Common clays as precursors for geopolymer-based construction materials

Zur Erlangung des akademischen Grades eines

Doktors der Ingenieurwissenschaften (Dr.-Ing.)

von der KIT Fakultät für

Bauingenieur-, Geo- und Umweltwissenschaften

des Karlsruher Instituts für Technologie (KIT)

genehmigte

DISSERTATION

von

M.Sc. Felix Dathe

Tag der mündlichen Prüfung: 14.02.2025

Referent: Prof. Dr.-Ing. Frank Dehn

Korreferent: Prof. Dr. rer. nat. Dietmar Stephan

Karlsruhe 2024

Abstract

The construction industry is increasingly seeking for sustainable materials to reduce overall environmental impacts, with a particular focus on minimizing the CO_2 footprint associated with the traditional cement production. In this context, geopolymers, synthesized from common clays, have emerged as promising alternatives, due to their versatile and tuneable properties, in terms of workability and mechanical properties, as well as their lower environmental impact. This thesis therefore explores the potential of geopolymers as green building materials through a comprehensive approach, examining their preparation methods, precursor selection, material properties, and performance characteristics.

In the first part of this thesis, a novel method for the evaluation of the suitability of clays as precursors for the formation of geopolymers using infrared (IR) spectroscopy is presented. With this technique the surface area under the OH stretching band in the IR spectrum of clays is determined, which directly correlates with the amounts of reactive components needed for the alkali activation process. This straightforward experimental approach not only simplifies the selection process of suitable clays, but also enables the estimation of the required amount of activator. Consequently, the alkali activation procedure is extremely simplified and no single-parameter screening is needed to identify a suitable mixing design. Additionally, the relationship between the IR spectroscopy data and the reactive clay components provides a predictive tool for assessing the quality of the resulting geopolymer mortars, particularly in terms of its compressive strength.

In the second part of this thesis, the impact of calcite-rich clays on the formation of geopolymer binders is explored. Through a controlled calcination procedure, it is possible to manage the thermal activation of the clay and the decomposition of carbonate minerals and the subsequent CO_2 release, independently. This procedure effectively separates the decarbonation of calcite from the dehydroxylation of layered silicates within the clay, enabling the formation of lime and other calcium-rich minerals. Despite the low content of reactive layered silicates and the presence of large amounts of unreactive minerals, such as calcite, the study demonstrates that mortars produced from these calcined clays can achieve compressive strengths exceeding 20 MPa, based on a tailored thermal activation. Hereby, the inclusion of portlandite significantly enhances the post-solidification characteristics and improves the carbonation resistance of the mortars.

Finally, the complex interplay of various factors impacting the geopolymerization reaction is investigated in depth. It was found that the water content and binder-to-aggregate ratio have a significant impact on the workability, the mechanical properties, and the porosity of the resulting geopolymer mortars. An increase in water content enhances the workability and reduces the air void content, due to an improved compaction of the material. However, it also leads to a decrease in compressive strength as a result of an increased capillary porosity. The mechanical properties of such mortars can be improved by optimising the binder-to-aggregate ratio through the addition of quartz sand.

In conclusion, this thesis aims to advance the understanding of geopolymers and the geopolymerization reaction itself to offer insights into the optimisation of the material properties for sustainable construction applications. The findings demonstrate the viability of geopolymers as eco-friendly alternatives to traditional cements and promote their adoption in green building practices.

Kurzzusammenfassung

Die Bauindustrie ist zunehmend auf der Suche nach nachhaltigen Materialien, um Umweltbelastungen und Treibhausgasemissionen zu verringern. Dabei liegt ein besonderer Schwerpunkt auf der Minimierung des CO_2-Fußabdrucks der herkömmlichen Zementherstellung. In diesem Zusammenhang gewannen Geopolymere als alternative Bindemittel, aufgrund ihrer vielseitigen und modifizierbaren Eigenschaften, beispielsweise in Bezug auf Verarbeitbarkeit und mechanische Festigkeiten, zunehmend an Bedeutung. In dieser Dissertation wird daher das Potenzial von Geopolymeren, auf der Basis calcinierter Tone, als umweltfreundliche Baumaterialien erforscht, wobei ihre Herstellungsverfahren, die Auswahl der Ausgangsstoffe, die Materialeigenschaften und die Leistungsmerkmale untersucht werden.

Im ersten Teil dieser Arbeit wird eine neuartige Methode zur Bewertung der Eignung von Tonen für die Bildung von Geopolymeren mithilfe der Infrarotspektroskopie (IR) vorgestellt. Mit dieser Technik wird die Fläche unter der OH-Streckungsbande im IR-Spektrum von Tonen ermittelt, welche direkt mit der Menge an reaktiven Komponenten korreliert, die für den alkalischen Aktivierungsprozess benötigt werden. Dieser unkomplizierte experimentelle Ansatz vereinfacht nicht nur die Auswahl geeigneter Tone für die alkalische Aktivierung, sondern ermöglicht auch die Abschätzung der erforderlichen Aktivatormenge. Folglich ist das Verfahren der alkalischen Aktivierung extrem vereinfacht und es ist kein Screening einzelner Parameter erforderlich, um ein geeignetes Mischungsdesign für die Herstellung von Geopolymeren zu ermitteln. Darüber hinaus bietet die Beziehung zwischen den IR-Spektroskopiedaten und den reaktiven Tonkomponenten ein Instrument zur Bewertung der Qualität der resultierenden Geopolymermörtel, insbesondere im Hinblick auf deren Druckfestigkeit.

Im zweiten Teil dieser Arbeit wird der Einfluss von Calcit-reichen Tonen auf die Bildung von Geopolymer-Bindemitteln untersucht. Durch ein kontrolliertes Kalzinierungsverfahren ist es möglich, die thermische Aktivierung der Tone und die Zersetzung von Karbonatmineralien mit anschließender CO_2-Freisetzung unabhängig voneinander zu steuern. Dadurch kann die Dekarbonatisierung von Calcit effektiv von der Dehydroxylierung von Schichtsilikaten getrennt werden, wodurch die Bildung von Calciumoxid und anderen Calcium-reichen Mineralien gewährleistet werden kann. Trotz des geringen Gehalts an reaktiven Schichtsilikaten und des Vorhandenseins großer Mengen an nicht reaktiven Mineralien zeigt diese Studie, dass Mörtel resultierend aus diesen kalzinierten Tonen, basierend auf einem angepassten Kalzinierungsprozess, Druckfestigkeiten von über 20 MPa erreichen können. Dabei verbessert die Zugabe von Portlandit die Nachverfestigungseigenschaften und die Karbonatisierungsbeständigkeit der Mörtel erheblich.

Im letzten Teil der Arbeit wird das komplexe Zusammenspiel verschiedener Faktoren, welche die Geopolymerisationsreaktion beeinflussen, eingehend untersucht. Es wurde festgestellt, dass der Wassergehalt und das Verhältnis von Bindemittel zu Gesteinskörnung einen erheblichen Einfluss auf die Verarbeitbarkeit, die mechanischen Eigenschaften und die Porosität von Geopolymermörteln haben.

Eine Erhöhung des Wassergehalts verbessert die Verarbeitbarkeit und verringert den Luftporengehalt aufgrund einer verbesserten Verdichtung. Sie führt jedoch auch zu einer Abnahme der Druckfestigkeit infolge einer erhöhten Kapillarporosität. Die mechanischen Eigenschaften von Geopolymermörteln können jedoch durch die Optimierung des Bindemittel-Gesteinskörnungs-Verhältnisses mittels der Zugabe von Quarzsand verbessert werden.

Zusammenfassend lässt sich sagen, dass diese Arbeit darauf abzielt, das Verständnis von Geopolymeren und der Geopolymerisationsreaktion selbst zu verbessern um somit Einblicke in die Optimierung der Materialeigenschaften für nachhaltige Bauanwendungen zu geben. Die Ergebnisse zeigen das Potential von Geopolymeren als Alternativen zu herkömmlichen Zementen und fördern deren Einsatz in umweltfreundlichen Baupraktiken.

Declaration

This cumulative dissertation entitled “Common clays as precursors for geopolymer-based construction materials” is submitted to the KIT-Faculty of Civil Engineering, Geo and Environmental Sciences. The work in this dissertation was carried out at the Institute of Concrete Structures and Building Materials under the supervision of Prof. Dr.-Ing. Frank Dehn between April 2018 and October 2024.

This dissertation is the result of my own work and is based on the three-following peer-reviewed publications:

Chapter 4:

F. Dathe, F. Dehn, Alkali Activation of Common Clay Deposits: Evaluation of the Suitability by an IR Spectroscopic Method, *Int. J. Concr. Struct. Mater.* **2024**, *18*, 1.

Felix Dathe conducted the experimental study, analysed the test results and drafted the manuscript. Frank Dehn contributed to the conception of the manuscript and supervision.

Chapter 5:

F. Dathe, V. Strelnikova, N. Werling, K. Emmerich, F. Dehn, Influence of lime, calcium silicate and portlandite on alkali activation of calcined common clays, *Open Ceramics* **2021**, *7*, 100152.

Felix Dathe was responsible for the experimental study, analysed the test results and drafted the manuscript. Vera Strelnikova supported the experimental work as part of her Master thesis. Nadja Werling and Katja Emmerich supported the analytics of the clay minerals. Frank Dehn contributed to the conception of the manuscript and supervision.

Chapter 6:

F. Dathe, S. Overmann, A. Koenig, F. Dehn, The role of water content and binder to aggregate ratio on the performance of metakaolin-based geopolymer mortars, *Minerals* **2024**, *14*, 823.

Felix Dathe, Andreas König and Frank Dehn were responsible for the conceptualization of the work and wrote and reviewed the publication. The experimental measurements and the visualisation were carried out by Felix Dathe, Steffen Overmann and Andreas König. Frank Dehn and Andreas König supervised the work.

Felix Dathe

October 2024

List of publications

- F. Dathe, V. Strelnikova, N. Werling, K. Emmerich, F. Dehn, Influence of lime, calcium silicate and portlandite on alkali activation of calcined common clays, *Open Ceramics* **2021**, *7*, 100152.

- F. Dathe, F. Dehn, Alkali Activation of Common Clay Deposits: Evaluation of the Suitability by an IR Spectroscopic Method, *Int. J. Concr. Struct. Mater.* **2024**, *18*, 1.

- F. Dathe, S. Overmann, A. Koenig, F. Dehn, The role of water content and binder to aggregate ratio on the performance of metakaolin-based geopolymer mortars, *Minerals* **2024**, *14*, 823.

- N. Werling, R. Schwaiger, F. Dathe, F. Dehn, K. Emmerich, Micromechanical properties of geopolymers with different calcined clay precursors, *Appl. Clay Sci.* **2024**, *250*, 107259.

- N. Werling, F. Dathe, F. Dehn, K. Emmerich, Calcined clay minerals as precursors for geopolymers and the influence of solubility on mixing ratios, *DuRSAAM 2023 Symposium Advancing alkali-activated materials* **2023**, 91.

- A. Koenig, A. Wuestemann, F. Gatti, L. Rossi, F. Fuchs, D. Fessel, F. Dathe, F. Dehn, F. Minelli, Flexural behaviour of steel and macro-PP fibre reinforced concretes based on alkali-activated binders, *Constr. Build. Mater.* **2019**, *211*, 583–593.

Acknowledgements

First and foremost, I would like to express my gratitude to my supervisor, Prof. Dr.-Ing. Frank Dehn. This work would not have been possible without his support and guidance.

I would also like to extend my thanks to Prof. Dr. rer. nat. Dietmar Stephan for being willing to take over the role as second reviewer of my thesis. His valuable insights and feedback have been greatly appreciated.

I am also very grateful to Prof. Dr. Frank Schilling, Prof. Dr. Kirsten Drüppel, and Prof. Dr.-Ing. Alexander Stark for being part of the examination committee. Their participation and evaluation have been crucial in the completion of this thesis.

Throughout the long journey of my thesis, I had the privilege of working with many outstanding scientists who contributed to my professional and private life. At the Institute of Mineralogy at the University of Leipzig, I would like to thank Andreas König, Annemarie Herrmann, Stefanie Thalheim and Klaus Bente for their collaboration and support.

I am also grateful to my colleagues at the Institute of Concrete Structures and Building Materials at the Karlsruhe Institute of Technology, including Laura Rossi, Richard Caron, Engin Kotan, Angelika Rußwurm, Martin Umminger, Moritz Zehmann, Patrick Wehres, Wolfgang Graf, Joachim Held, and Stephan Gehlsen, for their support. A special thanks goes to Julia Sonntag for earning "10 out of 10 babysitting points," which truly made a difference in balancing work and personal life.

Special thanks go to Katja Emmerich and Annett Steudel for their guidance with the analysis of clay minerals.

For their invaluable assistance at the institute, I would like to thank Petra Schlager, Andreas Bogner, and Astrid Hirsch.

I would also like to thank the students who worked with me as part of their theses: Tobias Dorn, Matthias Jakob, Bastian Oberleiter, Tien Nguyen, Vera Strelnikova, Steffen Overmann, David Maier, Ben Hopf, and Benjamin Bär. It was a pleasure to work with each of you.

Lastly, I am incredibly grateful for the support of my family and especially of my wife Schirin. Their encouragement and strength have been a constant source of motivation, and I could not have succeeded without them.

Table of contents

1. Introduction

Inorganic construction materials are considered as fundamental in the building industry, due to their robust mechanical properties.[1] The use of inorganic construction materials is driven by their advantageous properties, such as their high compressive strength, fire resistance, and durability. Applications of such construction materials span over a wide range, from residential buildings and infrastructure projects to specialised uses in marine and high-temperature environments.

Inorganic construction materials, which include concrete, mortar, and various composites, are characterised by the use of mineral binders, such as cement, lime, and gypsum, to create durable and versatile structures. In all of these cases, the addition of water triggers the hardening process, leading to their denotation as hydraulic binders (Figure 1).[2] Despite the great properties of cement as binder material, such as the flexible workability, the turnability *via* the use of additives, as well as the great mechanical properties of the thereof resulting concrete, the manufacturing of concrete is a significant contributor to the global CO_2 emissions. This is due to the raw materials preparation and the clinker production, whereby a high temperature is needed for the calcination, which causes the release of CO_2 from calcium carbonate. As stated by both the International Energy Agency (IEA) and the United Nations Environment Program (UNEP), the construction sector accounts for over 40 % of the global energy consumption and contributes to approximately one-third of the greenhouse gas emissions.[3] Within this context, the manufacture of concrete poses a substantial environmental challenge, as it is responsible for approximately 8 % of the total anthropogenic CO_2 emissions worldwide.[4,5]

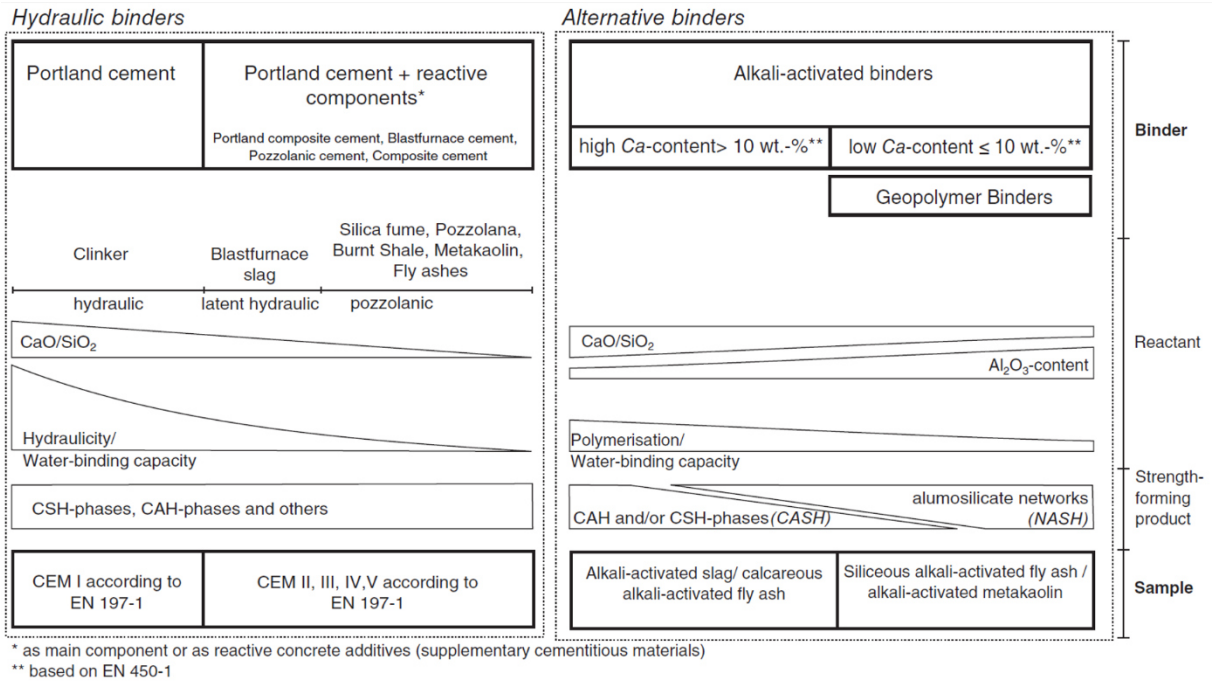

Figure 1: Classification of classical hydraulic and alkali-activated binders, reprinted from reference.[6]

Efforts to reduce the carbon dioxide footprint of the cement production have therefore been focused on the reduction of cement clinker *via* the addition of supplementary cementitious materials, such as

limestone.[7] Also, current research efforts go towards the use of alternative binder materials, such as alkali-activated materials (AAMs) and geopolymers, for the manufacture of construction materials.[8] Alternative binders are more sustainable compared to traditional binders, as they can incorporate industrial by-products, such as fly ash and slag, reducing waste, and naturally occurring precursors, such as common clays, and therefore promote a sustainable use of resources. Also, due to their alternative activation procedure, no high temperature treatments, which cause the major CO_2 emissions in the conventional cement production, are required. As Table 1 shows, alternative binders can clearly compete with hydraulic binders based on ordinary Portland cement (OPC) in terms of their mechanical performance.

Table 1: Comparison of the compressive strengths of different binders after 28 days at room temperature.

Type of binder	Binder	Strength [MPa]	Reference
Hydraulic binder	Ordinary Portland cement (CEMI 32.5)	32.5–52.5	DIN EN 197-1
	Ordinary Portland cement (CEMI 42.5)	42.5–62.5	DIN EN 197-1
	Ordinary Portland cement (CEMI 52.5)	>52.5	DIN EN 197-1
Alternative binder	Alkali-activated material based on ground granulated blast-furnace slag	40.0	[9]
	Geopolymer based on metakaolin	38.5	[10]

1.1 Cement

In the construction industry, cement is one of the most widely used binder materials.[11] It serves as fundamental ingredient in concrete and mortar, and contributes to their adhesive and cohesive properties. The versatility of cement has made it an indispensable material in the construction industry and has laid the foundation for its wide-ranging applications, from residential buildings to transportation. Based on that, the production of cement and the therewith involved the concrete industry, as major cement consumer, are an essential pillar of the world's economy with a pivotal role in the urbanisation and economic growth.[12,13]

Cement is generally derived from limestone, clay, and other raw materials, in a three-stage process, which involves the preparation of raw materials, the subsequent clinker production followed by the grinding with other components (Figure 2). In general, there are two approaches for the production of clinker, namely a wet or dry process, depending on the water content of the raw materials. The latter

one is more energy-efficient, due to the fact that no water has to be evaporated, and therefore this process is widely used to date. Whereas the wet process requires 5.29 GJ of specific energy per ton of clinker production, the dry version of cement manufacturing only utilises 3.40 GJ.[14] To begin the cement production process, the precursors of choice with respect to the product performance requirements, will be crushed typically to less than 10 centimetres in size and eventually mixed with other materials, such as iron oxide, alumina or silica. The materials then undergo a homogenisation process to achieve the required chemical composition. In a subsequent step, the pre-calcination and calcination in a rotary kiln at temperatures up to 1450 °C takes place. During the pre-heating moisture is removed, whereas during the calcination the decarbonation of calcium carbonate under the release of CO_2 is taking place. The high temperatures within the kiln are generated by the combustion of fuels, such as coal or natural gas, in the kiln. During the rotation of the kiln, the material moves progressively into hotter areas of the oven towards the flame. After the kiln-firing process, the clinker is cooled down very rapidly using air blowers or water-cooling systems. The rapid cooling is required to maintain the desired crystal structure and reduce the formation of undesirable crystalline phases. The clinker is then mixed with other materials, such as gypsum for example, blended and subsequently grinded to afford a powdered cement or blended-cement material.[15]

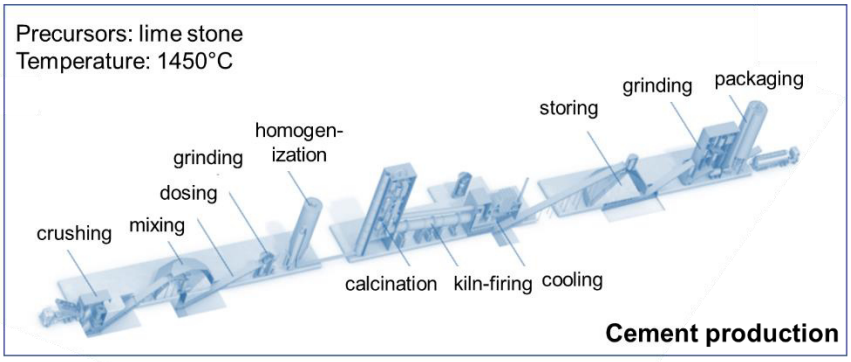

Figure 2: Overview of the cement production starting from lime stone.

Cement clinker primarily consists of calcium silicates, such as tricalcium silicate (C_3S) and dicalcium silicate (C_2S), together with other Ca-containing compounds, such as calcium aluminates and calcium ferrites (Table 2).[16] Within the clinker, alite is the most important phase with a portion of 50-70 % of the total composition. Alite is also responsible for the early strength development. 15-30 % of the clinker are comprised of belite, which contributes to the late strength development of cement, since it usually is less reactive than alite. Other phases, such as aluminate and ferrite, contribute each to about 5-10 % of the total clinker composition and also influence the early strength development. The temperature and duration of the decarbonation within the rotary kiln as well as the cooling process influence the phase composition and the homogeneity of the clinker material tremendously. Hereby it has been sown that slower cooling rates lead to larger and more homogenously distributed crystallites.[17]

Table 2: Overview of the components in cement clinker.

Name	Abbreviation	Chemical formulae
Alite	C_3S	$3\ CaO \cdot SiO_2$
Belite	C_2S	$2\ CaO \cdot SiO_2$
Aluminate	C_3A	$3\ CaO \cdot Al_2O_3$
Ferrite	C_4AF	$4\ CaO \cdot Al_2O_3 \cdot Fe_2O_3$

There are numerous types of cement available, due to the use of different Ca sources and the application of various additives to modulate the cements properties. The most widely used cement is the ordinary Portland cement (OPC), with the primary components being calcium oxide, silicon oxide, aluminium oxide, iron oxide and magnesium oxide. In general, OPC consists of 95 % clinker and 5 % gypsum, which is thought to improve the workability of the cement. Beside its versatility and economic value, OPC is not an optimal binder for all construction applications, since it suffers from durability issues, when applied in aggressive environments, such as high acidity or high sulphate concentrations. In addition to OPC, blended cement, in which sustainable supplementary materials, such as fly ash, slag, or silica fume are added, and white cement with a low iron content, are known among others.[18]

When cement is mixed with water, it undergoes a hydration reaction, in which a calcium silicate hydrate (C-S-H) gel is formed. This gel fills the voids between the cement particles and creates a dense interconnected network of the hydrated cement paste. In addition, calcium hydroxide is formed as by-product of the hydration reaction and contributes to the alkalinity of the resulting concrete and plays a role in its long-term strength development. As the hydration process progresses, the cement paste gradually solidifies and the hardening of the mixture is taking place, which retains its strength. The rate and extent of the hydration reaction depend on various factors, including the type of cement, water-cement ratio, temperature, and curing conditions.[19]

1.1.1 Environmental footprint of the cement production

According to the International Energy Agency, concrete is considered to be the most-used manufactured substance on the planet based on the volume.[20] Therewith involved is the production of cement, which acts as binder within concrete to aggregate the components being present. Currently, 4 Gt/year of cement are being produced, whereby over the past 65 years the production increased by a factor of 10, as shown in Figure 3.[21]

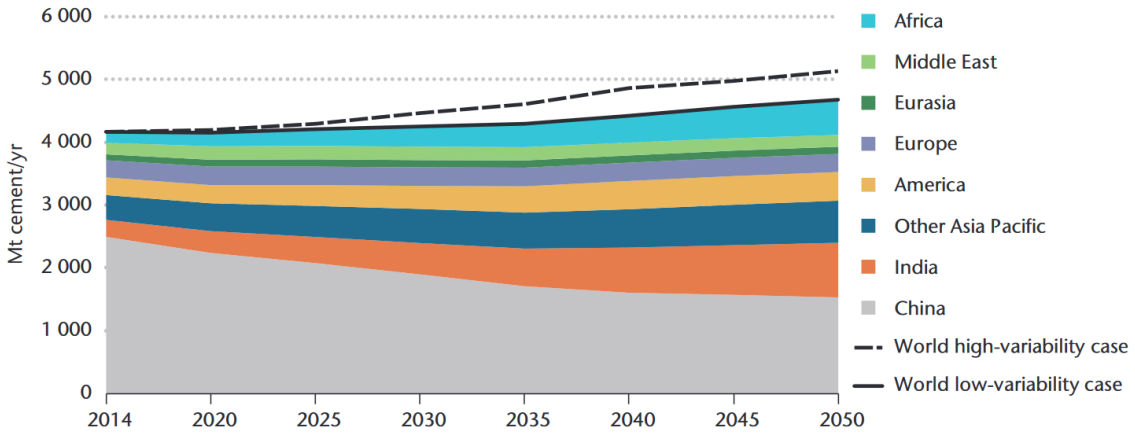

Figure 3: Cement production in dependence of the geographic location. Graphic reprinted from reference.[20]

The environmental impact of the cement production is significant, primarily due to its substantial contribution to greenhouse gas emissions and resource mining and consumption. The latter one is particularly pronounced, since minerals applied in the sector of construction materials, have a large energy demand despite their low energy intensities. This is based on the large amounts of minerals that have to be extracted prior to the cement and concrete production.[22]

Along with the before mentioned production capacity of 4 Gt/year, around 2300 Mt of CO_2 are emitted.[20] This number is thought to increase by 12-23 % by 2050 with respect to 2014, due to growing economies, especially in the Asian area.[20] Currently, the production of cement contributes to about 8 % of the global anthropogenic CO_2 production, which is mainly due to the high-temperature firing of raw materials, such as limestone, but also due to inefficient production technologies.[5] In this context, the production of cement contributes 36 % of the CO_2 emissions generated by construction materials[23] and at least 70 % of the CO_2 emissions from the concrete manufacture.[24] It is well established that the increase of greenhouse gases, such as CO_2, in our atmosphere is the main contributor to climate change, which cause an increase in the Earth's temperature.

The CO_2 emissions in cement manufacturing, mainly stem from the calcination of the carbonate rich precursors, such as limestone, in the rotary kiln. The calcination process contributes to about two third of the greenhouse gas emissions from cement production,[25] and also explains why the production of cement cannot be decarbonised completely, since these material-related CO_2 emissions cannot be avoided.[26] In addition, to the material-inherent CO_2 release, the high energy demand of the firing process is an important factor to consider.[27] The latter can be reduced tremendously through an enhanced kiln efficiency.[20] Other steps of the cement production, such as grinding, blending and backpacking only have a minor influence, according to life cycle assessments from "cradle to gate".[28]

To address these issues and to lower the environmental impact of the cement manufacture, alternative approaches and production technologies, have been investigated. As mentioned before, the majority of CO_2 emissions during the cement production comes from the clinker production. Therefore, there has been considerable progress to enhance the energy efficiency of the clinker production, especially with

respect to the kiln development along with heat recovery and recycling. Also, the flexibility of kilns with respect to the fuel source has greatly been enhanced and paved the way for the use of waste materials as "alternative fuels".[29] One other approach to reduce the environmental footprint of the cement production, is based on the reduction of the clinker content by the addition of so-called supplementary cementitious materials, such as such as limestone, gypsum, slag or fly ash. The most widely used supplementary materials is ground lime stone, which is not heated to avoid the release of CO_2.[7] In addition fly ash and blast furnace slags, which are formed as by-products in the coal and steel industries, have been used to reduce the clinker amount in cement.[30] However, the availability of these materials will most likely decline, since the production of coal is reduced through the use of alternative energy sources. In addition to the measures described, carbon capture and storage (CCS) has to be implemented on clinker production sites to really reach CO_2 neutrality.

Beyond the approaches to reduce the CO_2 footprint of the cement production, the complete substitution of clinker through alternative binders, such as alkali-activated materials or geopolymers, has gained academic interest in the last decades.[31,32]

1.2 Alternative binders

Alternative binders are classified based on the Ca-content of the raw materials used. Whereas alkali-activated materials result also from calcium-rich raw materials, such as blast furnace slag and other calcium-rich industrial by-products, raw materials with a low Ca-content, such as fly ash or clay-based raw materials, are utilised for the production of geopolymers (Figure 1). In both cases, the binding process of alternative binders involves chemical reactions, such as condensation and polymerisation reactions, which result in a hardened matrix.[33] Hereby, the reaction and the solidification process depend strongly on the choice of raw materials and are also dependent on the alkaline solution used for the activation step.[34] In the case of Ca-rich precursor materials, the activation is carried out in alkaline solutions of medium basicity. From this, calcium silicate hydrates-like phases can be obtained as reaction products. In the case of raw materials with a low Ca-content or Ca-free materials, highly alkaline solutions are utilised for the activation procedure, resulting in polymeric networks of amorphous phases similar to zeolites.

In Figure 4 an attempt is made, in analogy to Provis *et al.*, [35] to schematically show the phase formation based on the composition of the raw materials used as precursors for the alkali activation procedure. Whereas calcium aluminosilicate hydrate (C-A-S-H) gels are formed from calcium-rich aluminosilicates, the alkali activation of aluminosilicates low in calcium content leads to the formation of so-called N-A-S-H gels. Depending on the Mg content either zeolite-type or hydrotalcite-type structures can be formed. However, the exact phase determination is challenging, due to the large experimental parameter space, such as the chemical composition of the raw materials, the nature of the activator solution, the mixing design and curing conditions, among others.

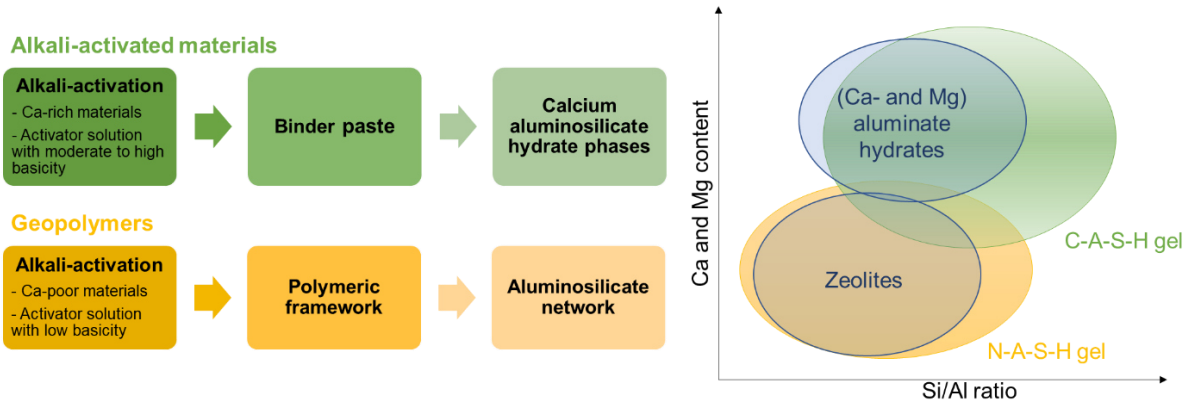

Figure 4: Schematic overview of the phase formation based on the composition of the raw materials used for the alkali activation procedure. Graphic partly adapted from reference.[35]

1.2.1 Alkali-activated materials

Alkali-activated materials (AAMs) represent a class of binders in the field of construction materials, which offer a sustainable alternative to traditional cement binders. In contrast to cement, which primarily consists of calcium silicates (such as Portlandite) and other Ca-containing compounds, such as calcium aluminates and calcium ferrites, AAMs are typically composed of aluminosilicate-rich precursors. During the manufacture of AAMs around 95 % less CO_2 emissions are produced in comparison to a similar mass of OPC.[36] In addition to that, industrial-by products can serve as starting materials, which again lowers the environmental footprint in contrast to the conventional production of clinker.

AAMs are synthesised through the activation of a precursor powder, based on calcium, magnesium, silicon or aluminium oxide, using alkaline solutions as activators.[37] These precursors are usually aluminosilicate-rich materials, which can be obtained from industrial by products, for example ground granulated blast furnace slag (GGBFS), resulting from the iron and steel industry, rice husk ash from rice milling or fly ash from coal combustion. Further, natural pozzolans, such as volcanic ash and calcined clays, as well as mine tailings can be utilised.[38] The choice of precursor depends on factors, such as the availability, cost, desired properties of the final product, and environmental considerations. The precursors will then be treated with an alkaline solution (e.g., sodium or potassium hydroxide) to undergo a process denoted as “alkali activation” (Figure 5). Firstly, the aluminosilicate material is dissolved in the activator solution. During this exothermic process, reactive units, consisting of covalently bound Si–O–Si and Al–O–Si units, are formed, which then undergo a condensation reaction. Hereby a cementitious matrix, also referred to as aluminosilicate gel is formed, which is based on the incorporation of Al into Si–O–Si units.[39] This leads to a binding process, which results in the generation of a three-dimensional network of silicon and aluminium bonds and subsequent crystallisation.[35]

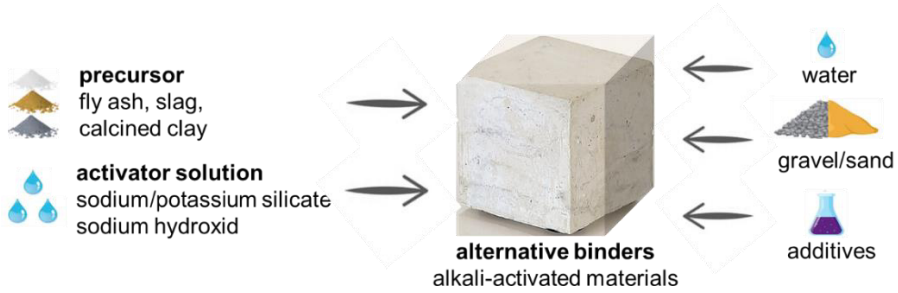

Figure 5: Schematic overview of the alkali activation processes to obtain alkali-activated materials as alternative binders.

The reaction progress of the alkali activation strongly depends on the precursor and activator type as well as the respective concentrations. The use of fly ash with a high silica content as precursor, for example, leads to a greater pozzolanic reactivity, which induces an enhanced strength development and durability in the final product.[40] The strength development is also positively influenced by the use of higher activator concentrations, which promote a faster reaction kinetics. However, an optimal activator concentration must be found, since a very large activator amount leads to the formation of detrimental effects, such as excessive shrinkage, cracking, and consequently to a reduced long-term durability.[41] Each of these components play a significant role in order to tune the properties and behaviour of AAM-based concrete, ultimately influencing its suitability for specific construction-related applications.[42]

The interest in the use of AAMs as alternative to conventional concrete stems from their exceptional mechanical characteristics, including a high compressive strength, remarkable durability, and resistance towards acids and various other chemicals. Furthermore, there are significant environmental advantages involved when using AAMs, since the production of AAMs typically results in significantly lower carbon dioxide emissions and a lowered energy consumption compared to ordinary Portland cement, a factor which contributes to the reduction of the construction industry's carbon footprint. Moreover, the incorporation of industrial by-products in AAM formulations fosters a sustainable use of resources, recycling and waste utilisation, aligning with sustainable development goals.

The applications of alkali-activated materials are diverse, ranging from traditional construction uses, such as structural and non-structural components, as well as specialised applications in areas, where an enhanced durability and resistance towards aggressive environments are required.

1.2.2 Geopolymers

Geopolymers, also a class of alternative binder materials, have gained significant attention for their unique chemical compositions and exceptional properties. The pioneering work of Davidovits in the 1970s laid the foundation for the development and understanding of geopolymers. Davidovits first coined the term "geopolymers" to describe a variety of inorganic binders based on alumosilicate polymers, which results from the chemical reaction of alumina-based silicates with a alkaline activator.[43] According to Buchwald's definition, geopolymer binders are inorganic two-component systems, consisting of a reactive solid component with SiO_2 and Al_2O_3 in sufficient quantity and reactive

form, and an alkaline activation solution, containing alkali hydroxides, silicates, aluminates, carbonates, sulphates or any combination thereof.[44] Geopolymer binders originate from natural pozzolans,[45] slags,[46] thermally-activated clays[47,48] and rice husk ashes,[49] as well as fly ash.[50] Alkaline solutions serve as activators, as seen before in the case of AAMs, which has led to the frequent use of the term "alkaline-activated binders".[33] However, geopolymers are clearly distinguished from alkali-activated materials based on the low Ca-content of the raw materials used.

These inorganic, aluminosilicate-based materials are synthesised through the reaction of alumina- and silica-rich materials with alkaline activators, forming a three-dimensional network of covalently bound Si–O–Al structures. Davidovits described the reaction for the geopolymer formation and illustrates that the addition of an alkaline solution leads to the dissolution of silicon and aluminium oxide. This dissolution process results in a "geopolymer precursor", which simultaneously undergoes a condensation reaction, which is typically base catalysed. This reaction leads to the formation of a three-dimensional network, as shown in Figure 6. Solid-state nuclear magnetic resonance (NMR) spectroscopic analyses (solid-state ^{27}Al and ^{29}Si MAS NMR) point towards the conversion of the four-fold coordinated aluminium centres to a three-dimensional cross-linked inorganic polymer, which consists of $NaAlO_4$ and SiO_4 tetrahedra.[51] These tetrahedra are interconnected by shared oxygen atoms, which leads to the formation of a three-dimensional polymeric structure with Al–O–Si units as main building blocks. The geopolymerization process forms amorphous alumosilicate networks with various structural motifs, whereby the hardening of the binder occurs due to network formation. Within these networks, cations, resulting from the activator, are present to maintain charge neutrality.[52] Interestingly, geopolymer products exhibit great structural similarity to zeolites. This is evidenced by X-ray-based studies, that have identified different zeolite structures within seemingly amorphous polymers.[53]

According to the Si:Al ratio of the three-dimensional alumino-silicate structures, which can be considered as amorphous to semi-crystalline, Davidovits established a classification into poly(sialate)-type (Si–O–Al–O–), poly(sialate-sil-oxo)-type (Si–O–Al–O–Si–O–) and the poly(sialate-disil-oxo)-type (Si–O–Al–O–Si–O–Si–O–) structures.[54] Hereby, the Si:Al ratio greatly influences the properties of the resulting mortars and therefore their potential application.

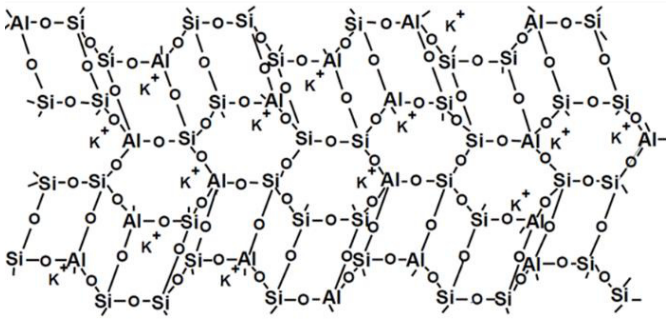

Figure 6*:* Structural network of a geopolymer according to Davidovits.[55]

Geopolymers exhibit a range of exceptional properties that render them highly advantageous for various applications. These properties arise from their unique chemical and structural characteristics, which distinguish them from traditional materials, such as ordinary Portland cement and ceramic-based materials. For instance, geopolymers demonstrate comparable compressive and tensile strength compared to conventional cementitious materials.[56] In this context it was shown, that geopolymers with a high compressive strength can be obtained when highly reactive precursor materials are utilised.[57] Hereby a higher strength can be correlated with a microstructure, which inherits a low content of undissolved mineral phases.[58] Additionally, geopolymers possess a remarkable durability, as they are typically resistant to acids, bases, and salts, which enhances their durability in harsh environments, including marine settings and areas with high chemical exposure. Furthermore, geopolymers exhibit a high thermal stability and minimal shrinkage and creep due to their three-dimensional network structure. Their low permeability to water and other fluids can also be attributed to their inherent structural features and their dense microstructure.[59] Geopolymers also offer good workability, allowing them to be moulded into various shapes and sizes. This lays the basis for a flexible design of geopolymer-based mortars.

1.3 Clays as precursors for geopolymers

For the production of geopolymers, clays can be used as versatile and abundant precursors. Clays are particularly suitable for the geopolymerization process, due to their high aluminosilicate content and their high reactivity after calcination. To obtain geopolymers from clay minerals, such as kaolinite, first a calcination step is required, which leads to the dehydroxylation of the clay mineral and the formation of a highly active nearly amorphous meta-state, also referred to as meta-clay. Despite the fact, that energy is required for the thermal treatment of the clay minerals prior to the alkali activation, the required temperature is still below the temperature that is needed for the conventional production of cement clinker. The from calcination obtained meta-clay is then reacted with an alkaline solution to initiate the geopolymerization reaction.

1.3.1 Structures of clay minerals

In general, clays are a type of clastic sediments, which include hard clay stones, deformable clays, and certain soil types with a predominant grain size distribution of less than 2 micro meters. Geological and geochemical estimates suggest that over 50 % of the Earth's sedimentary rocks contain such fine clastic sediments.[60] To exclude rocks with predominantly carbonate components (such as marl), clays are considered sediments with primarily silicate-based mineral components.

The components of clays mainly correspond to the mineral relics of their crystalline parent rocks, including mica, quartz, and small amounts of alkali feldspar, whereby the composition of a clay deposit depends on various factors, such as the climatic conditions, parent rock types in the weathering zone, and sediment transport.[61] Layered silicates and their weathering products can be considered actual clay minerals. Additionally, iron-rich and carbonate weathering products, such as pyrite, hematite, goethite,

dolomite, and calcite can contribute to several percentages. In minor quantities, plant and animal decomposition products in the form of humic substances may accumulate in fractions less than 0.2 µm.

The main building blocks of clay minerals are SiO_4 tetrahedra, in which silicon ions are coordinated by oxygen (Figure 7). These tetrahedra are connected *via* three of their edges to form a tetrahedral layer, which is also referred to as T-layer. This T-layer represents a fundamental component of clay minerals or so-called phyllosilicates. One of the vertices of the SiO_4 tetrahedra stick out from the T-layer and generally point in one direction, resulting in an infinite layer with a composition of $[Si_2O_5]^{2-}$. Occasionally, foreign cations such as Fe^{3+} and Al^{3+} can occupy the tetrahedral coordination sites, which leads to an increase in overall negative charge and a distortion of the T-layer.[62]

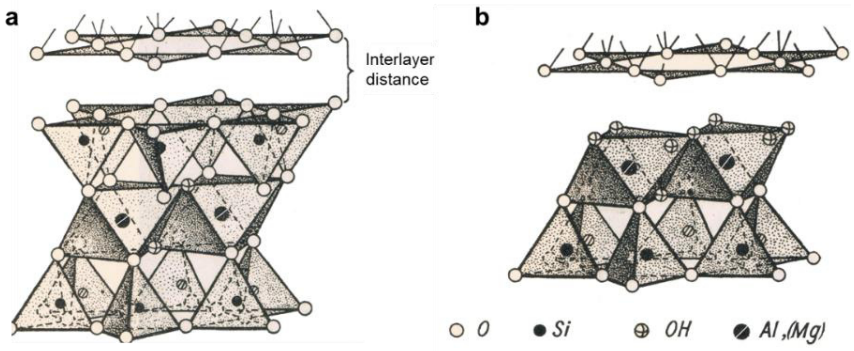

Figure 7: Schematic structures of clay minerals. a) Montmorillonite as three-layer mineral and b) kaolinite as four-layer mineral. Graphic adapted from reference.[63]

Other prominent coordination polyhedra, which can be found in clay minerals, are octahedra (Figure 7). In these octahedra, divalent and trivalent metal cations are coordinated by six hydroxide ions. Some minerals, like aluminium hydroxide and magnesium hydroxide, consist solely of such octahedral layers, which are denoted as O-layers. Common central ions include Al^{3+}, Fe^{3+}, Mg^{2+}, and Fe^{2+}. Depending on whether divalent or trivalent metal ions occupy these sites, the octahedral layer is described as trioctahedral or dioctahedral structure, respectively.[64] However, the occupancy of the coordination sites is strongly radius-dependent and therefore alkali ions cannot be found in octahedral coordination sites. As seen before in the case of the tetrahedral layer, an inhomogeneous occupancy may also occur in the octahedral layer.

The connection between T- and O-layers occurs through the free vertices of the SiO_4 layer, which leads to the stacking of alternating layers (Figure 7) and the formation of two-, three- and four-layer minerals. Furthermore, interlayers (Z-layers) exist, which are primarily responsible for the wide-ranging properties of clay minerals. These layers may be occupied by cations and/or water or may simply remain empty.

Two-layer minerals

Two-layer minerals describe a type of clay minerals, which consist of one tetrahedral sheet linked to one octahedral sheet. This motif is repeated throughout the whole mineral. Two-layer minerals can be

mainly distinguished based on the occupancy of the octahedral layers. Dioctahedral minerals include kaolinite and its rarer derivatives nacrite and dickite. In these minerals, hydrogen bonds bridge the interlayer. If this Z-layer is completely filled with water molecules, halloysite forms with a layer distance of 10 Å.[65] Trioctahedral two-layer minerals include serpentine group members, which exclusively have Mg^{2+} ions occupying the octahedral coordination sites, as well as Fe^{2+}-rich minerals, such as greenalite, berthierine, and cronstedtite.

Within the two-layer minerals, kaolinitic clays, characterised by a particularly high content of kaolinite, are a very unique group. Kaolinite is the most common two-layer mineral with a theoretical composition of 2 $SiO_2 \cdot Al_2O_3 \cdot 2\ H_2O$, which corresponds to 46.53 wt. % SiO_2, 39.49 wt. % Al_2O_3, and 13.98 wt. % H_2O. The water is bound in the form of OH-groups in the octahedral layer, forming van der Waals forces that connect to the next layer.[66] Due to slight deviations in the lateral dimensions of the tetrahedral and octahedral layers of kaolinite, tensions occur in the structure, which limit the crystal growth perpendicular to the layers to a maximum of 30 layers. By examining the overall structure (Figure 8), the morphology and properties of kaolinite can be derived and understood. Kaolinite crystals appear in nature as pseudohexagonal platelets that can be several hundred nm thick, whereby their hexagonal shape is given by the silicon tetrahedral layer.

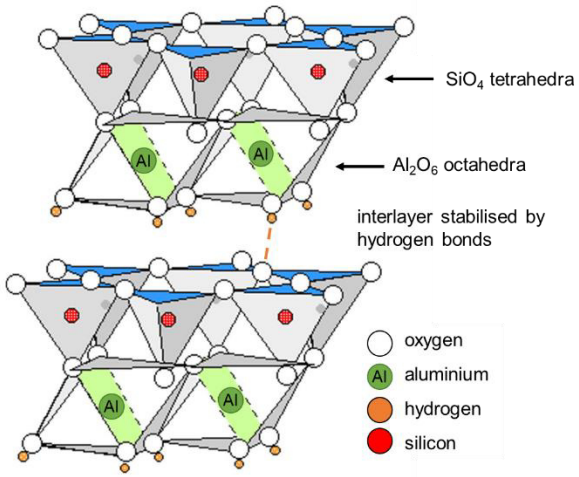

Figure 8: Structure of kaolinite as two-layer mineral. Interlayers are stabilised by hydrogen bonds. Graphic adapted from reference.[65]

Kaolin has a wide range of applications in various technical processes, such as in the ceramic industry and as a pigment and filler. However, deposits with high kaolinite content are rare and often contaminated with other clay minerals.

Three-layer minerals

Three-layer clay minerals display a T-layer - O-layer - T-layer structure, as shown in Figure 7. The resulting interlayer is responsible for the minerals' intra-crystalline swelling capacity. In general, three-layer minerals can be classified based on their swelling capacity and the occupancy of the octahedral layer. The swelling capacity depends on the overall charge, developed across the layers, and can range

from limited lattice expansion (about 15 Å for smectites) to unlimited expansion and layer disintegration in vermiculites. Smectites and vermiculites are differentiated by Bailey[67] based on interlayer charges, with dioctahedral smectites (e.g., montmorillonite, beidellite, and nontronite) being the main representatives. Vermiculites mainly occur as weathering products of biotites and magnesium-rich rocks in trioctahedral form. Trioctahedral smectites are rarely found in nature. Non-swelling minerals include dioctahedral micas, such as muscovite and illite, with biotite being the main representative of trioctahedral non-swelling three-layer minerals.

Four-layer minerals

The four-layer minerals exclusively correspond to aluminosilicates, which means that the tetrahedral layers are partially occupied by aluminium ions. Within four-layer minerals the tetrahedral and octahedral layers are arranged alternately. Depending on the occupation of the octahedral layer, four-layer minerals can be further classified into dioctahedral, ditrioctahedral, tri-dioctahedral, and trioctahedral four-layer minerals. Some examples of these minerals include donbassite, soil chlorites, sudoite, and cookeite.

Mixed-layer minerals

A closer examination of clays often reveals mixed-layer minerals with varying atomic layer structures. Regular mixed-layer minerals often have their own mineral names, as shown by the name rectorite, which refers to a combination of paragonite and dioctahedral smectite. A detailed overview of mixed-layer clay minerals and their X-ray crystallographic identification can be found in Brindley & Brown.[68]

1.3.2 Properties of clay minerals

Based on their inherent structural features, clay minerals exhibit interesting properties. For example, dried clay absorbs water through capillary and osmotic forces between particles, when there are being moistened. In non-swelling clays, water molecules only wet the particle surfaces, whereas in swelling clays, they penetrate the interlayers and expand them. This expansion can be influenced by various solvents, allowing for the distinction of clay minerals using X-ray powder diffraction. Another property arising from the existence of interlayers, is the ability for ion binding and exchange, where cations within the interlayers can be replaced by electrolytes. This effect is particularly noticeable in montmorillonite.

Clays also exhibit interesting rheological properties, such as a high viscosity and plasticity, which form the basis of the entire ceramic industry. The particle composition allows the formation of a water layer on the surface, which leads to a reduction of the cohesion forces and enables the deformation of the clay under pressure. This property is significantly influenced by the number of particles per unit volume. In clay suspensions, thixotropy occurs, where a structure forms at a finite speed, leading to a transition from the liquid to the solid state. This process is being fully reversible with mechanical energy input. The rheological properties of clays have great practical significance in the field of construction science.

In addition to the rheological properties, the reactivity of the clays after a thermal treatment must be highlighted. When clay minerals are treated thermally, dehydration and dehydroxylation occurs, which results in a release of the built-in OH-groups in the form of water. During this process, defects in the crystal structure up to a complete destruction of the structure and the formation of an amorphous material can occur. Hereby, the calcination temperature and type of clay mineral play crucial roles. The lattice defects formed during the calcination form the basis for the alkaline activation of clay minerals and the subsequent geopolymer formation. At higher calcination temperatures, phase rearrangements can even occur, leading to new phases, such as cristobalite and mullite, which are responsible for the strength of conventional pottery.

2. Aim of this thesis

As highlighted in the introduction of this thesis, the production of cement is a major contributor to anthropogenic carbon dioxide emissions, which significantly impact global warming and climate change. Therefore, there is an ongoing societal and political effort is made to reduce the greenhouse gas emissions in the cement and construction sectors. A key strategy to address this issue is the development and utilisation of alternative inorganic binders, which can be derived from the alkali activation of various precursor materials. In the field of alternative inorganic binders, geopolymers, which are defined based on their low calcium content, have attracted attention. Such geopolymers can be obtained from the geopolymerization reaction of calcined clays, which occur as locally available raw materials. However, the geopolymerization reaction of clays is a very complex process influenced by numerous factors, including:

- **Choice of raw materials:** the selection of the common clay precursors and therewith involved their mineralogical composition affects not only the reactivity and the activation procedure, but also impacts the properties of the geopolymer materials, such as their workability, mechanical strength and durability.
- **Precursor pre-treatment:** the thermal activation of the common clays is required prior to the alkali activation, which leads to the dehydroxylation of the clay and the subsequent formation of a highly active meta-clay. The conditions of this pre-treatment again affect the success of the alkali activation procedure.
- **Alkali activation procedure:** For the alkali activation of common clays the choice and concentration of base, the molarity and composition of the water glass and the water content are crucial. All these factors influence the geopolymerization reaction.
- **Binder composition:** the addition of additives, such as plasticizers and aggregates, as well as the binder to aggregate ratio strongly affect the final properties of the geopolymer materials.
- **Post-synthetic curing conditions:** the curing conditions, after the geopolymerization reaction itself influence the geopolymer materials properties. This includes the choice of temperature and humidity over a certain period of time.

This thesis therefore aims to contribute to a better understanding of the geopolymerization reaction of common clay precursors by looking at the factors described before. The ultimate aim is to enable the targeted formation of high performance geopolymer-based mortars, which combine a good workability of the fresh mortar, good mechanical properties and a high durability of the mortars.

3. Structure of this thesis

The present cumulative doctoral thesis is based on three peer-reviewed publications under the overarching topic of geopolymer-based construction materials, as depicted in Figure 9.

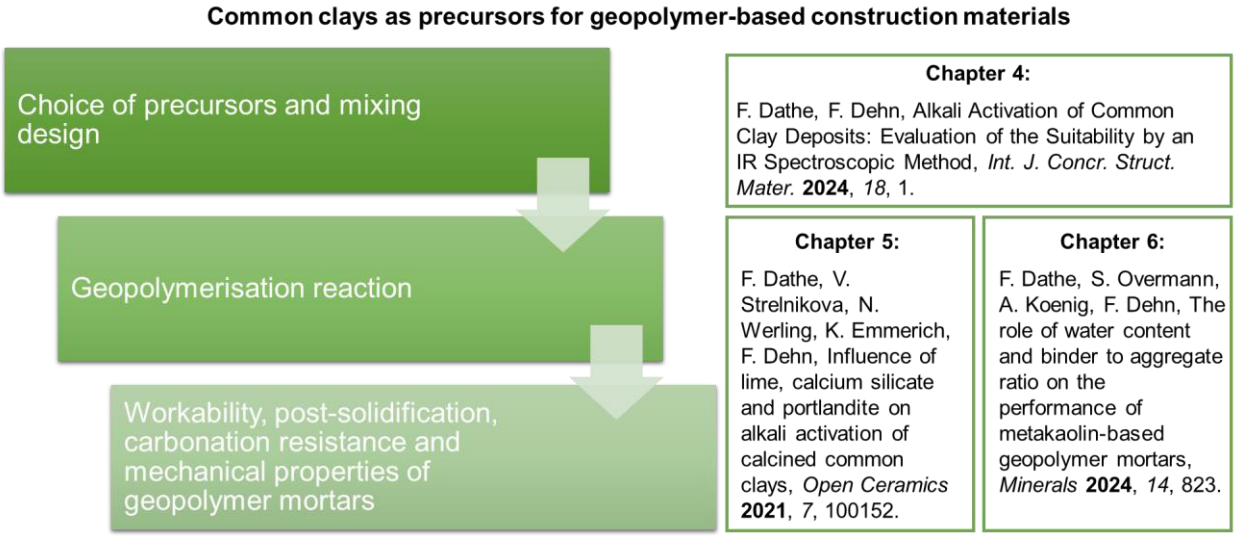

Figure 9: Structure of the cumulative thesis titled "Common clays as precursors for geopolymer-based construction materials".

In **chapter 4**, a methodology study concerning the identification of suitable clay-based precursors for the alkali activation procedure is presented. Therefore, an in-house developed infrared spectroscopy setup was developed, with which the surface area under the OH stretching band in the IR spectrum of common clays could be correlated with the amounts of reactive components, which are necessary for the alkali activation. Based on this correlation and a thorough calibration, the required activator amount could be determined directly without the need of iterative tests of the mixing design.

In **chapter 5**, the effects of calcite-rich clays on the geopolymer binder formation is investigated. Hereby, it could be shown that through a tailored calcination process, the thermal activation of the clay and the calcium carbonate decomposition can be controlled independently. Despite the low content of reactive silicates, mortars made from clays after this calcination procedure could achieve compressive strengths over 20 MPa, with enhanced post-solidification characteristics and carbonation resistance due to the inclusion of portlandite.

In **chapter 6**, various factors influencing the geopolymerization reaction have been investigated. It could be shown that the water content and the binder-to-aggregate ratio significantly affect the workability, mechanical properties, and porosity of geopolymer mortars. While an increased water content improves the workability and reduces the air void content, a decrease in compressive strength due to a higher capillary porosity is witnessed. Through an optimised binder-to-aggregate ratio *via* the addition of quartz sand the mechanical properties can be improved.

4. Alkali activation of common clay deposits – evaluation of the suitability by an IR spectroscopic method

Reproduced from: F. Dathe, F. Dehn, Alkali activation of common clay deposits – evaluation of the suitability by an IR spectroscopic method, Int. J. Concr. Struct. Mater 2024, 18, 1.

Abstract: In the context of a sustainable use of resources with the aim of the reduction of the CO_2 footprint, the development of alternative concrete materials has attracted a great deal of attention. In this context, geopolymers, obtained from common clay deposits, are found to be interesting construction materials with very versatile properties. In this paper, a completely novel approach for the evaluation of the suitability of clays for the geopolymer formation is investigated. The method is based on simple and easy-to-handle IR spectroscopic measurements, through which the surface area under the OH stretching band in the IR spectrum of the clay can directly be correlated to the amount of reactive clay components. These reactive components are required for the success of the alkali activation of the clays in order to access geopolymers. Based on the theoretical reaction pathway of the geopolymer formation, the linear relationship between the OH stretching band area and the reactive components can be used for the estimation of the required activator amount for the alkali activation of calcined clays and predict the quality of the casted geopolymer mortar in terms of strength. This new method not only gives an insight into the suitability of a common clay for the geopolymer formation, but also facilitates a straightforward alkali activation procedure without tedious preliminary testing of the required activator amount.

4.1 Introduction

The components of clays are mainly based on the mineral relicts of their parent rocks. This fact causes a vast variety of clay deposits to occur. Most common clays are associated with sheet silicates, which are vital for the alkali activation of clays, since they comprise suitable hydroxyl groups for the calcination process prior to the alkali activation.[69] Despite the sheet silicates also other minerals, such as quartz, hematite and feldspar, can be found in clay deposits. These minerals are inert towards calcination and activation processes.[70]

The alkali activation of raw materials has been studied in more depth recently, since it provides versatile access to novel construction materials. These materials are referred to as alkali-activated binders or geopolymer binders, depending on the calcium content of the raw material.[71] Furthermore, alkali activation represents a suitable and environmental friendly alternative to the cement production, which has a negative influence on the carbon dioxide content in the atmosphere.[72] So far, the focus has been mainly on the alkali activation of fly ash, slag and metakaolin[40] and not so much on common clays, due to the complexity of the clay material itself. This versatility of common clays causes difficulties, since it is necessary to investigate the exact mineral composition of the clay before the activation to evaluate the right conditions for the calcination and subsequent activation of the raw material.[73] The calcination as well as the activation processes are extremely important not only for the development of new construction materials, but also for the application of calcined clay as an additive for ordinary

concrete, due to its pozzolanic activity.[74,75] Although there is a close relationship between the pozzolanic activity and the alkali activation, the hardening of the binder is caused by a different chemical reaction and makes a comparison difficult.

To obtain a geopolymer binder based on common clays the raw material must be calcined first. During this step, the crystalline nature of the sheet silicates is destroyed under elevated temperatures and at the same time the hydroxyl groups of the crystal structure are eliminated in the form of water.[76] The calcination process significantly impacts both the crystallinity of the material and its solubility in a basic pH solution. The after the calcination obtained amorphous material, represents the starting material for the alkali activation. During the alkali activation process, an aqueous base and water glass are commonly added to the calcined clay which leads to the formation of a geopolymer precursor. This precursor then undergoes a condensation reaction and forms an amorphous alumosilicate network (Figure 10).[55]

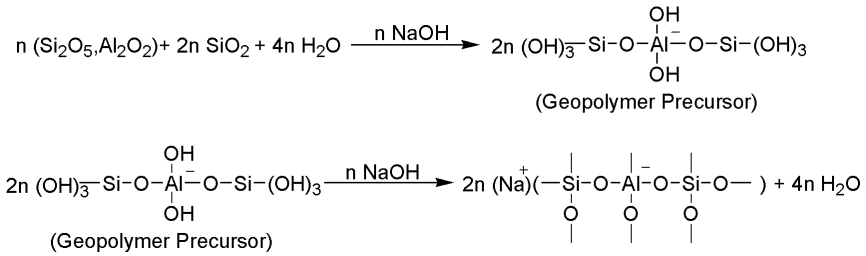

Figure 10: Process of the formation of geopolymers based on metakaolinite.[43]

One of the major factors to consider during this process is the amount of base and water glass that is required for the geopolymer formation. Based on the studies of Davidovits *et al.* in 1994 it can be assumed that for 1 mole of metakaolin (which is a dehydroxylated form of kaolinite) 2 moles of water glass and in total 2 moles of base are required. However, if a calcined clay is used instead of pure kaolinite, which consists of a variety of mineral components, the situation becomes more complex. Therefore, it is necessary to determine the number of reactive components within clay deposits before the alkali activation. The amount of reactive components in the clay strongly depends on the OH groups present in the structure, since during the calcination process the clay structure is losing its OH groups in the form of water. This leads to the formation of so-called reactive centres, where the OH groups were present before, and the subsequent formation of geopolymer precursors. The positions of these reactive centres can then be cross-linked during the activation process via a condensation reaction.[39,77]

Encouraged by this, a suitable method for the investigation of the amount of reactive components in clay deposits was developed. Therefore, a clay activation index, which represents the alkali activation potential of common clays, based on an IR spectroscopic method, is introduced. This clay activation index allows to estimate the suitability of a certain clay for the geopolymer formation but also gives an estimation of the amount of activator that is required for the alkali activation of the calcined clay.

4.2 Materials and methods

4.2.1 Clay materials

Eight different deposits of common and materials (clays A – H) were analysed by powder X-ray diffraction (XRD) and simultaneous thermal analysis (STA) to gain information about their composition (Table 3). The phase components usually exhibit error values around ± 2 %.

For the qualitative analysis of the composition of the clays the programme EVA™ was used, whereas the quantitative analysis was obtained by Rietveld analysis of the data, employing the programme PROFEX.

Table 3: Composition of the clays A to D (in %).

Mineral component	Clay A	Clay B	Clay C	Clay D	Clay E	Clay F	Clay G	Clay H
Albite	-	-	4	-	-	3	2	-
Phyllosilicates*	94	65	61	33	93	77	82	24
Quartz	2	28	29	44	2	20	12	74
Orthoclase	4	4	4	2	-	-	4	2
Anatase	-	3	1	1	2	-	-	-
Anhydrite	-	-	-	1	-	-	-	-
Haematite	-	-	2	-	-	-	-	-
amorphous content	**-**	**-**	**-**	19	-	-	-	-
***Phyllosilicates**								
Kaolinite	78	40	23	12	87	68	5	6
Muscovite	16	10	19	21	6	9	4	18
Smectite	-	5	3	-	-	-	-	-
Montmorillonite	-	-	**-**	-	-	-	71	-
Chlorite	-	-	3	-	-	-	2	-
strata Chlorite/Smectite	-	5	3	-	-	-	-	-
strata Illite/Smectite	-	5	10	-	-	-	-	-

MetaMax® from BASF was used as reference material, since it is a high-reactivity pure metakaolin product, which shows no contamination of other minerals. The chemical purity of the kaolinite was investigated by powder XRD and STA. As aqueous base a 50 wt. % sodium hydroxide solution and as water glass a sodium metasilicate with a molar proportion of SiO_2 to Na_2O of 3.4 was used.

4.2.2 Analytical methods

Powder X-ray diffraction (XRD) was carried out using a D8 Advance diffractometer (Bruker GmbH Karlsruhe, Germany) with a Lynxeye Detector (5° opening angle). Experiments were carried out with Cupper Kα radiation in a 2θ area between 5 and 70° in steps by 0.02° with a scanning time of 0.2

seconds. The quantitative analysis was carried out with the software PROFEX Version 4.1.0, by using an internal standard of 10 wt. % corundum.

Infrared spectroscopic measurements (IR) were carried out on a Bruker Tensor 27 FT-IR Spectrometer, with a modified ATR-IR Diamond set-up. During the measurements, attention was paid on constant pressure on the sample.

Simultaneous thermal analysis (STA): About 100 mg of the raw materials were heated up to 1000 °C with a heating rate of 10 K/min under nitrogen atmosphere in corundum crucible, using a STA 409 apparatus (Netzsch, Selb, Germany).

Scanning electron microscopy (SEM) images were obtained using a Philips XL 30 FEG environmental scanning electron microscope (ESEM; FEI Europe, Eindhoven, The Netherlands). For the measurements all samples were glued onto aluminium SEM-holders using conductive tape (Leit-C, Plano GmbH, Wetzlar, Germany). To improve the quality of the SEM images, the samples were sputtered with a thin conductive layer (5 nm Au/Pd 80/20) and were investigated using an acceleration voltage of 20 kV.

4.2.3 General preparation of the clay samples

Prior to the activation process, all clays were calcined in 1 kg charges, which were tempered to 700 °C for 3 h in a muffle oven under air. Afterwards, different components were added to the calcined clay to obtain mortar specimens (according to a slightly modified DIN EN 196-1:2005-05 approach). Firstly, the calcined clay was placed in the mixer with the aqueous base. After 30 seconds of stirring, sand was added over 30 seconds and subsequently water glass was added to the mixture while the mixture was stirred (140 rpm). Afterwards, the mortar was stirred for another 30 seconds under stirring (280 rpm) and the specimens were casted in steel moulds.

Before the IR measurements of the clay, the samples were grinded and sieved to obtain a particle size ≤ 32 µm. Furthermore, the clays and the material for the calibration were well dried under vacuum to remove any residual water. For the IR spectroscopic measurements of the common clays non-calcined samples were used. For the generation of the calibration curve (Figure 13a) a certain amount of pure kaolinite was added to the calcined kaolin.

4.2.4 Strength measurements

The compressive strength of the mortar specimens was determined according to DIN EN 196-1:2005-05 with a TESTING Blum & Feuerherdt GmbH servo hydraulic compression and bending test device of the type RT 200/10-1s. After casting, the specimens were stored at 20 °C with a relative humidity of 65 % for 7 days until the specimens were tested.

4.3 Results and discussion

In order to measure the clay activation index of the clay samples and evaluate the activator amount that is needed for the alkali activation of common clay deposit, it is important to know the amount of reactive

components within the clay. As mentioned before, this reactive amount is directly associated with the OH groups that are present in the clay. Therefore, IR spectroscopic measurements were utilised to gain information about the composition of the clay and the presence of hydroxyl groups.

4.3.1 Description of the experimental setup

The developed experimental IR setup is shown in (Figure 11). The setup consists of a modified diamond ATR-IR unit from "PIKE Technology". In order to obtain a constant pressure on the sample, a load cell was installed in axial position to the pressure stamp. With the aid of a fine thread, the contact pressure can be adjusted precisely. To guarantee a constant sample volume, a plate with a drilling was drafted on top of the IR diamond. This not only gives the possibility to use a certain sample volume, but also enables an efficient cleaning of the instrument after the measurement.

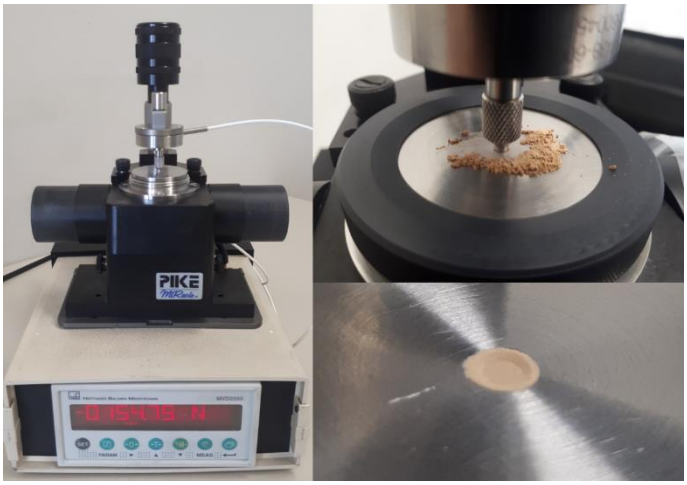

Figure 11: Picture of the experimental IR setup for the determination of the clay activation index of common clays.

In Figure 12 an example of an IR spectrum of a clay material using the before described setup is shown. The important region for the determination of the clay activation index is in the area of 3800 – 3500 cm^{-1}.

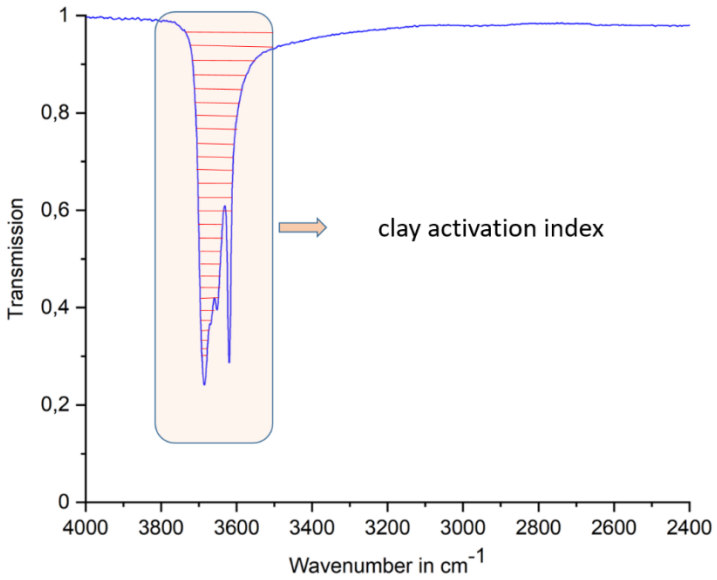

Figure 12: Example of an IR measurement of a clay using the before described experimental setup.

4.3.2 Calibration of the experimental setup

As starting point for this method, different mixtures of pure kaolinite with amorphous calcined kaolin, which was used as hydroxyl free support material, were prepared. The proportion of the mixtures were 0 to 100 wt. % of the kaolinite content with a stepwise increase of 5 wt. %. Kaolinite was the mineral of choice, since it represents the sheet silicate with the most hydroxyl groups and therefore a material that can easily be used for alkali activation.[78] The samples were dried under vacuum prior testing to ensure that no free water influences the measurement. The purity of the samples was previously determined by powder XRD and STA measurements. Also, the samples were analysed via SEM imaging, showing the sheet like structure of the clay minerals. The mixtures were then further examined by the before introduced ATR-IR setup. As expected, an increase of the surface area of the OH stretching band around 3800 – 3500 cm^{-1} was observed moving from mixtures with a small kaolinite content to a higher kaolinite content (Figure 13). To verify this observation quantitatively, the surface area under the OH stretching band was integrated and plotted against the kaolinite content, resulting in a linear correlation. Based on this, it can be assumed that the kaolinite content/the amount of OH groups correlate directly with the number of reactive centres present after the calcination process.

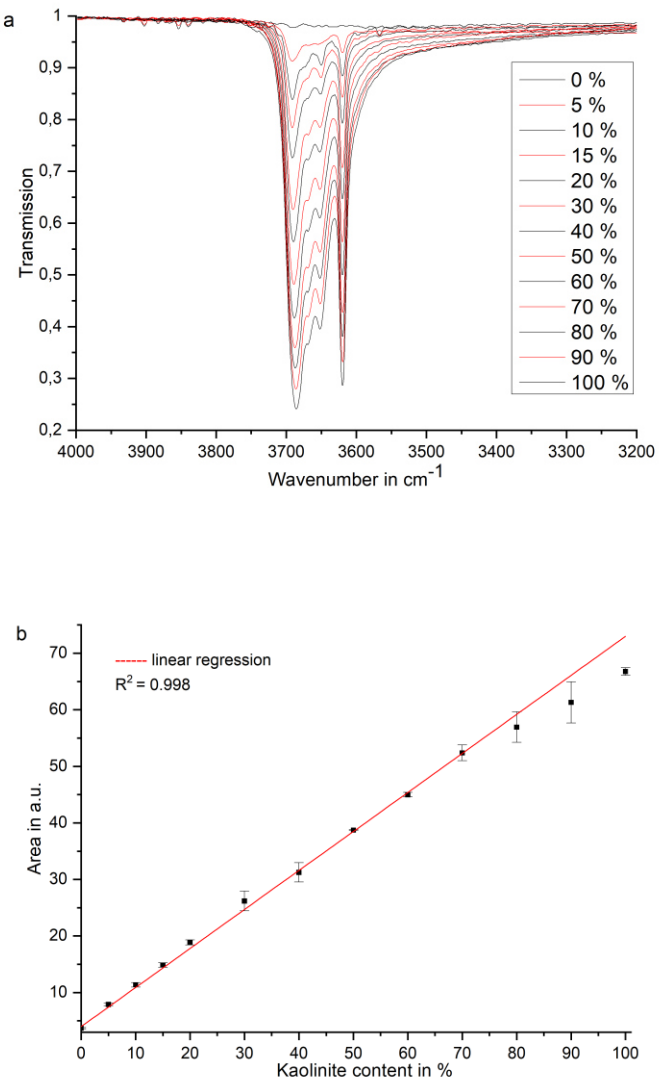

Figure 13: (a) Investigation of different kaolinite/kaolin mixtures by IR spectroscopy and (b) the relationship between the area under the OH stretching bands and the kaolinite content.

4.3.3 Clay activation index of common clays

After the calibration procedure, the clays were also analysed by ATR-IR spectroscopy using the developed setup. Figure 14 provides a clearer overview by displaying only four of the investigated clays. It is essential to note that all clays underwent vacuum drying before being utilised in this study.

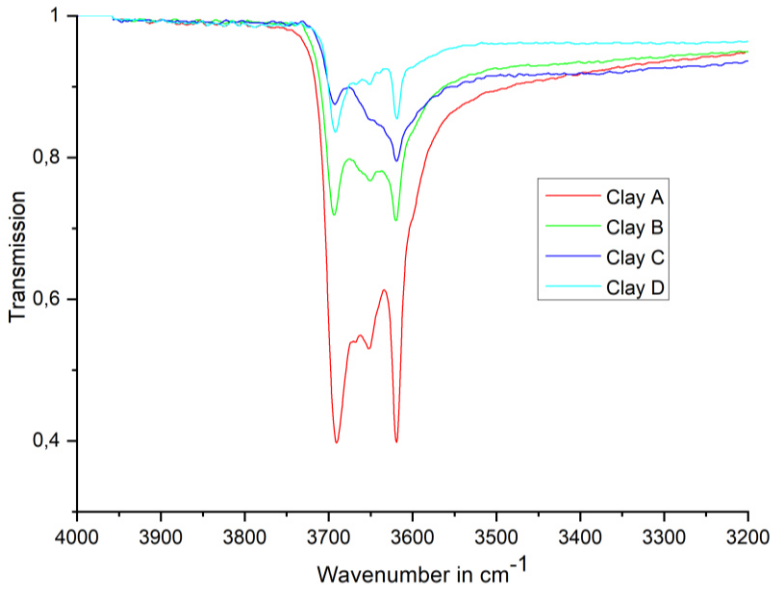

Figure 14: Investigation of four different clay deposits by ATR-IR spectroscopy.

The integrals of the OH IR stretching bands of the different clays were then related to the calibration curve obtained before (Figure 15). Since, the integral is related to the amount of OH groups present in the clay sample, which is crucial for the alkali activation process, it can be converted into the clay activation index based on the calibration shown before. The clay activation index varies from 0 to 100 % depending on the content of the active species within the clay that can be used for the alkali activation process.

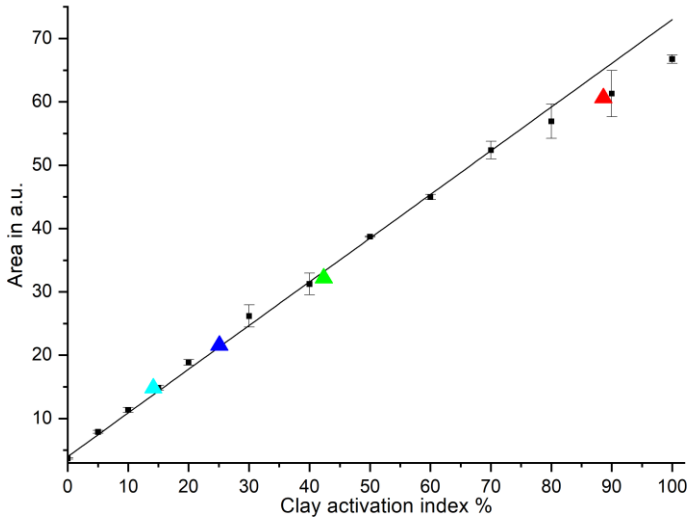

Figure 15: The relationship between the surface area under the OH stretching bands and the clay activation index of the common clays (A black; B red; C blue; D light blue) and the kaolinite/kaolin calibration curve (black).

4.3.4 Application of the clay activation index for the alkali activation of clays

The observations made during the ATR-IR spectroscopic measurements and the calculated clay activation indexes were now applied to the design of a suitable mixture of calcined clay, water glass and base during the alkali activation process to form a geopolymer binder mortar. Therefore, clays were calcined prior to the alkali activation process.

For the mixing design for the alkali activation procedure, it was assumed that a high hydroxyl content within a clay and thus a high clay activation index is related to large amounts of reactive centres. Therefore, a high clay activation index should also result in good mortar quality after the alkali activation. The stoichiometry of the different components was based on Davidovits' studies, in which 1 moles of metakaolin, 2 moles of water glass and in total 2 moles of base were used.[55] The previously defined clay activation index (Figure 15) can now be utilised to calculate the required activator dosage (Table 4). In this context water glass as well as the aqueous base were both considered as activators, since the addition of base without water glass to the calcined clay only leads to the formation of a crystalline material (zeolite).[79] In case of a lower clay activation index, the clay demands a smaller amount of activator solution, because the amount of reactive centres responsible for forming geopolymer precursors is lower. The reference mixture with a pure metakaolin (MetaMax®) consumes the highest amount of activators during the chemical reaction.

Table 4: Alkali activation mixtures based on the IR spectroscopic determination of the clay activation index. All mixtures consisted of 450 g calcined clay, 1350 g CEN-sand and the calculated activator amount.

Calcined clay sample	Clay activation index in %	NaOH in mol	Na_2SiO_3 in mol
Clay A	88.6	1.77	1.77
Clay B	42.4	0.85	0.85
Clay C	25.1	0.5	0.5
Clay D	14.2	0.28	0.28
Clay E	95.3	1.9	1.9
Clay F	64.4	1.29	1.29
Clay G	20.2	0.4	0.4
Clay H	4.3	0.09	0.09
Ref. pure metakaolin	100	2	2

For the examination of the geopolymer binder specimens, which were obtained by the alkali activation described before, the compressive and flexural tensile strength was measured (Figure 16).

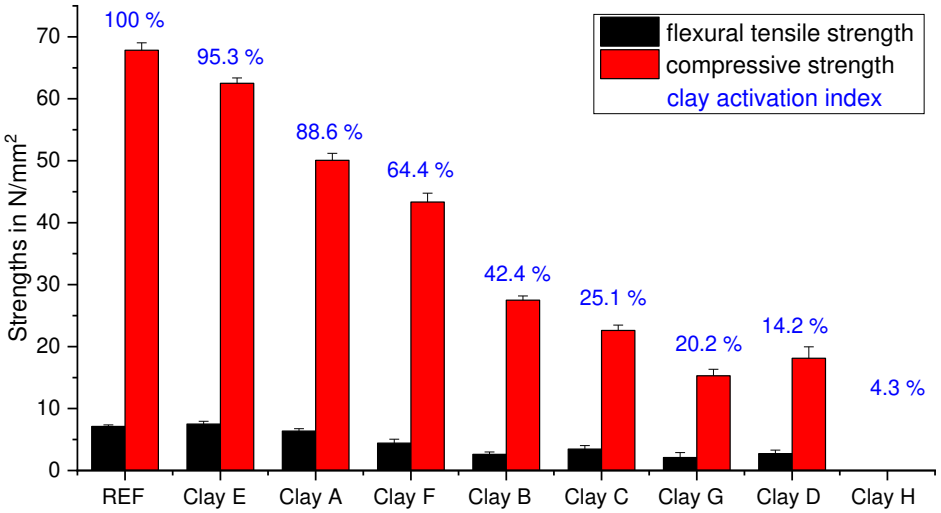

Figure 16: Compressive strength and flexural tensile strengths of the geopolymer mortars, sorted by decreasing clay activation index.

These investigations have shown, that almost all specimens hardened without any special treatment (heat, etc.), which was not observed when random mixtures of calcined clay, activators (water glass, base) and sand were used. This already shows the success of this IR spectroscopic method for the evaluation of the necessary activator content for the alkali activation. Only clay H did not harden and consequently no compressive and flexural tensile strength measurements could be carried out.

As expected, the reference material MetaMax®, with the highest clay activation index, has shown the highest compressive strength among all clay materials. The compressive strengths then decrease with decreasing clay activation index from clay E to clay G. Therefore, the clay activation index is not only a great tool to estimate the suitability of common clays for the alkali activation but it also gives clear information about the mixing design for the alkali activation procedure. Only in the case of clay D a slight inconsistency can be witnessed, since clay D shows a little higher compressive strength than clay G, despite the lower clay activation index. This points out, that not only chemical processes, like the alkali activation process, are responsible for the mortar performances but also physical effects, such as the grain size or the porosity, influence the material characteristics.

The obtained results were also verified via SEM imaging. Clays with a high activation index, and a therewith-associated high compressive strength, such as clay E, show a well-structured binder surface, whereas samples with a lower clay activation index, such as clay D, exhibit a more inhomogeneous microstructure that leads to a fragile connection between the particles.

4.4 Conclusions

The current study has shown a linear correlation between the surface area of the ATR-IR OH stretching band in kaolinite mixtures, and the kaolinite content using the developed ATR-IR setup. Based on this correlation and a subsequent calibration, the clay activation index, which gives insights into the amount

of reactive components after the calcination process, of various common clays was determined. This allowed the calculation of the activator (water glass and base) amount required during the alkali activation of the calcined clay based on Davidovits' proposed geopolymer formation. This completely novel approach simplifies the alkali activation of clay material enormously and provides a straightforward access to a variety of geopolymer binders without the need of preliminary empirical and often iterative testing of the necessary activator amount. Tests of the compressive as well as the flexural tensile strength have underlined the stability of the geopolymer binders after the activation process and therefore shown the success and the wide applicability of this method.

4.5 Acknowledgements

This work would not have been accomplished without the Faculty of Chemistry and Mineralogy of Leipzig University. We also like to thank the staff of the Competence Center for Material Moisture (CMM) from KIT for the support during this work, and the German Research Foundation (DFG) for funding (Projektnummer 325967999).

4.6 Supporting information

4.6.1 Powder X-ray diffractograms

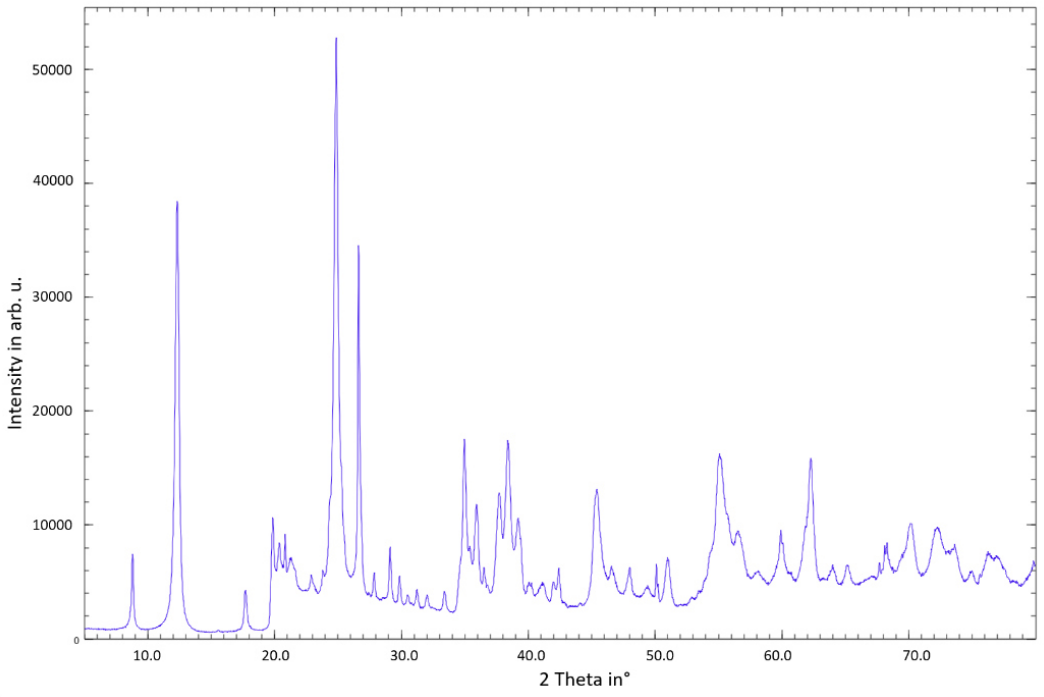

Figure 17: Powder X-ray diffractograms of clay A.

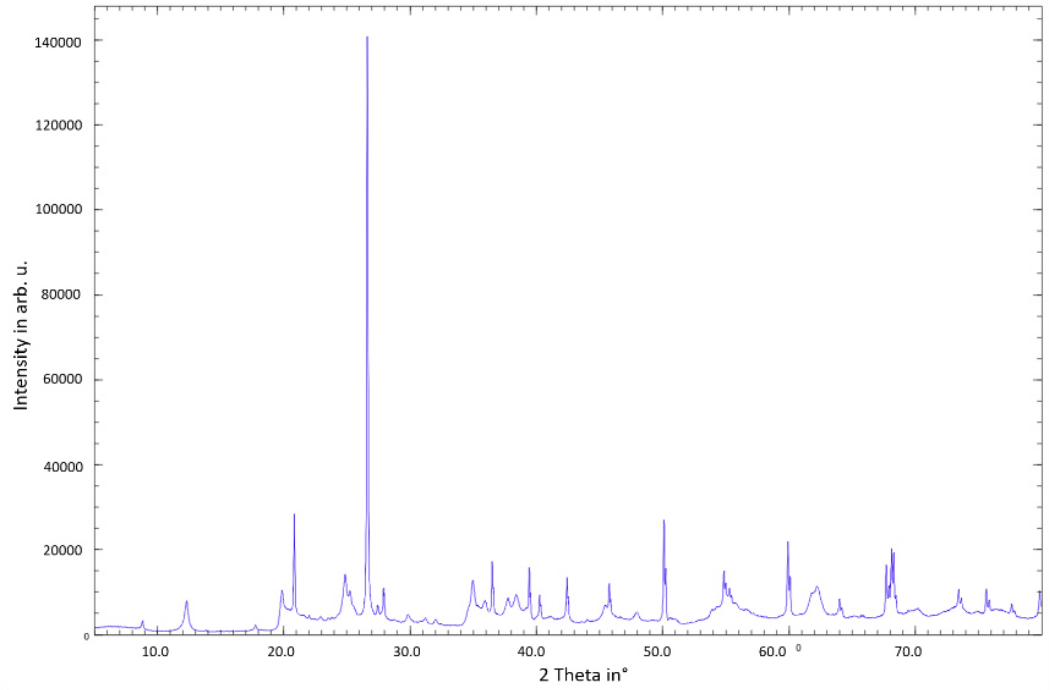

Figure 18: Powder X-ray diffractograms of clay B.

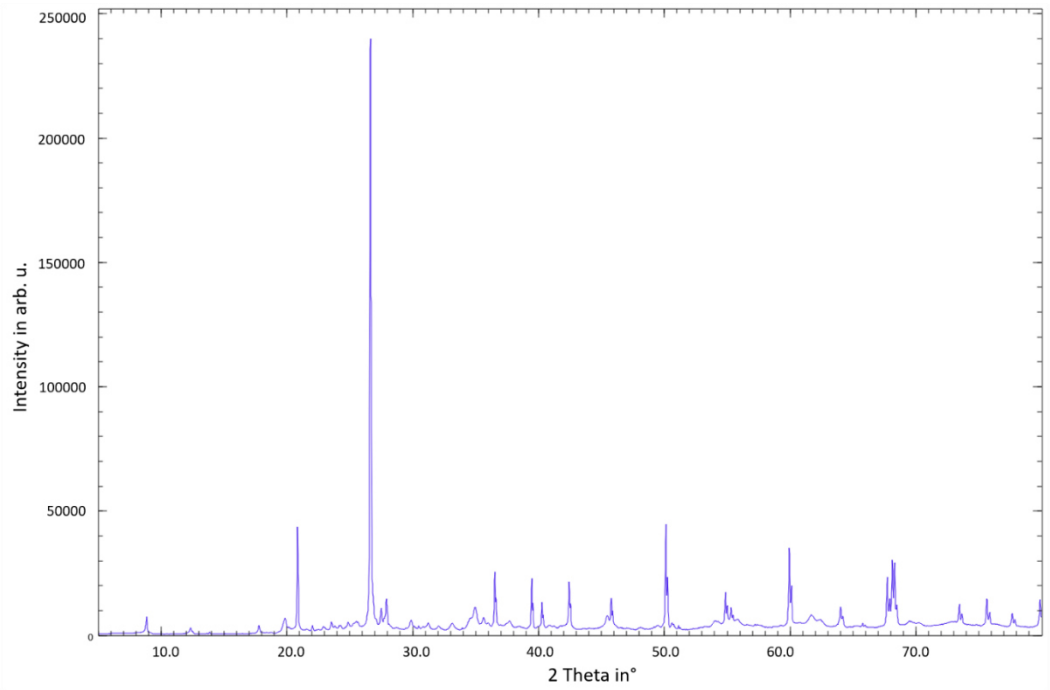

Figure 19: Powder X-ray diffractograms of clay C.

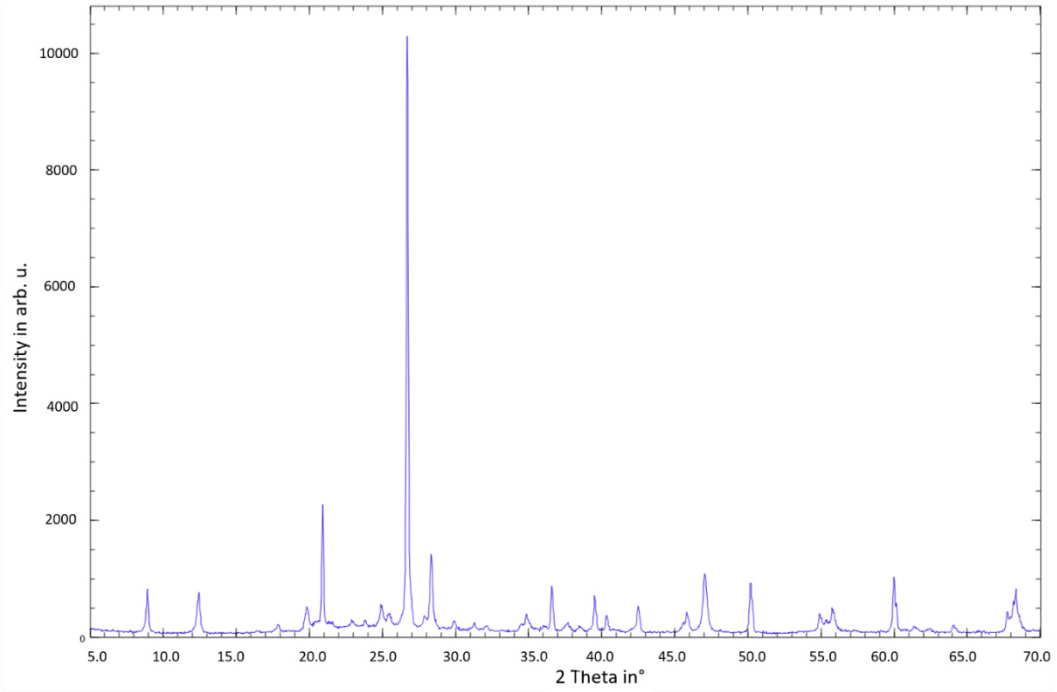

Figure 20: Powder X-ray diffractograms of clay D.

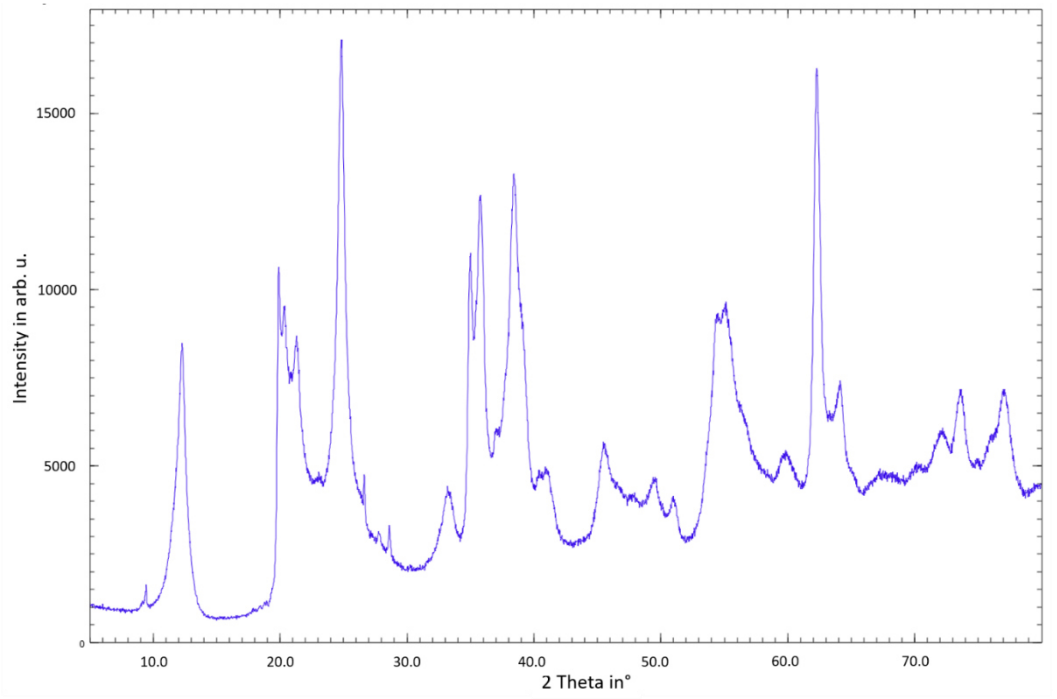

Figure 21: Powder X-ray diffractograms of clay E.

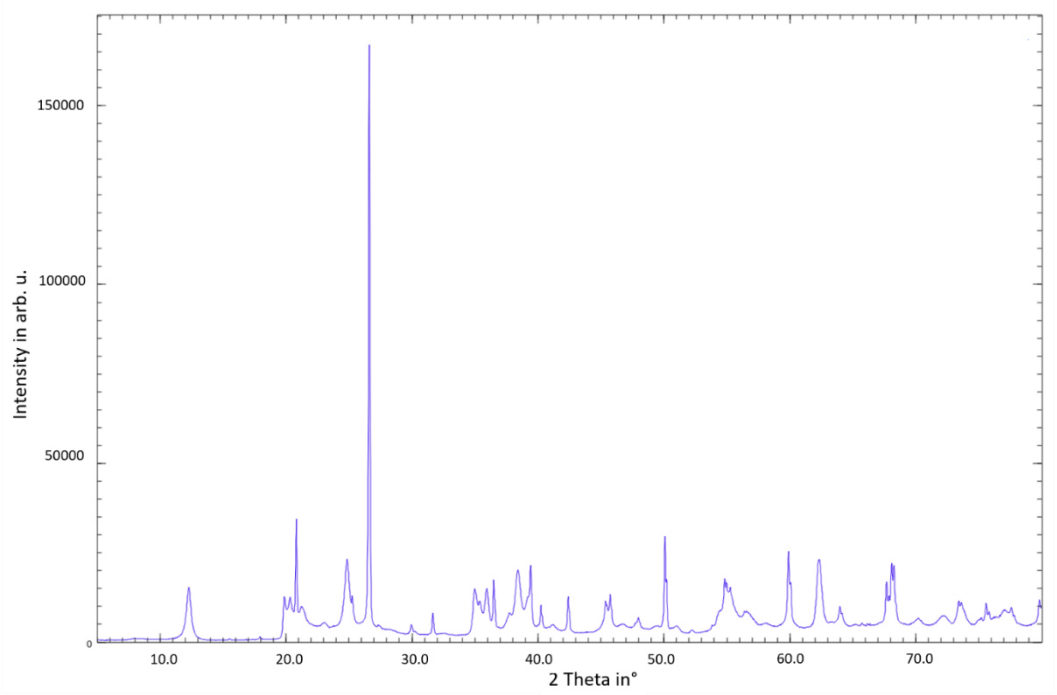

Figure 22: Powder X-ray diffractograms of clay F.

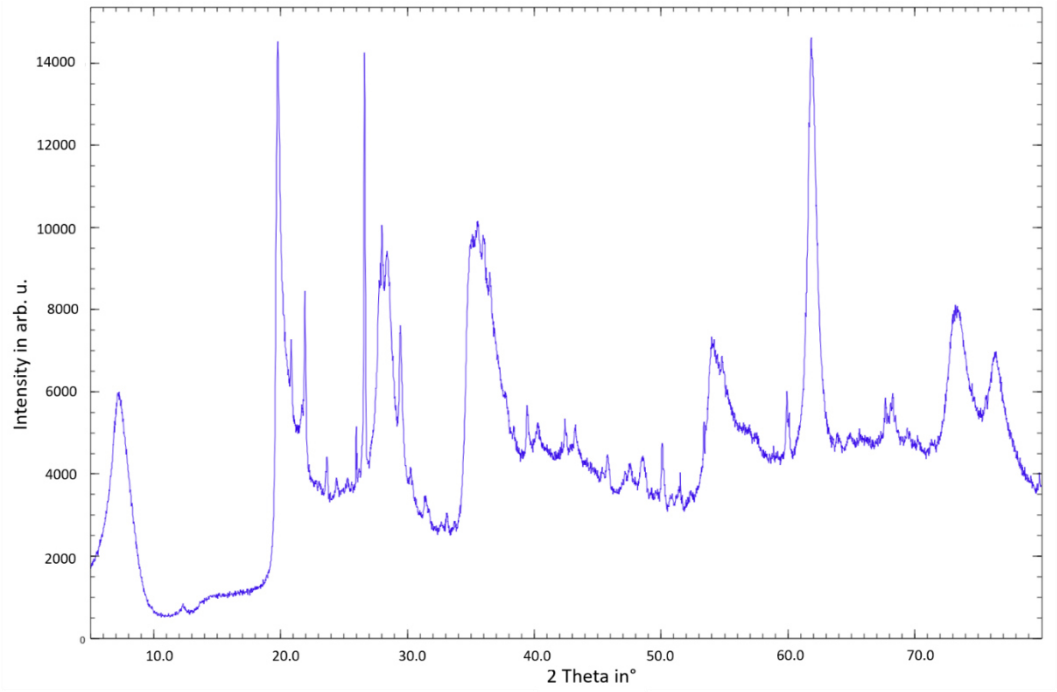

Figure 23: Powder X-ray diffractograms of clay G.

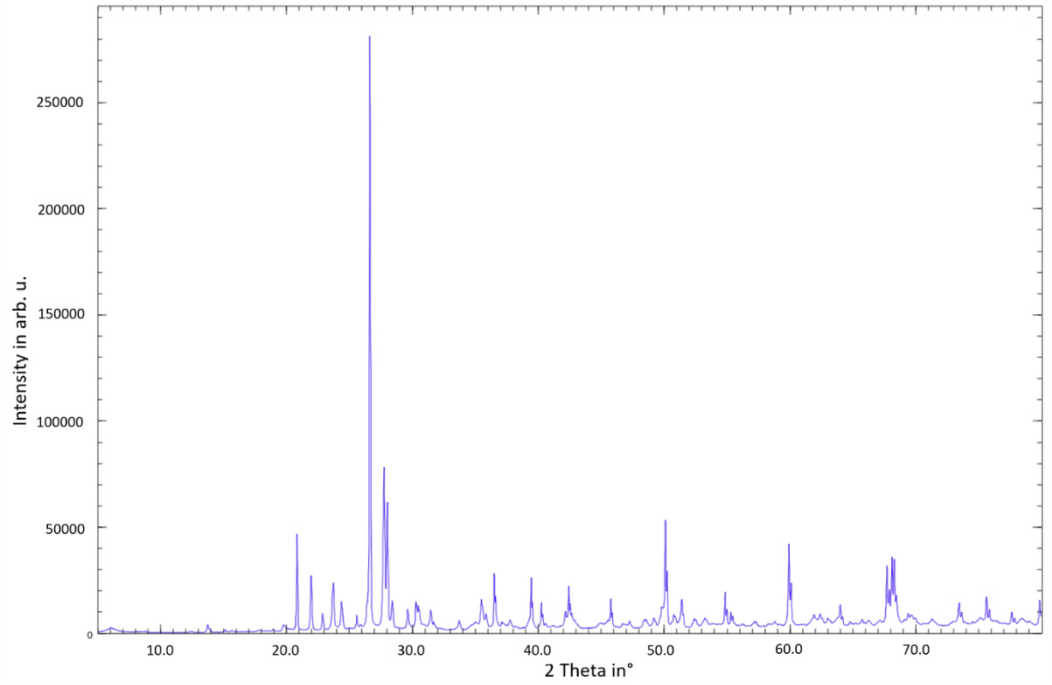

Figure 24: Powder X-ray diffractograms of clay H.

4.6.2 Selected SEM images

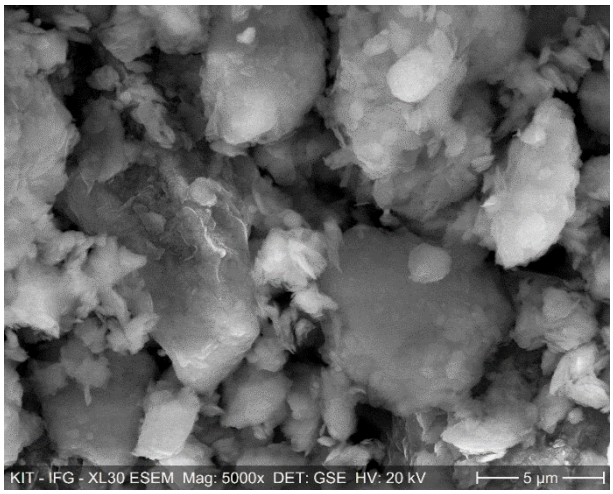

Figure 25: SEM image of clay D.

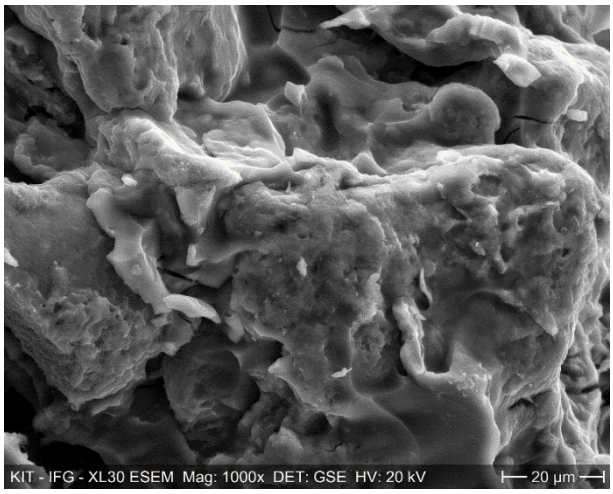

Figure 26: SEM image of mortar D after the alkali activation.

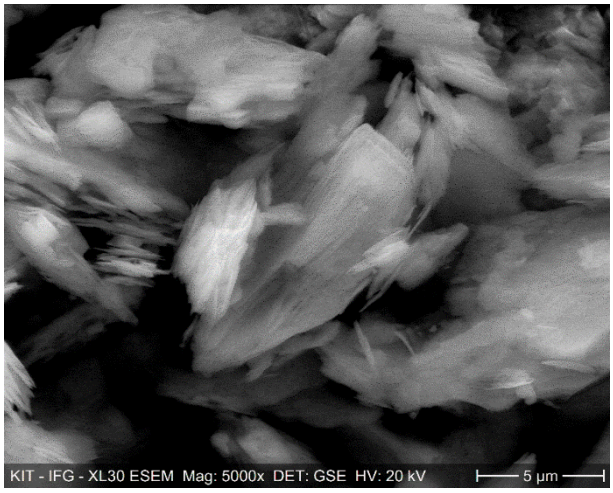

Figure 27: SEM image of clay E.

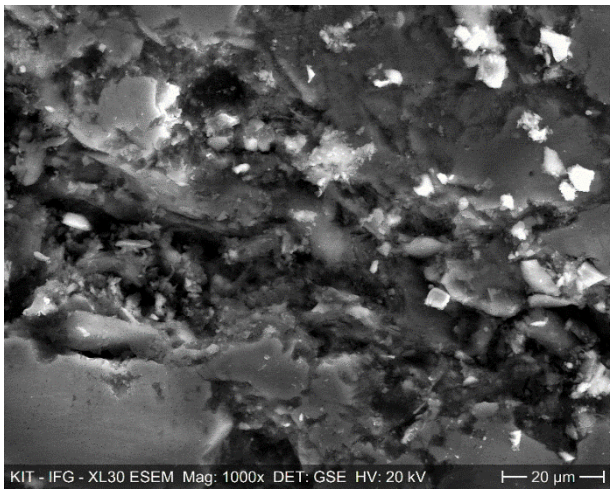

Figure 28: SEM image of mortar E after the alkali activation.

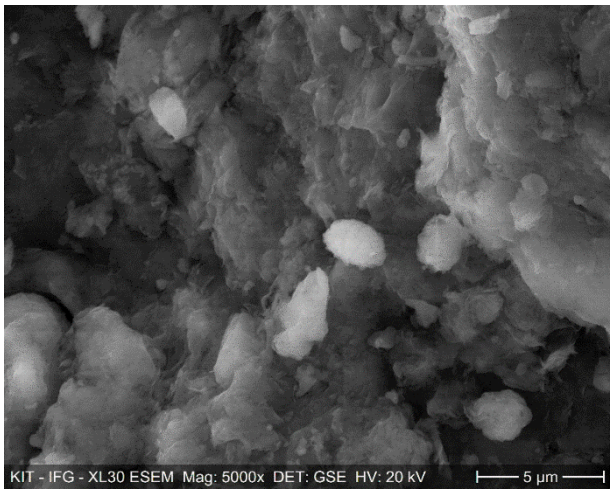

Figure 29: SEM image of clay H.

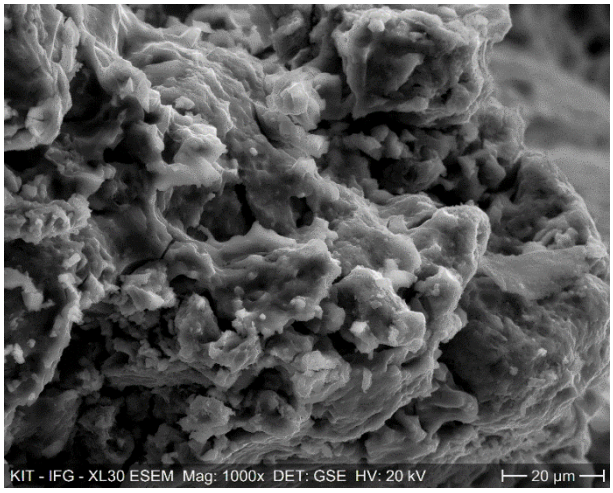

Figure 30: SEM image of mortar H after the alkali activation.

5. Influence of lime, calcium silicate and portlandite on alkali activation of calcined common clays

Reproduced from: F. Dathe, V. Strelnikova, N. Werling, K. Emmerich, F. Dehn, Influence of lime, calcium silicate and portlandite on alkali activation of calcined common clays, Open Ceramics, 2021, 7, 100152.

Abstract: The application of calcite rich common clays has marked impact on the formation of alkali-activated binders. Experiments have shown that the carbonate decomposition can be well controlled via the calcination procedure, whereby the majority of the decomposition and the subsequent CO_2 release occurs above the calcination temperature of 750 °C. The decarbonation of the calcite can mostly be separated from the dehydroxylation of the layered silicates. Depending on the composition of the raw clay material, the $CaCO_3$ decomposition leads either to the formation of lime or other Ca rich minerals. The mechanical properties of the alkali-activated binders were investigated and despite the very low amounts of layered silicates of the clay raw materials and the high content of unreactive minerals, compressive strengths of above 20 MPa of the mortars could be obtained. The presence of lime in calcined clays up to an adequate amount has a positive effect on post-solidification and the carbonation resistance of the mortars

5.1 Introduction

Recently, geopolymer (GP) and alkali-activated binders (AAB) have attracted a great deal of attention in research as alternative to conventional binding materials.[80] In contrast to the state-of-the-art construction material cement, the CO_2 footprint can be tremendously reduced through the application of such alternative binders in the field of civil engineering.

Both geopolymers and alkali-activated binders can be obtained from condensation reactions of Si and Al-rich precursors in the presence of a base. This process is also referred to as alkali activation. The transition from a geopolymer to an alkali-activated binder depends strongly on the soluble Ca content of the raw material, since this is crucial for the formation of different amorphous phases, such as N-A-S-H (low Ca content), C-A-S-H, C-(N)-A-S-H, and C–S–H(I) (very high Ca and low Al content).[40] The nature of these amorphous phases is very complex and key to ongoing studies.[39] In general, GPs are considered as Ca-poor AABs with a high Al and Si content and whereas products resulting from fly ash with more than 7 wt % of CaO (according ASTM C618, type F) or 10 wt % CaO (according to DIN EN 450–1), respectively, are classified as AAB, a lower calcium content is thought to result in the formation of a geopolymer. Further classification criteria are based on the Ca content within the crystallographic structure of the reaction products (< 20 wt % CaO → geopolymer)[81] or the performance of the concretes/mortars (< 10 wt % CaO → geopolymer).[6,71]

For the production of alkali-activated binders, usually industrial by- products, such as fly ash (FA) and ground-granulated blast-furnace slag (GGBS), have been used. The exploitation of these industrial by-

products for the production of construction materials has been emphasised recently, especially with respect to a circular economy.[82] However, the availability of fly ash and slag in the European area is limited. This is mainly due to the continuous decrease of coal production and mining in the context of the energy revolution and the use of sustainable energy resources. In addition, the amount of ground-granulated blast-furnace slag lag from iron production cannot cover the global demand for mineral binders.

For these reasons, common clays have been investigated as precursors for the production of alkali-activated binders and as substitute in conventional cementitious systems with the ultimate aim of decreasing the amount of required cement clinker.[83] The term common clays is referring to structural clay products, which are fine grained and typically exhibit plastic behaviour when exposed to water.[84] The main benefit of using common clays as precursors for alternative binders is the great availability since clay deposits are distributed widely around the globe. A further advantage of using clays for the GP production, are the moderate temperatures in the range of 700 °C–850 °C, which are required for the calcination. Consequently, only H_2O is released by the decomposing of the clay minerals and no CO_2 is formed as by product during the thermal treatment. The calcium-poor geopolymer binders, resulting from the alkali activation of these calcined clays, are very different from conventional cementitious systems in terms of their mineralogical properties and their microstructure. The very high thermal stability, the resistance towards acids[85–89] and the good mechanical performance[40,90,91] are particularly worth mentioning here.

Despite these advantages, the consumption of NaOH and the therewith-associated rapid decrease of pH of the binder during the condensation reaction is challenging since the basicity of binders is one of the most important material parameters in concrete technology. To protect the steel reinforcement of corrosion processes, a constant pH value above 11 is required to maintain the durability of the structure.

In ordinary Portland cements, the basicity results from the hydration product portlandite ($Ca(OH)_2$). The formation of $Ca(OH)_2$ in the micro- structure of the cement will automatically stabilise the pH value at a constant level above 13.[92,93] However, since during the hardening process of alkali-activated binders no portlandite is formed and the generation of sodium carbonates from sodium hydroxide through the presence of CO_2 in the air takes place,[94] the basicity of the binder is reduced.[95] The consumption of NaOH and the thereof resulting reduction in the pH value influences in the corrosion of steel reinforcement.[96–98]

As part of this study, calcite rich common clays were investigated as precursors for alkali-activated binders. Earlier studies focused almost exclusively on the utilisation of kaolin-rich deposits, which contain only very low amounts of calcium carbonate.[99] However, since carbonates, such as calcite and dolomite, are often geologically associated with layered silicates, the investigation of calcite rich common clays to produce AABs seems logical. Spurred by this, the author's attention in this area has turned towards the exploration of calcite rich common clays and their alkali activation. To investigate

the influence of calcite on the alkali activation, the calcination temperature has been varied and the formation of CaO and the impact on the AAB properties have been explored. In that sense, the mechanical properties, such as the compressive and tensile strengths, of specimens made of alkali-activated common clays, have been measured. The investigation on calcium carbonate bearing clays for alkali activation leads us to the grey area between the calcium-free geopolymers and calcium-rich alkali-activated binders and all because of the low solubility of the calcium carbonate and the high reactivity of lime.

In addition, the carbonation resistance has been looked at in detail, since through the formation of CaO from $CaCO_3$, an internal buffer is formed, which can react with the CO_2 from the air and consequently counteracts the-afore mentioned reduction in pH value.

5.2 Materials and methods

5.2.1 Raw materials

As part of this study two naturally occurring common clays were used, namely one clay from the Rhine Graben (Clay1) and one from a clay pit in central Germany (Clay2), both clays are secondary clay deposits. As a reference material (denoted as Refclay), a kaolin with a high purity of kaolinite from Hampshire UK mixed with 25 wt % $CaCO_3$ was utilised. For the reference materials pulverised $CaCO_3$ with a purity of >98.5 % and a grainsize d50 of 1 µm as well as pulverised $Ca(OH)_2$ with a purity > 96 % were selected (Carl Roth GmbH & Co.KG, Karlsruhe, Germany). All materials were milled and sieved to a grainsize below 90 µm and the particle sizes were determined by a particle size Analyser CILAS 1064 (LG), (3p instruments, Odelzhausen, Germany). The mineral composition of the two common clays was determined via powder X-ray diffraction (XRD) and X-ray fluorescence (XRF) analyses (Table 5 and

Table 6)

As activators, a saturated NaOH solution with a concentration of 19.05 mol/L (50 wt %) and sodium silica solution Betol39T were blended. The applied water glass is based on a solution of sodium silicate with a solute concentration of 34.5 wt % and a molar ratio of SiO_2 and Na_2O of 3.4 (Woellner, Ludwigshafen, Germany).

Table 5: Proportions (wt. %) of the mineral phases within the common clays and the references clay obtained from powder XRD analysis and particle size from laser granulometric measurements.

	Clay1 Rhine Graben	**Clay2 Central Germany**	**Kaolin Hampshire UK**
Calcite	25.4 ± 0.5	27.5 ± 0.5	0
Dolomite	4.9 ± 0.5	0	0
Quartz	21.3 ± 0.5	26.5 ± 0.5	3.2 ± 0.5
K-feldspar	2.5 ± 0.8	0	0
Plagioclase	5.3 ± 0.4	3.8 ± 0.8	0
Kaolinite	8.7 ± 1	14.5 ± 1	94.5 ± 1
Muscovite/Illite	16.6 ± 1	15.0 ± 0.5	2.2 ± 0.5
Smectite	6.7 ± 0.4	10.0	0
Microcline	1.7 ± 0.5	0	0
Chlorite	4.8 ± 0.6	2.5 ± 0.5	0
Hematite	0	1.8 ± 0.5	0
Particle size			
d(0,5) % < [μm]	8.5	27.8	9.4

Table 6: Elemental compositions of the raw materials in wt. % determined by XRF analysis. LOI = loss of ignition.

Constituents	**SiO_2**	**Al_2O_3**	**CaO**	**Fe_2O_3**	**MgO**	**Na_2O**	**K_2O**	**LOI**
Clay1	44.5	11.5	14.4	4.7	3.1	0.7	2.1	18.0
Clay2	45.3	17.5	15.7	8.1	0.2	1.5	0.8	12.5
Kaolin	44.3	42.9	0.1	0.7	0.1	0.3	0.1	10.5

5.2.2 Analytic techniques

5.2.2.1 Powder X-ray diffraction (XRD)

For the powder X-ray diffraction analysis a D8 Advance diffractometer (Bruker GmbH Karlsruhe, Germany) with a Lynxeye Detector (5 opening angle) was used. Experiments were carried out with Copper Kα radiation in a 2θ area between 5 and 70 in steps by 0.02 with a scanning time of 0.2 s. The quantitative analysis was carried out with the software PROFEX Version 4.1.0, by using an internal standard of 10 wt % corundum.

5.2.2.2 X-ray fluorescence (XRF)

The elementary composition was determined using a S4 Explorer for the raw clay and the surface of the AAB specimens investigated by a M4 Tornado (Bruker GmbH Karlsruhe, Germany) using energy dispersive X-ray fluorescence (XRF) spectrometer.

5.2.2.3 Simultaneous thermal analysis (STA)

About 100 mg of the raw materials were heated up to 1000 °C with a heating rate of 10 K/min under nitrogen atmosphere in corundum crucible, using a STA 409 apparatus (Netzsch, Selb, Germany).

5.2.2.4 Simultaneous thermal analysis (STA) coupled mass spectrometry (MS)

About 100 mg of the raw materials were heated up to 1000 °C with a heating rate of 10 K/min under nitrogen (50 mL/min)/synthetic air (25 mL/min) atmosphere (Jupiter 449, Netzsch, Selb, Germany). The coupled mass spectrometer was a Quadrupol 409 (Aeolos, Netzsch, Selb, Deutschland).

5.2.2.5 Calcination

100 g of each clay were calcined at different temperatures in a laboratory muffle furnace (Heraeus Instruments, Hanau, Germany). Based on the STA results, one of the following temperatures 650, 700, 750, 800 and 850 °C was selected. These temperatures are based on the decomposition of the carbonate species and crystallisation of lime or calcium silicates in the clays. The clays were analysed quantitatively and qualitatively via powder XRD after the thermal treatment. After the calcination, the clays were milled with a vibrating mill to destroy the small aggregates that were formed.

5.2.2.6 Determination of the lime content

The soluble calcium content was determined by the following procedure developed by Franke.[100] Therefore, 50 g of the calcined clay samples were taken and completely sieved to 0.063 µm. Weighted with the accuracy of 0.001 g, 1.0 g of the sieved sample was mixed with 12 mL of ethyl acetoacetate and 80 ml of 2-butanole. The mixture was heated under reflux for 3 h and subsequently filtered. The precipitate was washed with 2-propanole and the washing liquid was combined with the mother liquor. To this clear solution, the indicator (TYP) was added, and the solution was titrated with 0.1 M HCl until a colour change from colourless to yellow occurred. This titration was carried out twice.

5.2.2.7 Alkali activation

After the calcination, the clays were mixed with the alkali activator solution and sand. The resulting mortars were then cased based on DIN EN 196-1.[101] Hereby, two different sample sizes were cased 2x2x8 cm³ and 4x4x16 cm³. For a better workability, the powder grain content of the used CEN standard sand was removed by sieving < 125 µm. The mix ratio is shown in

***Table* 7**.

The development of the formulation started from the theoretical hypothesis given from Davidovits[43] for the optimal proportion for a geopolymer network. From the former research done on zeolite materials is known that the most stable ratio of silicon to aluminium is 3 to 1 because of the fourfold bonding of

Al as energetic unstable coordination sphere. Considering these aspects and calculating with pure metakaolin as precursor, a theoretical optimal proportion of precursor to sodium silicate and sodium hydroxide can be achieved estimating a complete reaction. On the other hand, the practical realisation is often difficult due to the different water demand of each calcined clay and the actually reactive amount of metaclay after the calcination process. Several different mixing designs were investigated always with the aim to minimise the activator amount with regard to environmental aspects. The chosen formulation was free of shrinkage cracks, showed good setting time and the specimens did not show efflorescence on the surface. However, a certain amount of activator had to be added to achieve an adequate workability for constructional applications which was determined via the slump test. The portlandite containing metakaolin mortar "$Ca(OH)_2$ Metakaolin Mortar" was cased with the same mix design from the calcined kaolin clay from the UK (Kaolin). There for 10 wt % of the metakaolin was replaced by portlandite $Ca(OH)_2$.

Table 7: Alkali activation procedure.

Mortar	Alumosilicate precursor calc. Clay (750 °C; 850 °C)	Activator solution Betol39T + NaOH (50 wt. %)	CEN standard sand 125 µm – 2 mm
Mix ratio	450 g	450 g Betol39T, 225g NaOH (162 g sodium silicate, 112,5 g NaOH, 400.5 g H_2O)	1350 g

5.2.2.8 Determination of the physical properties

Like in DIN EN 196-1[101] described, the fresh mortars were tested for their slump, density and solidification time based on DIN EN 196-3:2017-03.[102] All three clays show a comparable water demand, so that the water binder ratio of 1:1 led to a stiff fresh mortar with a resulting slump test around 15 - 20 cm. All samples were demoulded 24h after casting and stored wrapped in foil at 65 % relative humidity and 20 °C until further tests were carried out. The compressive and flexural strengths were measured 7 and 28 days after casting on a ToniPRAX testing station Model 2031 (Toni Technik, Germany).

5.2.2.9 pH value

The hardened mortars were ground and powdered. 5 g of this powder < 90 µm, were suspended in 50 mL distilled water and the pH value of this suspension was measured with a pH electrode.

5.2.2.10 Carbonation tests

Based on DIN EN 13295:2004,[103] a accelerated carbonation testing was performed on 4x4x16 cm^3 mortar pricks after 7 days of curing wrapped in foil at 65 % relative humidity (RH) and 20 °C. The

specimens were transferred to a carbonation cabinet, with an atmosphere of 2 % CO_2 atmosphere and 65 % RH. After a certain time of CO_2 exposure, the depths of carbonation were determined by cracking the specimens and spraying a 1 % phenolphthalein solution on the freshly broken surface. After 60 seconds, the carbonation depth was measured on four sides of the specimens and an average value was calculated. Hereby it became obvious, that the carbonation depth was not dependent on the determination time. Similar observations were already reported by Gluth *et al*.[80]

5.3 Results and discussion

5.3.1 Characterisation of raw materials

The two clays and the reference material were analysed by simultaneous thermal analysis (Figure 31). During the STA experiments, different phase transitions were observed. At around 100 °C the loss of water bound in the materials can be observed. All three clays showed a dehydroxylation of the clay minerals, especially the dehydroxylation of kaolinite, around 520 °C. However, differential scanning calorimetry (DSC) and the thermogravimetric analysis (TG) of this decomposition process are overlapping with the dehydroxylation of the minerals. The CO_2, formed by the decomposition of dolomite, could be detected starting at 700 °C by STA coupled to a mass spectrometer (see supporting information).[104] Further, mass losses starting at around 700 °C occurred, which result from the decomposition of the dolomite and calcite in the raw materials. At temperatures above 850 °C, all carbonates were decomposed. Afterwards no further mass losses could be observed by TG. However, for Clay1 and Clay2 the formation of a high temperature phase could be observed at 902 °C via differential scanning calorimetry (DSC) and for the reference clay the formation of spinel phase at high temperatures consisting of Si and Al could be witnessed at 994 °C.

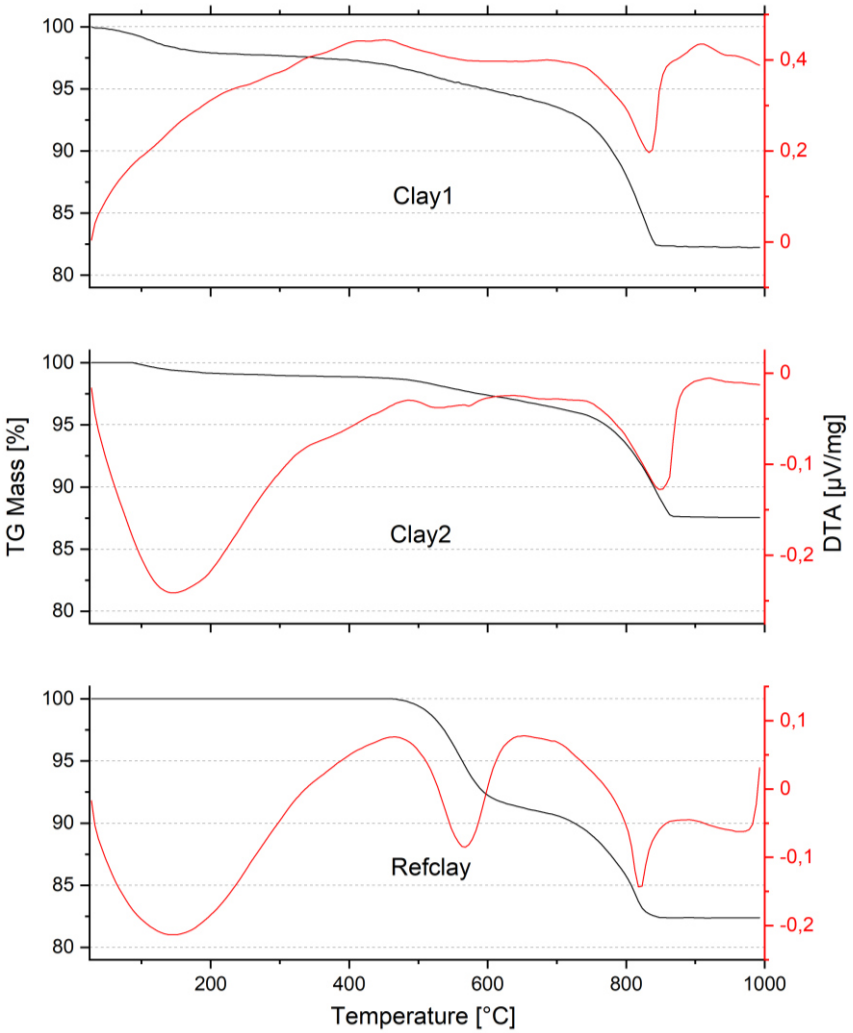

Figure 31*:* STA measurements of the three investigated clays heated from room temperature to 1000 °C; Sample weight 100 mg, atmosphere 75 mL/min N_2.

To gain further insight into the before described phase transitions, the clays were calcined at different temperatures (650, 700, 750, 800, 850, 950 °C) and the resulting materials were analysed via powder X-ray diffraction (Figure 32). Clay1 consists of a broad range of minerals and the calcination at 650 °C results in the disappearance of kaolinite and dolomite. Nevertheless, still a strong reflex, which can be attributed to calcite, can be observed. When Clay1 is calcined at higher temperatures, the intensity of the calcite reflex is decreased, however, only very little recrystallisation of calcite to lime does occur even at a calcination temperature of 850 °C. With Rietveld analysis only a lime content of 2 wt. % could be determined. The calcium oxide within the clay (14.4 wt. % in the raw material) forms most likely an insoluble amorphous phase during the thermal treatment, which is not detectable via powder X-ray diffraction. This is confirmed by the fact, that when Clay1 is calcined at temperatures above 902 °C, different calcium minerals, such as gehlenite ($Ca_2Al[AlSiO_7]$) and wollastonite ($CaSiO_3$) can be observed. The transition of the calcite to gehlenite and wollastonite via an amorphous transition state is favoured over the formation of crystalline lime. In addition, the variation of the calcination duration could not change the outcome of the powder diffraction experiments.

In the case of Clay2, the decomposition of calcite starting at 750 °C leads mainly to the formation of lime 10 wt. % (15.7 wt. % in the raw material). However, again not the whole amount of calcite is converted into lime. At 850 °C gehlenite and wollastonite can already be observed, which shows that not all the calcium is bound in the form of crystalline lime after the calcination. At higher temperatures above 950 °C the lime reacts further with the aluminosilicate to form more gehlenite.

For the reference clay, kaolinite is decomposing when the material is calcined at temperatures in the range of 650 to 750 °C. At a calcination temperature of 850 °C the complete decomposition of calcite to lime can be observed. When the Refclay is heated up further to 950 °C, the lime and the amorphous metakaolin forms gehlenite ($Ca_2Al[AlSiO_7]$). Also, small reflexes belonging to wollastonite ($CaSiO_3$) can be detected.

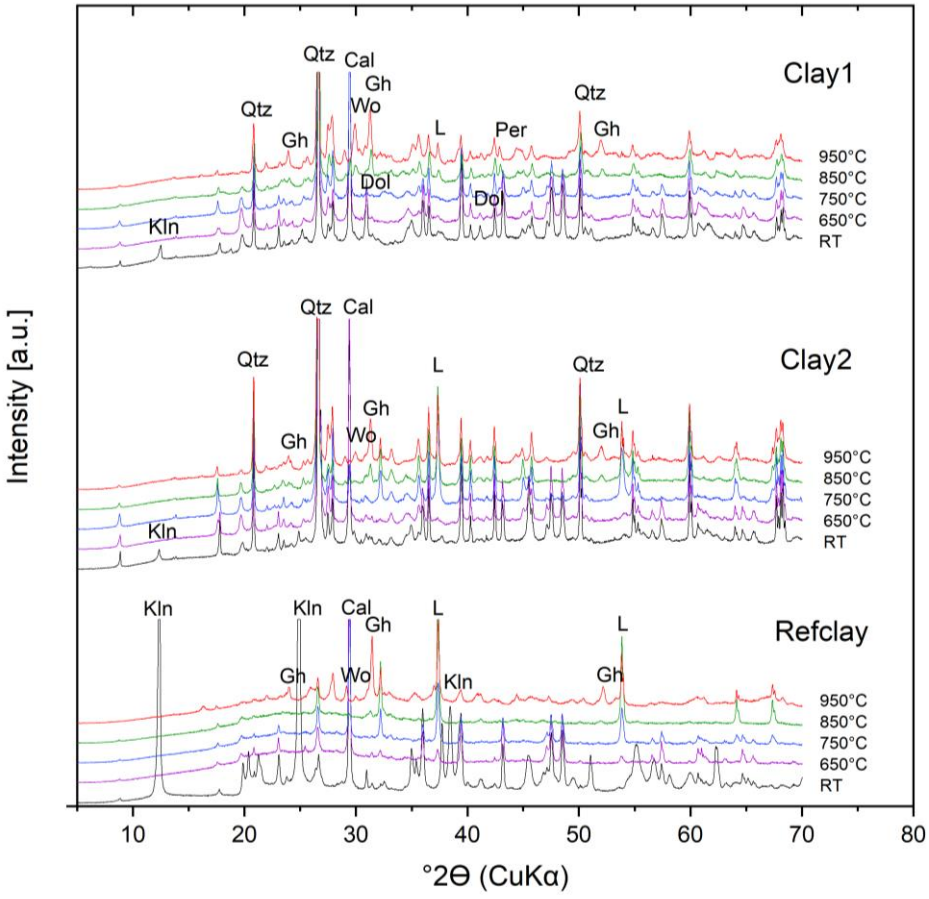

Qtz Quartz; Cal Calcite; L Lime; Kln Kaolinite; Gh Gehlenite; Wo Wollastonite; Dol Dolomite; Per Periclase

Figure 32: Powder X-ray diffractograms of the two clays and the reference material, which were calcined at different temperatures (RT, 650, 750, 850, 950 °C).

The information gathered by powder XRD is underlined by the measurement of soluble free calcium in the calcined clays according to the method described by Franke.[100] The results are depicted in Figure 33. It becomes obvious, that the soluble content of calcium follows different trends for the three clays. Whereas for Clay1 with 14.4 wt. % CaO in the raw material only 1.7 wt. % calcium oxide is soluble after the complete decarbonation of the calcite, in Clay2 9.3 wt. % out of 15.7 wt. % in the at 850 °C

calcined material are soluble. In the case of the reference clay, consisting of 14 wt. % CaO in the raw material, a soluble CaO content of 13.6 wt. % was determined.

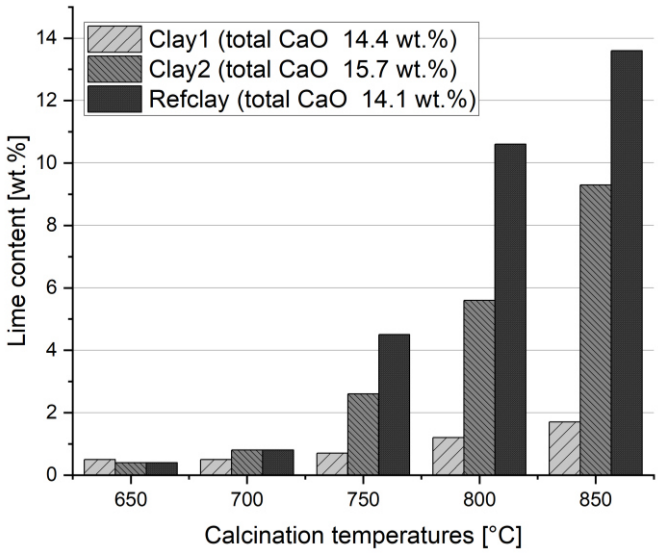

Figure 33: Calcium oxide content depending on the calcination temperatures. The soluble CaO content was determined according to Franke *et al.*[100]

5.3.2 Exploration of the mortars

Alkali activations of the calcined common clays and the reference kaolin were carried out to obtain mortars prisms. Hereby it has to be mentioned that CaO is quite reactive and reacts with water to form $Ca(OH)_2$ with an exothermic reaction enthalpy of 65.19 kJ/mol. This high exothermic head release may influence hardening process and leads to changes in the mechanical strength development. The compressive strengths of these specimens were analysed depending on the calcination temperature of the clays 28 days after casting (Figure 34). All three mortars show an enhancement of the compressive strength until a calcination temperature of 750 °C. Hereby a maximum compressive strength of 65.3 MPa could be obtained for Refclay, whereas compressive strengths of 28.6 MPa for Clay1 and 23.4 MPa for Clay2 were measured. The reason for the lower compressive strengths of the clays, in comparison with the reference clay, is the lower amount of reactive layer silicates, which can be calcined and converted into the strength giving N-A-S-H phases. Whereas the reference clay contains 94.5 wt. % kaolinite, Clay1 consists of 8.9 wt. % and Clay2 14.5 wt .% kaolinite. When the clays are calcined at temperatures above 750 °C a tremendous decrease of compressive strength can be witnessed.

Comparable calcite-free clays show usually a very similar increase of the compressive strength up to calcination temperatures of 750 °C. However, such calcite-free clays do not exhibit a significant loss in compressive strengths in temperature ranges between 750 °C and 900 °C. Only when calcination temperatures above 900 °C are applied, a decrease in compressive strength is observed for calcite-free clays, due to the formation of unreactive spinel's formed from the metaclay minerals.[105] The observed loss of compressive strength up to 50 % is therefore a direct consequence of the presence of high calcium contents, since Ca species influence the hardening process of the binder paste.

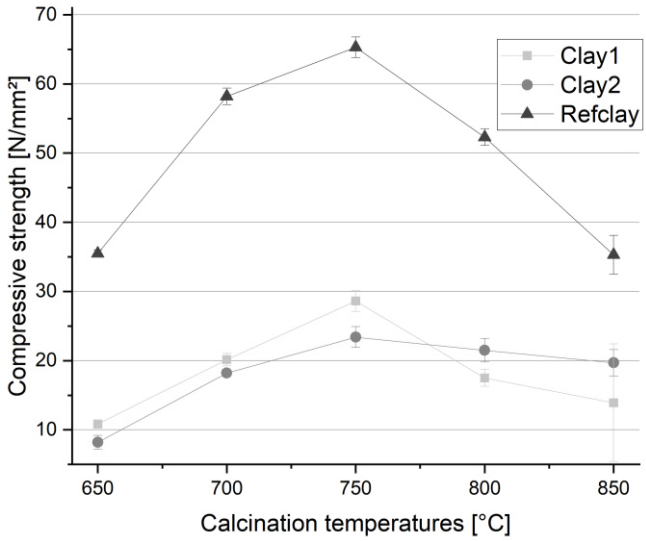

Figure 34: Compressive strengths of the two clays and the reference clays depending on the calcination temperature. Strengths were measured 28 days after casting.

Based on the results of the compressive strengths in dependence of the calcination temperature, only clays calcined at 750 °C and 850 °C were considered for further testing.

During the casting of the specimens, also the properties of the fresh mortar properties were explored. There was a major change in workability and the solidification time observed depending on the calcination temperature of the clays.

With constant activator/clay ratio for the alkali activation, the workability of the mortars is clearly increased for all three clays when the calcination temperature is enhanced. This is based on the fact, that the particle size is enhanced with increasing calcination temperature, as laser granulometric measurements have shown (Table 8). This leads to a reduced water consumption and consequently to a higher flow spread of the fresh mortars. As shown in Table 8, the slump test results of all three materials were significantly increased.

Table 8: Particle size, slump test and hardening time for 750 °C and 850 °C calcined clays

	Particle size d(0,5) % < [μm] 750 °C → 850 °C	**Slump test [cm] 750 °C → 850 °C**	**Solidification time [h] 750 °C → 850 °C**
Clay1	10.5 → 13.5	15.5 → 20	5 → 2
Clay2	30.5 → 35.4	17 → 21.5	6 → 1.5
Refclay	9.4 → 12.1	15.5 → 19.5	4.5 → 2.5

Especially for Clay1 calcined at 850 °C, an inhomogeneous solidification was observed, whereby the softer binder covers solidified areas. This inhomogeneous solidification also leads to a high standard deviation of the obtained compressive strengths (Figure 36).

To study the inhomogeneous solidification further, the mortars casted of Clay1 were analysed in more detail by powder X-ray diffraction and micro x-ray fluorescence. Thereby it could be shown, that two phases were formed with very different crystallographic and mechanical properties (Figure 35). In the hard areas crystalline sodium silicate hydrate (Na_2SiO_3 x H_2O) crystallised (Figure 36). This observation can most likely be attributed to the fact that the activator solution of Betol39T does not react with the amorphous clay minerals to form N-A-S-H or C-A-S-H phases, but directly crystallises and forms Na_2SiO_3. This leads to a local inhomogeneous distribution of aluminium and calcium as shown in Figure 35.

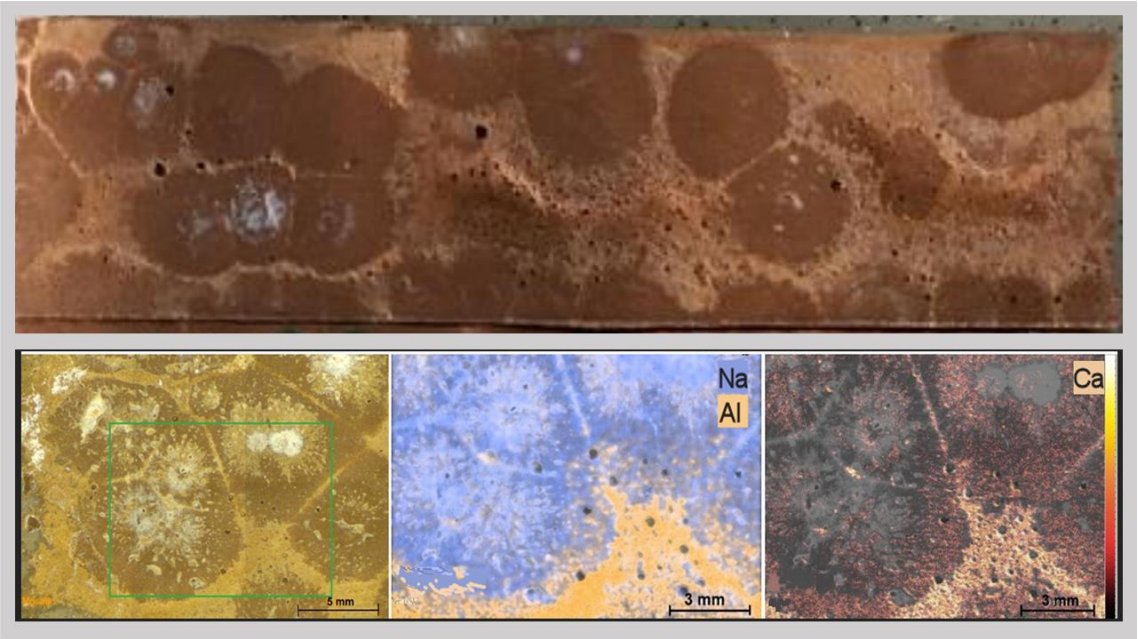

Figure 35: Top: surface of the mortar specimen of Clay1 calcined at 850 °C. Bottom: the inhomogeneous distribution of Al, Na and Ca determined by µXRF.

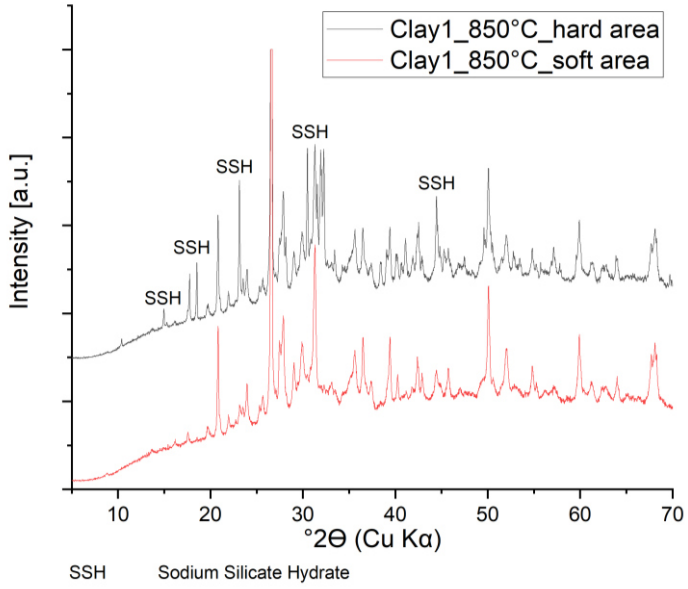

Figure 36: Powder X-ray diffractograms of the inhomogeneous solidification measured on two different parts of one specimen, soft and hard area. The formation of sodium silicate hydrate is shown.

The compressive strength development over the first 28 days (Figure 37) shows that there is a significant post solidification from 7 days to 28 days. Such a development is typical for cementitious systems or slag based AABs, since a reaction is occurring through which strengthening crystalline phases, such as calcium silicate hydrate (CSH) phases, are formed. Also in the case of the calcite containing clays, the post solidification could be due to the formation of CSH phases. This assumption is supported by the appearance of the typical reflex of CSH phases in the XRD of the reference clay after six days (Figure 39). In contrast, for alkali-activated calcite free clays, which form N-A-S-H phases, usually no major post solidification can be observed over time.

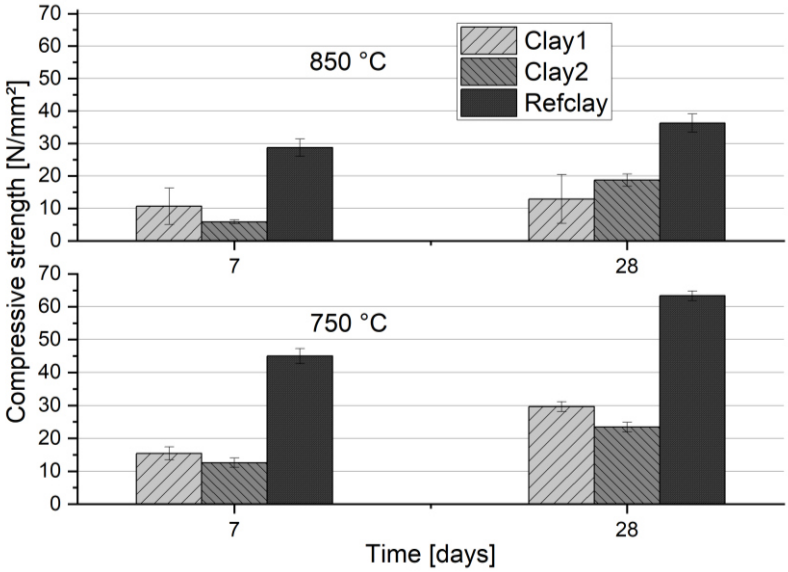

Figure 37: Post-solidification of the mortar specimens between 7 and 28 days after casting.

5.3.3 Lime consumption

The solidified binder paste was analysed by powder XRD 7 days after casting (Figure 36). These investigations show that the calcite stays untouched by the activation process. In addition, a lot of other minerals such as quartz, albite, hematite and muscovite show an inert behaviour. The binder paste of Clay2 calcined at 850 °C shows no Ca species in crystalline form, such as lime. This finding points towards the fact, that Ca is taking part in the alkali activation reaction and is consumed during this reaction.

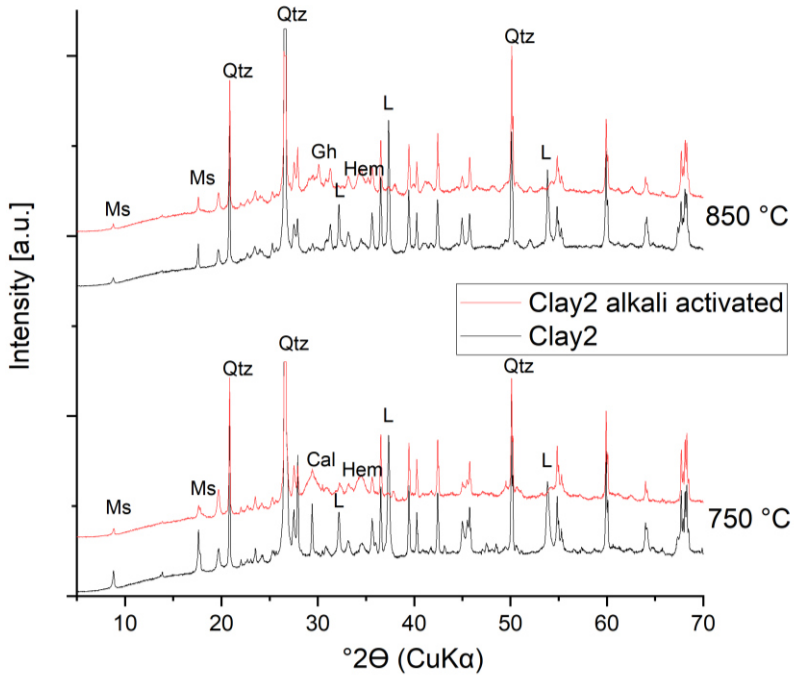

Qtz Quartz; Cal Calcite; L Lime; Gh Gehlenite; Ms Muscovite; Hem Hematite

Figure 38: Powder X-ray diffractograms of binder paste casted from calcined Clay2 at two different calcination temperatures.

A similar behaviour can also be observed for the alkali-activated reference clay (Figure 39). Again, CaO in the binder is consumed over the time and Ca species are implemented into amorphous networks. Further, the beginning formation of calcium silicate hydrate phases can be observed.

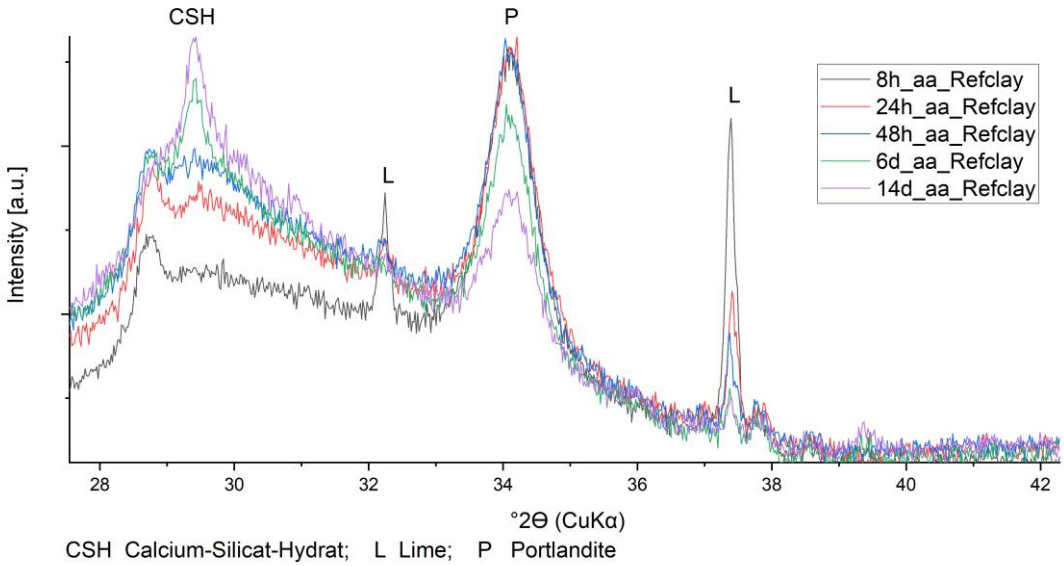

CSH Calcium-Silicat-Hydrat; L Lime; P Portlandite

Figure 39: Powder X-ray diffractograms of the reference clay mortar showing the CaO consumption over the time of 14 days.

5.3.4 Carbonation resistance

Since measurements of the pH values of the ground mortars have shown higher values than expected (Figure 40), the question arose whether the CaO within the mortar can protect the specimen from carbonation, similar to the role of $Ca(OH)_2$ in concrete systems.

As it is shown in Figure 40, the pH value inside the mortars is decreased over time. Starting from 14, due to the pure NaOH used for the activation, the pH value is reduced to 10.8 after 90 days for a calcium free metakaolin mortar. In contrast, the investigated calcite containing clays show a higher pH value after 90 days, which was found to be between 12 and 13. Based on these results, accelerated carbonation experiments were carried out (Figure 40).

For comparison, a reference mortar consisting of pure metakaolin without any calcium content was also investigated, named further as (MKref). It becomes obvious that the carbonation depths of the clays significantly differ from the Ca-free mortar. The carbonation depth was measured by spraying phenolphthalein on the fresh broken cross-section of the specimens. After 90 days the calcium free system shows a carbonation depth of 9.5 mm. In comparison, the three investigated clays show a carbonation depth between 4.8 and 7.2 mm. That underlines that the attack of CO_2 on the specimen is occurring much slower due to an enhanced OH^- content in the pore solution.

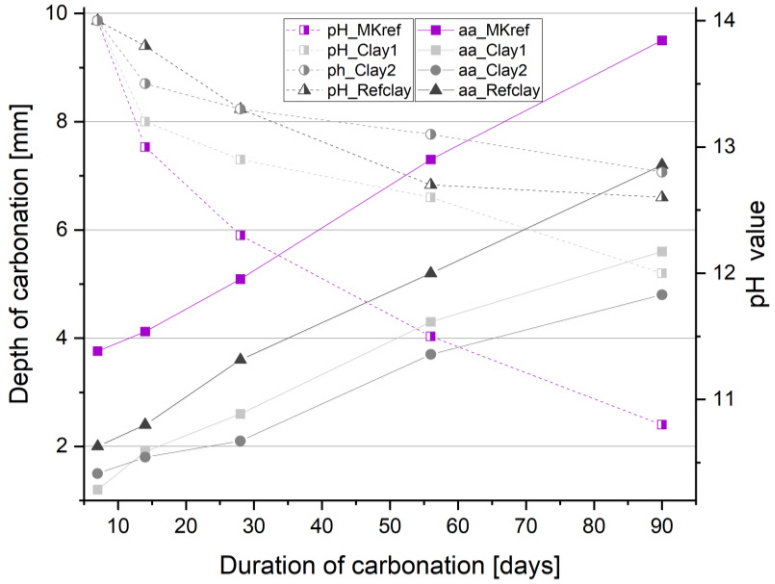

Figure 40: Accelerated carbonation test 2 % CO_2 atmosphere. The depths of carbonation of all three mortars made of the clays calcinated at 750 °C and the overall pH value of the hardened mortars are shown. A comparable Ca-free Metakaolin mortar (MKref) is used.

5.3.5 Replacement of calcite by portlandite

Based on the before described results, two CaO-free mortars were casted, since very high CaO contents were found to have a negative impact on the solidification time and the compressive strength. More precisely, a standard metakaolin mortar, referred to as “Metakaolin Mortar” and a metakaolin mortar mixed with $Ca(OH)_2$, denoted as “$Ca(OH)_2$ Metakaolin Mortar”, were utilised for the investigations. The intention was hereby to implement an alternative Ca-source beside CaO, which does not react that exothermically with water and is therefore thought to be a more unreactive Ca species in the context of this study.

The $Ca(OH)_2$ Metakaolin Mortar was casted replacing 10 wt. % of the metakaolin binder by $Ca(OH)_2$. The resulting specimens reached to a compressive strength of 61.3 MPa (Metakaolin Mortar) and 60.7

MPa ($Ca(OH)_2$ Metakaolin mortar). The fresh mortar properties were similar. The investigation of the mechanical properties have shown that the $Ca(OH)_2$ does not have a negative impact on solidification time and the mechanical properties, as seen before for the CaO containing clays. Also, the accelerated carbonation tests of the $Ca(OH)_2$ Metakaolin Mortar show a very high carbonation resistance. Again, as seen before for the calcite containing clays, the soluble Ca is consumed after the alkali activation and most likely imbedded in amorphous Al and Si containing phases. 24 hours after casting the XRD investigation show that the crystalline portlandite hast been completely dissolved.

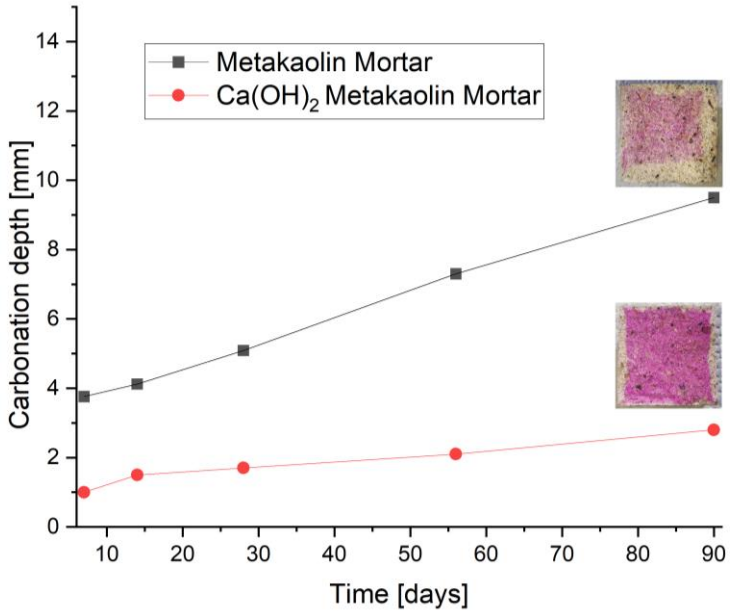

Figure 41. Carbonation depth of $Ca(OH)_2$ tuned Metakaolin mortar. The pictures in the graph show the freshly broken cross sections sprayed with phenolphthalein.

5.4 Conclusions

Calcium rich common clay deposits have gained more and more attention recently in the field of construction materials, due to the frequent occurrence of such clay deposits. In this context, also the utilisation of calcium rich common clays as precursors for the alkali activation and formation of alternative binders has been considered.

In this work, the authors investigated the influence of calcium compounds on the properties of the alkali-activated binders. In this context, it could be shown that, if calcium was present in the form of calcite, the two investigated common clays showed expected mechanical properties after calcination and alkali activation. However, if calcite decomposition occurs during the thermal treatment, the properties of the alkali-activated binders are altered tremendously. Although the calcination of Clay1 and Clay2 leads to calcite decomposition, different reaction products are observed. Whereas Clay1 forms an amorphous Ca rich transition phase, the thermal treatment of Clay2 leads to the formation of crystalline lime. The formation of lime has an enormous impact on the mechanical properties, such as the setting behaviour and the workability of the mortars. With very large lime amounts, undesired damage processes can be observed, such as the crystallisation of sodium silicate, which leads to an inhomogeneous solidification

of the binder. Ultimately, this makes the binder not suitable for any application as construction material. However, lime in adequate amounts leads to an increase in basicity and consequently an enhancement of carbonation resistance, which is beneficial for the application of such binders in steel reinforced components. Combined whit the high acid resistance that alkali-activated systems naturally show an application in agriculture buildings could be an interesting place of use.

As part of this work, the authors could show that the calcium carbonate decomposition can be well controlled via the calcination process. It became obvious that for pure calcium carbonate, the carbonate decomposition and the dehydroxylation of the layered silicates can be separated via the temperature. Only for MgCa carbonates, such as dolomite, the decarbonation and dehydroxylation takes place simultaneously within a similar temperature range. Based on this, the desired amount of lime can be adjusted via the calcination of the calcite rich common clays without any recrystallisation processes of the amorphous layered silicates. The consideration of the free lime content is not only important for the formation of alkali-activated binders but has also to be considered when common clays are applied as additives in conventional cementitious systems.

The mechanical properties of the alkali-activated binders were investigated and despite the very low amounts of layered silicates of the clay raw materials and the high content of unreactive minerals (60 wt. % quartz, illite) compressive strengths of above 20 MPa of the mortars could be obtained. We are convinced that after the addition of additives, such as super plasticisers and retarders, and the optimisation of the activator species, compressive strengths of 32.5 MPa similar to standard ordinary Portland cementitious systems are feasible. Such investigations are part of our ongoing studies.

The investigations have confirmed that even low amounts of free lime lead to an increase of basicity and have therefore a positive impact of the carbonation resistance of the mortars. Thereby, no negative effect on the mechanical properties was observed and even a post-solidification of 50 % from 7 to 28 days of the mortars were observed for the first time in the field of alkali-activated binders based on common clays.

In ongoing studies, the mechanism of the $CaCO_3$ decomposition in combination with different clay minerals should be clarified further, since it can react either to form lime, as expected, or to form Ca rich amorphous phases, which leads to an immobilisation of the calcium.

5.5 Supporting information

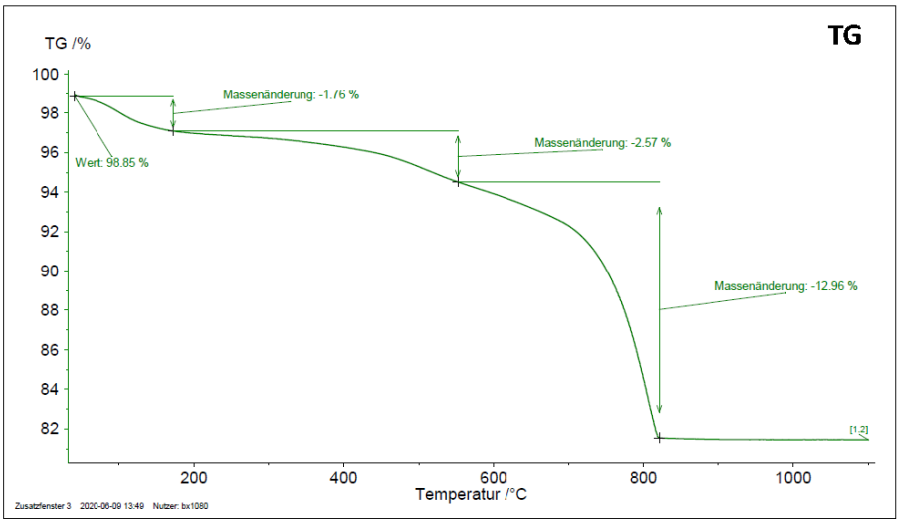

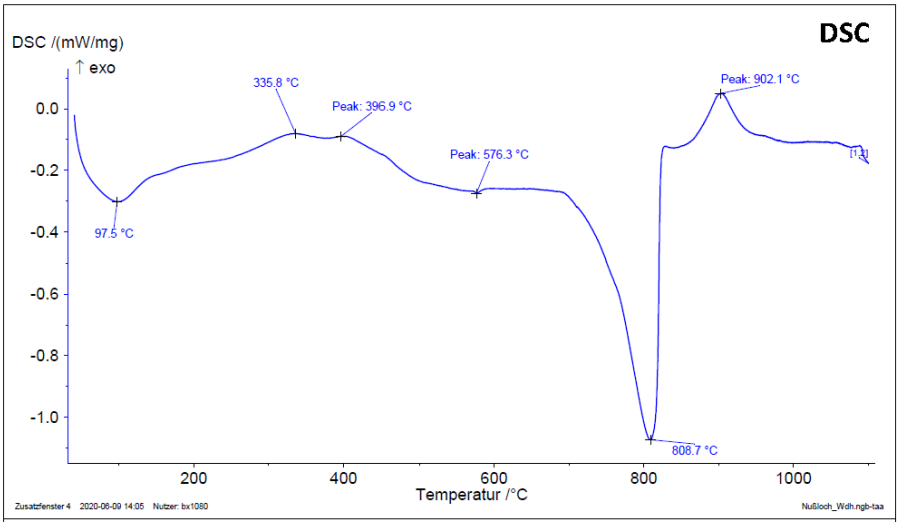

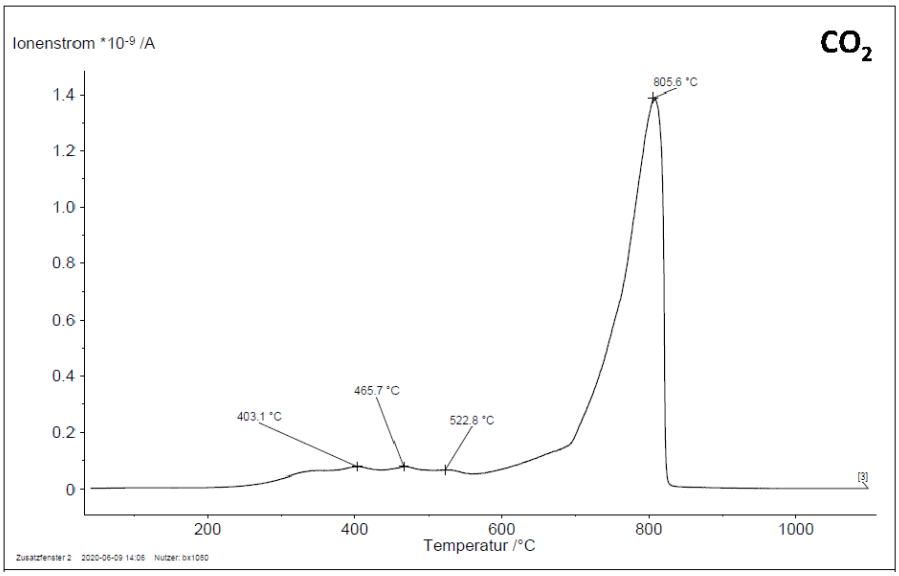

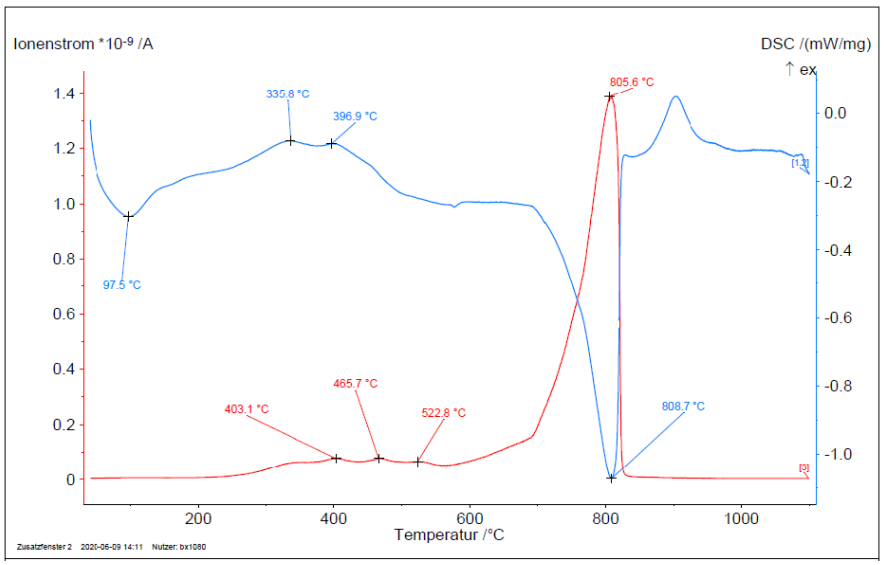

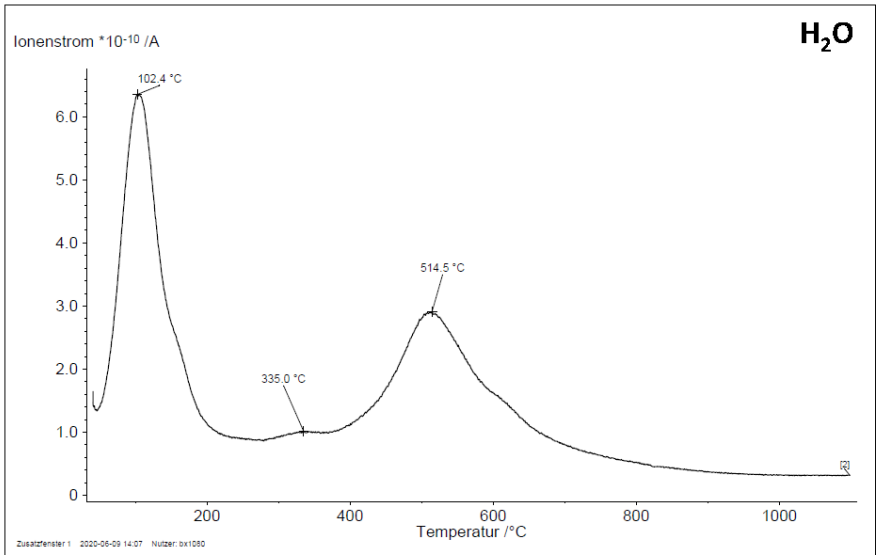

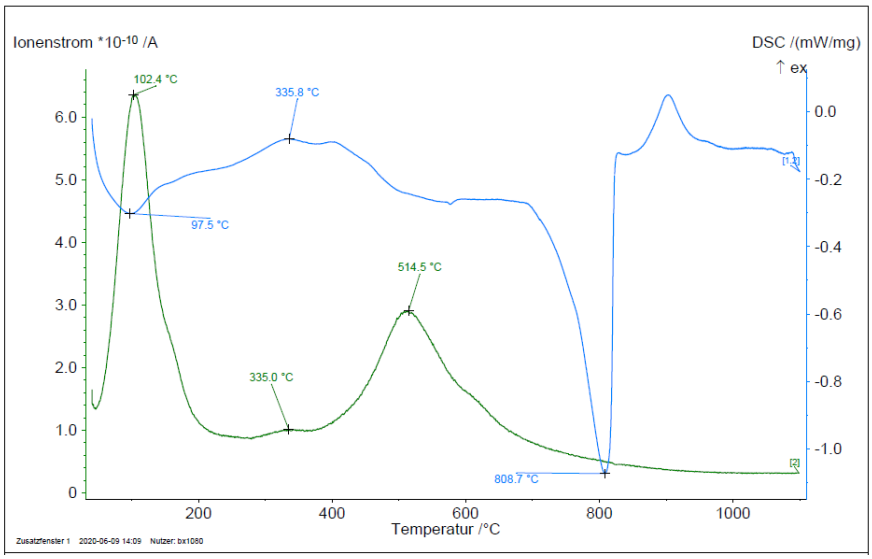

Figure 42: STA coupled mass spectroscopy.

6. The role of water content and binder to aggregate ratio on the performance of metakaolin-based geopolymer mortars

Reproduced from: F. Dathe, S. Overmann, A. Koenig, F. Dehn, The role of water content and binder to aggregate ratio on the performance of metakaolin-based geopolymer mortars, Minerals 2024, 14, 823.

Abstract: Geopolymers are in many applications a perfect alternative to standard cements, especially regarding a sustainable development of green building materials. This experimental study therefore deals with the investigation of different factors, such as the water content and the binder to aggregate ratio, and their influence on the workability of fresh mortar, the mechanical properties and various porosity parameters. Although increasing the water content improved the workability and flow behaviour of the fresh mortar, at the same time a reduction in compressive strength in particular and less in flexural strength could be demonstrated. This finding can be attributed to an increase in capillary porosity, as demonstrated by capillary water uptake and mercury intrusion porosimetry measurements. At the same time, the increasing water content led to an improved deaeration effect (low air void content) and to initial segregation (see µXCT measurements). An alternative approach to enhance the compressive and flexural strengths of the mortar specimens, is the optimisation of the binder to aggregate ratio from 1 to 0.25. This study paves the way for a comprehensive understanding of the underlying chemistry of the geopolymerization reaction and is crucial for the development of sustainable alternatives to cementitious systems.

6.1 Introduction

According to the International Energy Agency (IEA) and the United Nations Environment Program (UNEP), the construction area contributes to more than 40 % of the energy consumption worldwide and adds about a third to the greenhouse gas emissions.[3] In this context, the production of concrete represents a significant environmental burden, since about 5 to 7 % of the man-made CO_2 emissions come from the global concrete production.[4] For the production of every ton of Portland cement about 1.5 tons of raw materials are needed, while about one ton of CO_2 is released.[5] These numbers are rising every year due to an increased demand of construction materials. The immense amounts of raw materials needed, and the high level of CO_2 emissions make the cement production extremely resource and energy intensive.

In order to ensure a sustainable development of the construction sector, alternatives to conventional cementitious binders with a low carbon footprint have to be found. In this context, geopolymers have attracted more and more attention.[106] The term geopolymer was established by Davidovits in 1978 and refers to binder materials based on alkali-activated alumosilicates.[55,107] Geopolymers can be obtained from a polymerization reaction of an alumosilicate material in the presence of an alkaline solution, such as sodium hydroxide, sodium silicate, potassium hydroxide or potassium silicate, as activator (Figure 43).

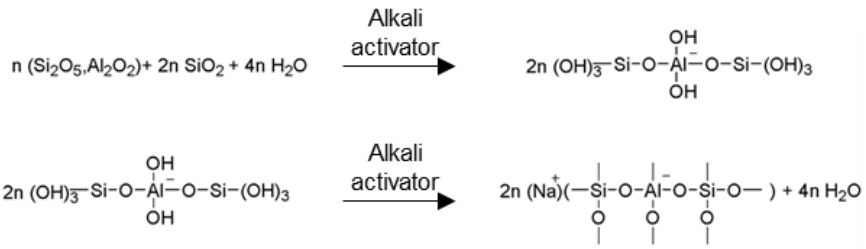

Figure 43: Geopolymerization reaction according to Davidovits.[55]

As starting material for the geopolymer production metakaolin, slag or alumosiliceous fly ashes are commonly used.[34,108] Metakaolin is a dehydroxylated form of the clay mineral kaolinite and its structure is based on an amorphous (non-crystalline) aluminosilicate network, which can be activated by a base to form a corresponding geopolymer. Recently, also common clays, as widely occurring and cheap resources, have been investigated as raw materials for the geopolymer production.[77,109–112] Such alternative binders based on sustainable resources are also being referred to as "Green Concrete".[113] In addition to improved sustainability, these mortars/concretes have improved resistance to chemical agents (acids, sulfates) or high temperatures due to their alumosilicate network.[87,114,115]

Despite the fact, that geopolymers are known for almost 50 years, the geopolymerization reaction is a very complex reaction, which depends on many experimental factors. Consequently, a targeted mixing design to afford defined geopolymers with predictable properties, such as the workability or the tensile and compressive strengths, is challenging. To overcome this, attempts to rationalise the experimental parameters for the mixing design of metakaolin-based geopolymers, such as the sodium silicate to sodium hydroxide ratio and the alkaline solids to metakaolin ratio, were for example reported by Al-Salloum *et al.* Hereby it was shown that the workability of the fresh mortars improved with an increased sodium silicate to NaOH ratio until a certain limit, while also the compressive strength was found to be increased.[116] In this context it was also shown that by using a higher NaOH concentration during the activation, the polymerization degree within the mortar specimens can be increased [117]. The compressive strength of geopolymers was also reported to be improved through the addition of waste, such as pent abrasive powder, which was mainly composed of corundum grains.[118] Down this road, also the addition of dyes, such as bromothymol blue, cresol red, phenolphthalein, and methyl orange, to the geopolymer mixture has been described with the aim to provide colored geopolymers, which are suitable for design and restoration applications. Hereby it was found that the fresh mortars exhibit a good workability, while there is no significant change in the microstructural 3D network of the geopolymer mortars observed.[119] Apart from these factors, also the water content of the mixture and the therewith associated solid to liquid ratio is crucial, since it not only influences the fresh mortar properties, but also the mechanical properties of the final mortar specimens.[111] Water is not only the reaction medium, in which the dissolution of the raw materials and the ions takes place, but also an integral part for the polymerization reaction itself, since it takes part in the hydrolysis and polycondensation of Al- and Si-containing oligomers.[118] In addition, water has a major influence on the workability of the fresh mortar. As the thickness of the water film on the particles increases, the

internal friction is reduced, which results in increased flowability of the fresh mortar. Beside the positive effect of water in the context of the geopolymer formation, it has been reported, that the addition of water and the therewith associated reduction in alkalinity of the reaction system[119] can lead to a migration of ions away from the reaction zone. Also, an excess of water might influence the chemical equilibrium of the geopolymerization reaction according to the principle of Le Chatelier and pushes the equilibrium to the side of the starting materials, which leads to a reduction of the polymerization rate.[120] This is complicated by the fact that the water is chemically bound to a lesser extent in the geopolymerization process compared to common cement hydration. This leads to the assumption that the porosity in the hardened geopolymer mortar/concrete is more clearly influenced by the water content. Therefore, the addition of water is a balancing act for a successful preparation of geopolymers via alkali solutions.

Although the role of water was investigated in some papers,[43,113,118,121,122] no comprehensive studies using advanced analytic techniques, such as micro X-ray computer tomography, were carried out. In this paper we therefore studied the alkali activation of metakaolin with the aim is to find a suitable water content and consequently an optimal formulation for the geopolymerization of calcined clay to produce geopolymer based mortars with low porosity and based on low porosity and high compressive as well as tensile flexural strengths. In this context, we also examined the binder to aggregate ratio in detail using various analytic techniques, such as X-ray powder diffraction (XRD), mercury intrusion porosimetry (MIP) and micro X-ray computer tomography (µXCT). This fundamental understanding of the geopolymer chemistry and the rationalisation of the factors, which can influence the geopolymerization reaction, is crucial for the sustainable production of green building materials.

6.2 Materials and methods

6.2.1 Raw materials

Metakaolin (Metamax®) was purchased from BASF (Ludwigshafen, Germany), while the aqueous NaOH solution (50 wt. % NaOH) was obtained from Carl Roth GmbH & Co. KG (Karlsruhe, Germany). A sodium silicate solution (Betol39T®) from Woellner GmbH (Ludwigshafen, Germany) with a concentration of 34.5 wt. % and a SiO_2 to Na_2O molar ratio of 3.4 was used. Either quartz powder (MILLISIL W3®, Quarzwerke GmbH, Frechen, Germany) and CEN standard sand (0.08 - 2 mm) according DIN EN 196-1:2016-11 were used as inert aggregates. The powder X-ray diffractograms of Metamax® and MILLISIL W3® are shown in the Supplementary Material (Figure 53 and Figure 54).

6.2.2 Sample preparation

All experiments were carried out under controlled laboratory conditions at 20 °C and 50 % relative humidity. The manufacture and casting of the mortar specimens was carried out according to a modified DIN EN 196-1:2016-11 procedure.[101] Based on previous experiments and the successful formation of suitable geopolymer mortars,[77] 450 g metakaolin powder was added to 225 g of an aqueous sodium silicate solution. While the mixture was stirred, aqueous sodium hydroxide solution (50 wt. %, 450 g)

and water (according to the mixing designs shown in Table 9 and Table 10) were added. The corresponding molar ratios are shown in the Supplementary Material (Table 14). Subsequently, CEN standard sand was given to the mixture while stirring. For the investigation of the influence of the binder to aggregate ratio on the workability of the fresh mortar and the strength of the mortar specimens, quartz powder was added as aggregate instead of CEN standard sand. Hereby the metakaolin/quartz powder ratio was varied from 100/0 to 20/80. The resulting mortars were then casted in standard prisms (40 × 40 × 160 mm^3) for the investigation of the influence of water or prisms of 20 x 20 x 80 mm^3 size for the investigation of the aggregate addition. The smaller prism size of the latter enabled a timely analysis of a large number of specimens. All samples were demoulded 24h after casting and stored wrapped in foil. The storing of the samples was taking place under controlled conditions (65 % relative humidity and 20°C) until further tests were carried out.

Table 9: Mixing design for the geopolymers mortars. W/S refers to the water to solid content of the fresh lime and the mortars, to which sand was added.

Code	Additional water in g	W/S (fresh lime)	W/S (mortar)
GP_Ref	0	0.57	0.20
GP_50	50	0.64	0.22
GP_100	100	0.71	0.25
GP_150	150	0.78	0.27

Table 10: Mixing design for the alkali activation of metakaolin and quartz powder (in g).

Code	Metakaolin	Quartz powder	Sodium silicate	50 wt. % NaOH	H_2O from sodium silicate and NaOH
GP_100/0	500	0	500	250	445.0
GP_90/10	450	50	450	225	400.5
GP_80/20	400	100	400	200	356.0
GP_70/30	350	150	350	175	311.5
GP_60/40	240	160	240	120	213.6
GP_50/50	200	200	200	100	178.0
GP_40/60	160	240	160	80	142.4
GP_30/70	120	280	120	60	106.8
GP_20/80	80	320	80	40	71.2
GP_20/80 +20 g H_2O	80	320	80	40	91.2

6.2.3 Methods

For the powder X-ray diffraction analyses a D8 Advance Bruker diffractometer with a Lynxeye Detector was used. Experiments were carried out with Copper Kα radiation in a 2θ area between 5° and 70° in 0.02° steps with a scanning time of 0.2 s. The powder X-ray diffractograms of the precursor materials (metakaolin and quartz powder) and the mortar specimens (GP_Ref and GP_150) are shown in the Supplementary Material (Figure 53, Figure 54 and Figure 59). The light microscopic determination of the air void content was carried out on polished mortars samples with an Olympus SZX 10 microscope according to DIN EN 480-11:2005-12.[123] The pore size distributions of all mortar specimens (GP_Ref, GP_50, GP_100, GP_150) according to incident light microscopy are shown in the Supplementary Material (Figure 55). A micro X-ray computer tomograph with a directional X-ray tube FXE 225.99 (≤ 225 kV, focal spot diameter ≤ 3 mm, tungsten target) by YXLON International GmbH (Hamburg, Germany) and a 2D-detector 1621xN (2.048 x 2.048 pixels, CsI, pitch size 200 x 200 µm^2) by PerkinElmer (Waltham, US) were used to determined macro pores and the grain distribution in the GP_Ref, GP_50, GP_100, GP_150 samples (Figure 47 and Figure 48). Measurements were carried out on drill cores of the diameter d = 6.5 mm and height h = 40 mm, which were extracted from the mortar specimens. The macro pores distribution analysis of the experimental data was carried out determined with software ImageJ 1.47v (National Institute of Health) and VG Studio Max 2.0v (Volume Graphics GmbH, Germany) based on.[124] For the SEM images a LEO 1530 Gemini Carl Zeiss microscope with a secondary electron detector was applied to investigated polished and unpolished fragments within the GP_Ref, GP_50, GP_100, GP_150 samples (Figure 49). For the water absorption measurements, a cube with an edge length of 40 mm of each sample was dried until a mass constancy was reached (24 h, 105 °C). Afterwards the dried cubes were placed in a vessel with 400 mL of water and weighed after 4 h and 24 h to confirm a constant mass of the cubes, which results in a complete saturation of the mortar specimens (GP_Ref, GP_50, GP_100, GP_150) with water to detect open pores. The results are depicted in Figure 3 and based on these experiments the pores filled with water can be calculated and the water absorption depending porosities were obtained (Table 12) according to the following equation.

$$\varepsilon_w = \frac{(m_s - m_d)}{\rho_w * V} * 100$$

ε_w = porosity determined for water m_s = mass of the water saturated specimens

m_d = mass of dried specimens p_w = density of water V = sample volume

Nitrogen adsorption measurements of GP_Ref were carried out using a NOVA Touch LX1 provided by Quantachrome under liquid nitrogen cooling to determined specific surface of pores with a diameter between 0.35 to 400 nm (Supplementary Material, Figure 56 and Figure 57). For the determination of the pore size distribution of GP_Ref, GP_50, GP_100, GP_150 via mercury intrusion porosimetry a Pascal 440 device from Thermo Fisher Scientific was used (Figure 46, Supplementary Material, Figure 58). The additional module 140 (low pressure) gave the possibility to cover the pore radii between 3.6

and 100,000 nm. The measurement was performed on fragments. The compressive and flexural strengths of all mortar specimens, in standard prisms (40 × 40 × 160 mm³) for the investigation of the influence of water or prisms of 20 × 20 × 80 mm³ size for the investigation of the aggregate addition, were determined seven days after their manufacture with a RT 200/10-1s device of the company Testing Bluhm & Feuerherdt according to DIN EN 196-1:2005-05.[101] The applied loading rate for the determination of the compressive strength was 2400N/s, whereas a loading rate of 50 N/s was used for the flexural strength. The results are depicted in Figure 51 and Figure 52 as well as in the Supplementary Material (Table 14). The workability of the fresh mortars (GP_Ref, GP_50, GP_100, GP_150) was tested via a flow spread test on a flow table according to DIN EN 1015-3:2007-05 (Table 11).[125] Right after the mixing process, the fresh mortar was placed in a truncated cone (Ø 100 mm) on the Hägermann flow table. After 15 hits, the spread of the fresh mortar was measured in both directions and the average flow spread was calculated.

6.3 Results and discussion

6.3.1 The role of the water content in the geopolymerization process

6.3.1.1 Workability of the fresh mortar

In order to evaluate the workability of the fresh mortar, flow spread tests were carried out depending on the water content of the samples. As shown in Table 11, the flow spread increases with an enhanced water content of the geopolymer mixture. This corresponds to an easier to handle mortar, which is beneficial for the subsequent casting process.

Table 11: Flow spread test results of the fresh mortars.

Code	Flow spread in mm	Relative flow spread	Consistency
GP_Ref	190	2.6	Plastic mortar
GP_50	245	5.0	Soft mortar
GP_100	275	6.6	Soft mortar
GP_150	>300	8.0	Very soft mortar

6.3.1.2 Investigation of the porosity of mortar specimens

The porosity of the mortar specimens was investigated in detail using light-based imaging methods, the examination of the water absorption, low temperature adsorption of nitrogen, mercury intrusion porosimetry and scanning electron microscopy (Figure 44).[126] In addition to these analytical techniques, we have used micro X-ray computer tomography to image micro-structures in three dimensions and to determine the porosity of the mortar specimens.[116] The existence of micropores (pores < 2 nm) within the mortar specimens was ruled out by N_2 adsorption measurements, as shown in the Supplementary Material (Figure 56 and Figure 57).

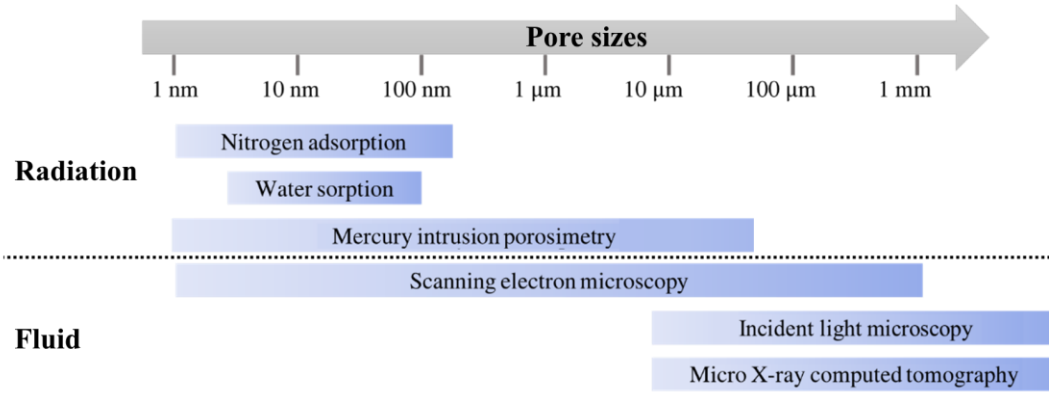

Figure 44: Relevant pore sizes and appropriate analytical methods for their determination.

The porosity of the mortar specimens was determined from the water absorption. During these experiments the mass difference between dried mortar specimens and mortar specimens, which were submerged in water, was determined (Figure 45).

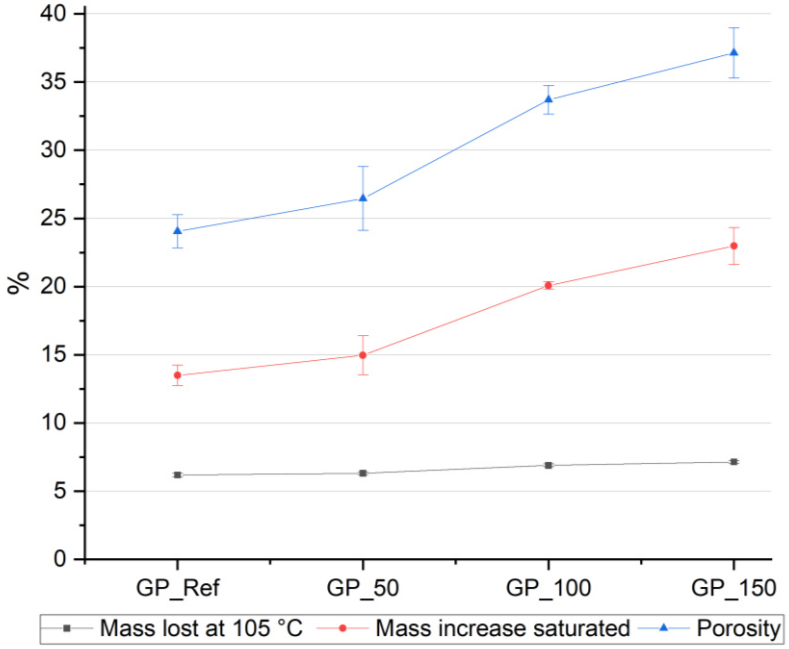

Figure 45: Determination of the water absorption and the porosity via drying and water uptake; mass loss at 105 °C to mass constancy (black); mass increase saturated (red); calculated porosity (blue).

During the drying process an almost linear mass loss of about 0.9 % is witnessed with increasing water content of the geopolymer mixtures. After the drying process fine cracks can be observed within the mortar specimens, which can be attributed to the shrinkage of the material and the different expansion coefficients of the various components. For the water uptake again an almost linear increase with increasing water content of the geopolymer mixture can be witnessed. The maximum difference amounts 7.4 % and is therefore about 10 times higher than the mass loss detected during the drying process.

Based on these experiments the pores filled with water can be calculated and porosities between 24.05 % and 35.8 % were obtained. As it becomes obvious from Table 12, the porosity increases with increasing water content of the geopolymer mixture.

Table 12: Porosity determined via the investigation of the water absorption measurements.

Code	Porosity by water absorption in %
GP_Ref	24.05 ± 1.2
GP_50	26.5 ± 2.3
GP_100	33.7 ± 1.1
GP_150	37.1 ± 1.8

The meso- and macropores of the mortar specimens were analysed by mercury intrusion porosimetry. The cumulative pore volume, the average pore diameter and the specific surface area obtained from mercury intrusion porosimetry are depicted in Figure 46. For these calculations based on the Washburn-equation[127] 3.050 nm was selected as upper threshold (Supplementary Material, Figure 58).

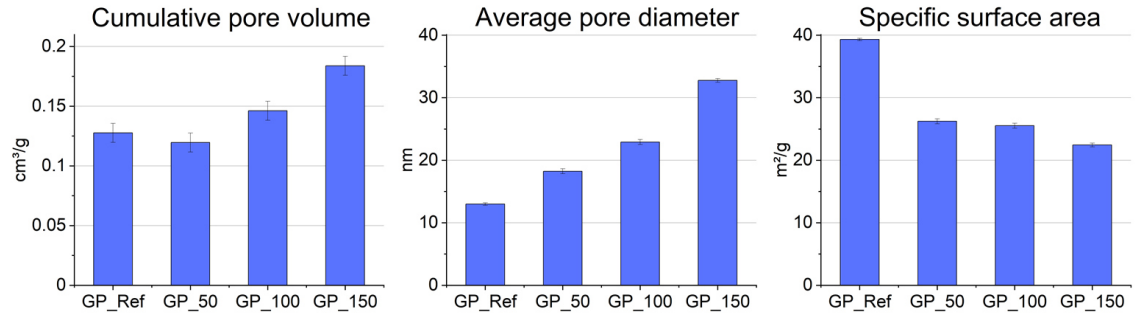

Figure 46: Results of the mercury intrusion porosimetry. Pore volumes are presented in cm^3/g of geopolymer with an error of ± 0.008 cm^3, according to literature evidence.[128]

The cumulative pore volumes (Figure 46) and the thereof resulting porosities (Table 13) show almost a linear increase with increasing water content. In case of the average pore diameter again an increase can be witnessed when the water content in the geopolymer mixture is enhanced. While an enhancement of the average pore diameter with increasing water content was witnessed, the specific surface area is decreased.

Table 13: Porosities of the mortar specimens determined via mercury intrusion porosimetry.

	Porosity in %	Cumulative pore volume in cm^3/g	Average pore diameter in nm
GP_Ref	24.2	0.128	13.0
GP_50	23.0	0.120	18.2
GP_100	26.8	0.146	22.9
GP_150	31.5	0.184	32.8

To gain structural information regarding the porosity in the size range of macro pores like air voids (Ø 0.020–10 mm), micro X-ray computer tomography (µXCT) measurements of the mortar specimens was carried out. Also, µXCT gives information about the distribution of the aggregated particles. With the used measurement setup resolution of 10 µm was achieved. The results of the µXCT of the drill cores for all mortar specimens are depicted in Figure 47.

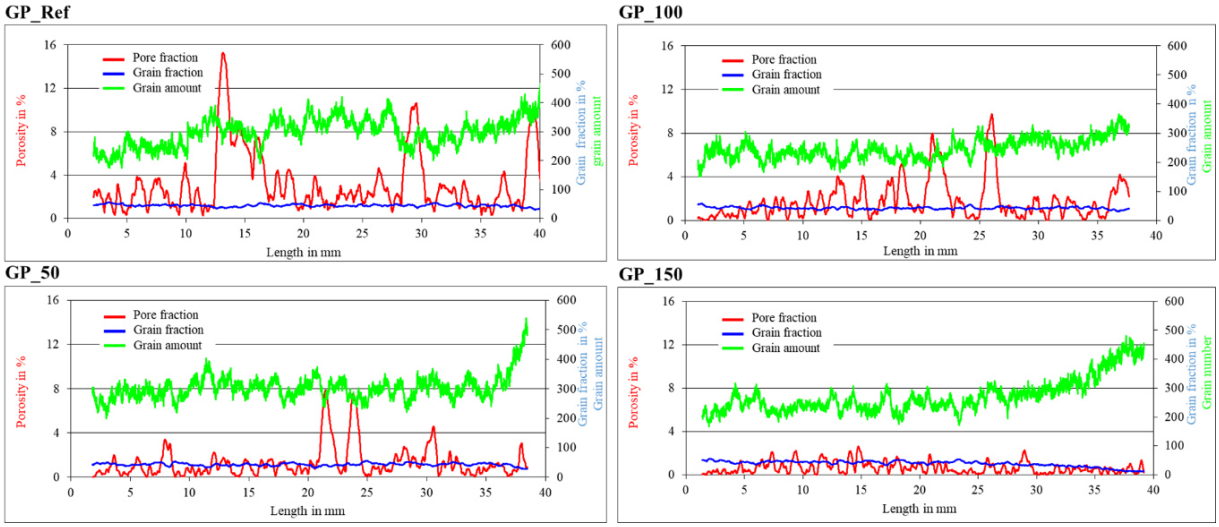

Figure 47: Pore and grain distribution through the cores of the mortar sample prisms obtained via µXCT measurements. The length of 0 mm corresponds to the bottom of the mortar sample prisms.

These results show that in the reference geopolymer mortar and in the mortars, to which 50 g and 100 g of water were added, the grain fraction stays constant over the whole length of the drill core. However, the spatially resolved analysis of the drill core of the mortar, to which the highest amount of water (150 g) was added, shows a decrease of the grain fraction starting at a height of 30 mm. This is due to the low viscosity of the fresh mortar of GP_150, which leads to a gravity related segregation of the grains and to the accumulation of the biggest grains within the bottom area of the drill core.

Obviously, not only the grain fraction is influenced by the water content of the mixture but also the porosity regarding air voids. It becomes clear that mixtures with a lower water content exhibit a higher amount of air voids than the samples with a higher water content (Figure 48). The higher amount of air voids can be attributed to the high viscosity of the fresh mortar and the therewith associated worse workability. Similar findings were made in the context of alkali-activated materials based on Sicilian volcanic precursors (i.e., volcanic ash and pumice), although here also the particle size of the applied precursors has shown to be a decisive factor for the porosity of the mortar specimens.[129]

The observed porosity trend is inverse to the porosities determined via water absorption and mercury intrusion porosimetry since these techniques always indicated an increase in porosity with an enhanced water content. However, in the case of the µXCT measurements, only air voids which consist of 8 voxels were analysed (Ø ~20 µm ≈ 8000 µm^3) and no smaller pores can be detected, which explains the different trends in comparison with the other analytical techniques. This finding is also supported by incident

light measurements, where GP_Ref shows the highest number of pores over whole size range as shown in the Supplementary Material (Figure 55).

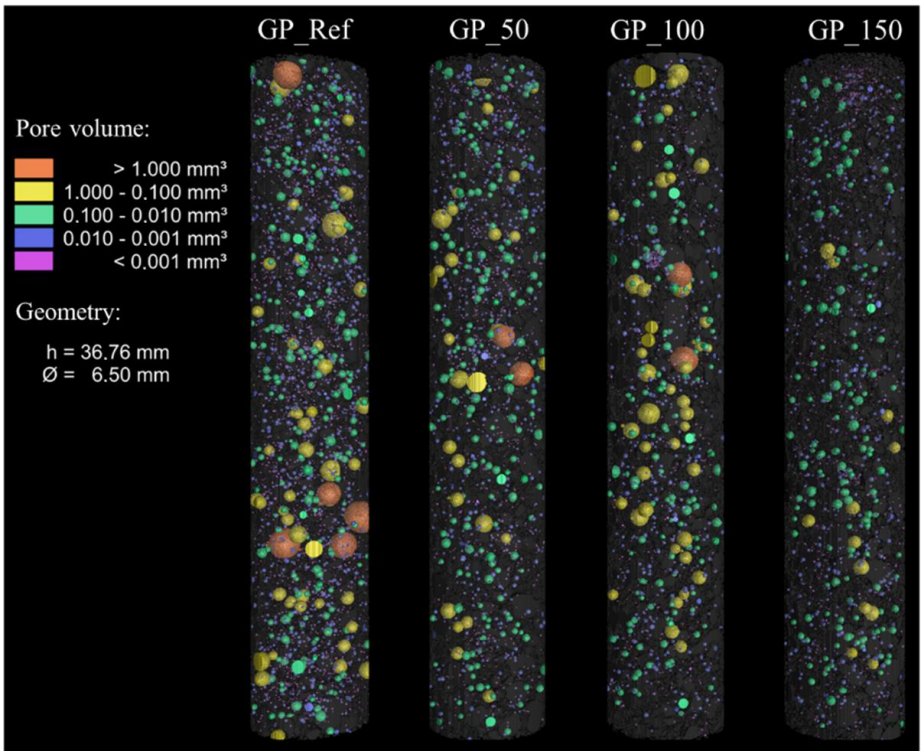

Figure 48: 3D representation of the pore size distribution within the drill core. The drill cores are oriented according to their casting direction, but cut off about 1.6 mm.

The microstructures and porosities of the mortar specimens were investigated by scanning electron microscopy (Figure 49). From the images a heterogeneous distribution of aggregates within the binder matrix becomes obvious. Also cracks within the specimens can be witnessed, which most likely stem from the drying process. Similar microstructures have been reported for other metakaolin-based geopolymers.[116]

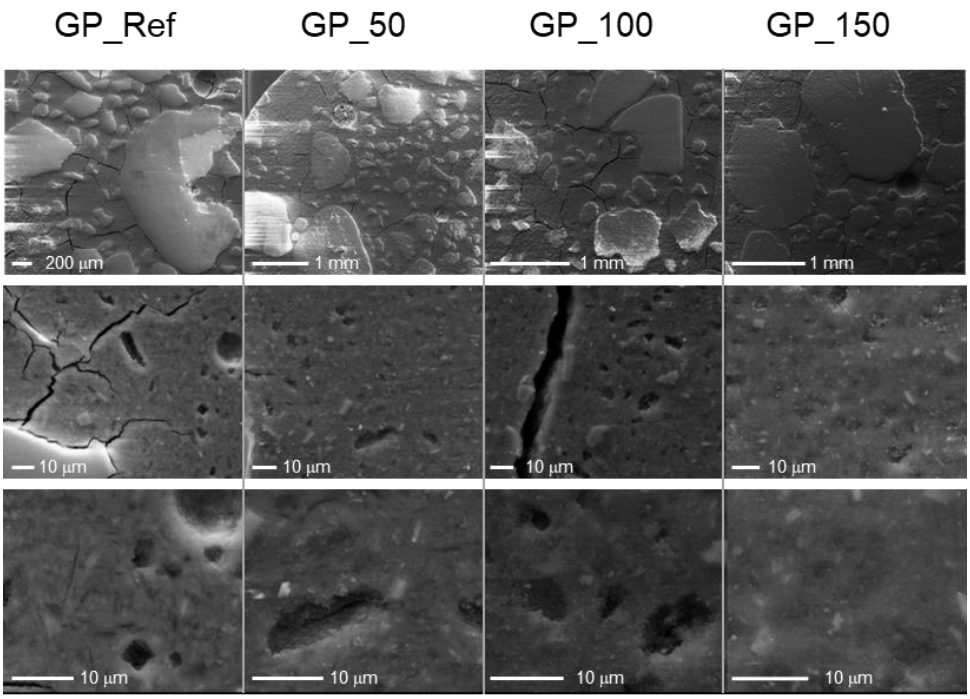

Figure 49: Scanning electron microscopy images of the mortar specimens. From left to right. GP_Ref, GP_50, GP_100, GP_150. The resolution increases from the top to the bottom.

The mortar specimens GP_Ref and GP_150 where crushed and investigated by powder X-ray diffraction. In the resulting diffractogramm (Figure 50) the crystalline phases quartz, anatase, muscovite and albite can be identified, these phases belong to the used aggregate in the mortar. The geopolymer binder is amorphous and leads not to any diffraction reflexes in the pattern. You see clearly that the crystalline composion of GP_Ref and GP_150 is identical. These results show us that the additional water does not lead to a change of crystallinity and the effect on porosity is due to other mechanisms.

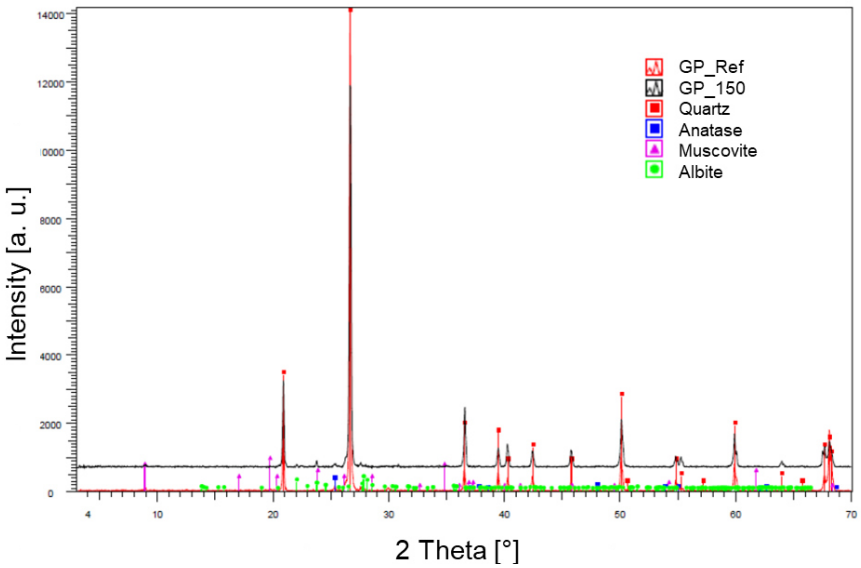

Figure 50: Powder X-ray diffraction of the mortar GP_Ref and GP_150

6.3.1.3 Mechanical properties of the mortar specimens

The compressive and flexural strengths of the mortar specimens were determined and it becomes obvious that a higher water content (w/s = 0.27 for mortar) leads to a reduction of the compressive strength (Figure 51). Subsequently, the compressive strength is inversely proportional to the water content of the geopolymer mixture, which is similar to observations made for the water to solid ratio in other metakaolin-based geopolymers[116] as well as for water-to-cement ratio in conventional cementitious systems.[130] Similar observations were made for the tensile flexural strength of the mortar specimens. Only the reference mortar shows a slight deviation from this trend, but in the same time the highest standard deviation.

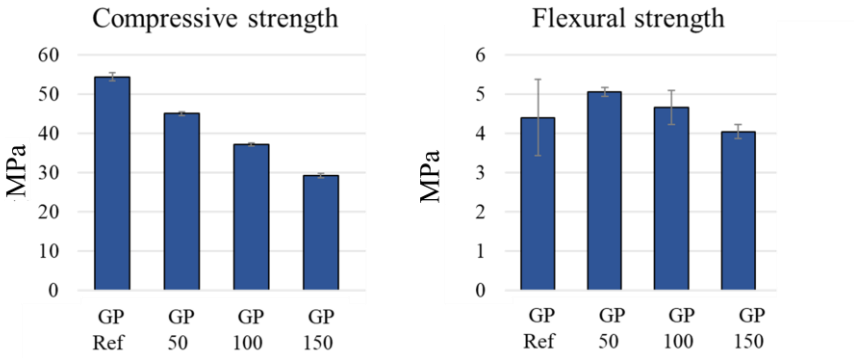

Figure 51: Compressive (6 values per mean value) and flexural (3 values per mean value) strengths with standard deviation of the mortar specimens.

The strength measurements clearly correlate with the porosities of the mortar specimens determined via capillary water uptake and mercury intrusion porosimetry measurements. It becomes obvious that a higher water content within the geopolymer mixture leads to an enhanced porosity of the mortar specimens, which results in a reduction of the compressive and flexural strengths. It is noticeable that the compressive strength decreases significantly more than the flexural strength due to the increasing water content. This behavior is unexpected. Normally, pores are usually compressed in compression testing and in flexural strength they reduce tensile cross-sectional area and have a crack-initiating effect.

However, a low water content significantly reduces the workability of the fresh mortar, as the flow spread tests carried out have shown. Also, a low water content leads to a high amount of air voids, which were observed via micro X-ray computed tomography (Section 3.3.3) as well as incident light microscopy (see Supporting Information). Therefore, the macro pores had a lower influence than the smaller pores (< 20 µm) on the mechanical performance. In order to produce geopolymers with good mechanical properties, the water content should be kept as low as possible.

6.3.2 The role of the binder to aggregate ratio

Although the increase of water content in the geopolymer mixture leads to a better workability of the mortar, a clear reduction of the compressive and less of flexural strengths was observed. Therefore, an alternative approach, namely the variation of the binder to aggregate ratio, is investigated with the aim to enhance the workability of the mortar, while good strengths of the mortar specimens are maintained.

Whereas in the case of GP_Ref, GP,50, GP_100 and GP_150 a fixed amount of CEN sand (1,350 g) was added as aggregate, in this section a systematic study of the ratio variation of metakaolin and quartz powder as aggregate was carried out. In this case quartz was selected as non-reactive aggregate in powder form. In order to optimise the formulation of the geopolymer mortar, various binder to aggregate ratios varying between 1.0 and 0.25 were prepared.

6.3.2.1 Mechanical properties of the mortar specimens

For the investigation of the effect of the quartz powder inclusion into the geopolymer mortars, the compressive and flexural strengths of the mortar specimens were determined depending on the binder to aggregate ratio (Figure 52). It becomes obvious that the geopolymerization of pure metakaolin without the addition of quartz powder results in mortar specimens with a compressive strength of 46.6 MPa and no detectible flexural strength. Very similar strength values were determined for the 90/10, 80/20 and 70/30 binder to aggregate mixtures. However, when the binder to aggregate ratio is reduced and the quartz powder content is increased an enhancement of the compressive and flexural strengths can be witnessed. The maximum compressive strength of 81.4 MPa was achieved with the 20/80 binder to aggregate ratio. It is known from the development ultra-high performance and eco-friendly concretes that the partial replacement of the reactive component (cement) by quartz powder can increase the packing density, due to the more finely tuned grain band, and thus the strength.[123] This physical mode of action can apparently be transferred for metakaolin-based geopolymer Li *et al.* demonstrated a similar increase in compressive strength (83/17 ratio) with heat-treated metakaolin-based geopolymer. When to the 20/80 mixture 20 g of additional water are added, the compressive and flexural strength decrease. This is in complete accordance with the water content results shown before.

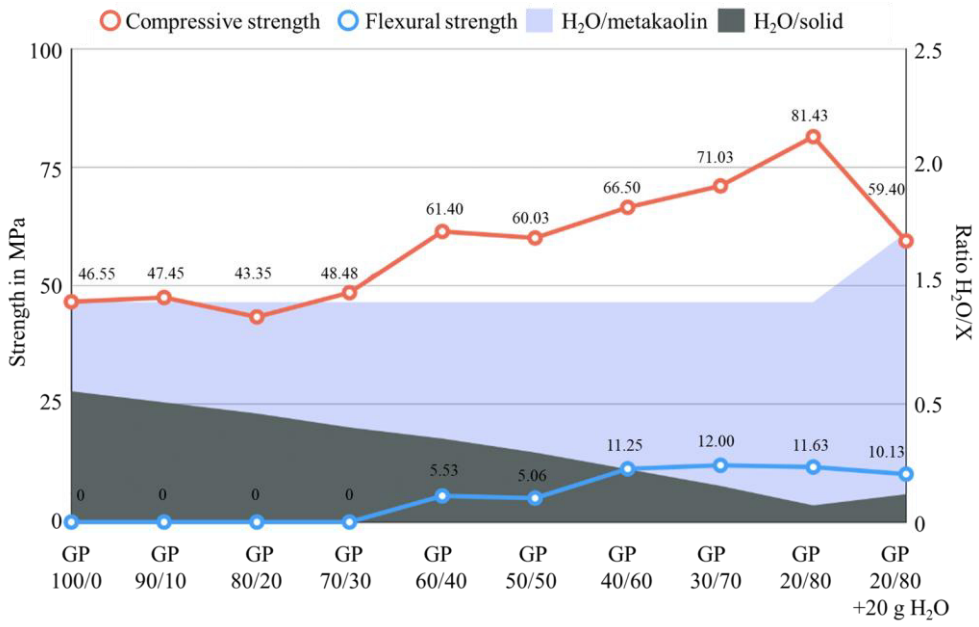

Figure 52: Compressive (six values per mean value) and flexural strengths (three values per mean value) of the mortar specimens depending on the metakaolin to quartz powder ratio.

These results are astonishing since the increase in aggregate ratio leads to an improvement of the compressive and flexural strengths of the mortar specimens within the investigated binder to aggregate ratio regime. Similar observations were made for geopolymer concrete made from alkali-activated fly ash, where an enhancement of the flexural strength of geopolymer concrete was observed with an increase in the total aggregate content.[124] Also, an increase in compressive strength has been observed for metakaolin-based geopolymers with a maximum at 73.8 % aggregate content. However, the reported compressive strengths were approximately 20 MPa below the compressive strength observed for the herein described mortar specimens.[116] Consequently, these experimental findings can be considered as model experiments for the geopolymerization of common clays, since common clays can be considered as natural mixtures of metakaolin with aggregate with a metakaolin content of below 50 %.

The rationalisation for this experimental observation is difficult, since the binder to aggregate interface within geopolymer binders is still poorly understood, especially at a molecular level. However, only recently, interfacial bonding including Al–O–Si, Na–O and H-bonding was investigated using molecular dynamics simulations. The simulations have shown that the Si/Al ratio is crucial for the interfacial strength due to a higher degree of interaction and more cross-linking within the geopolymer.[131] In order to increase the interfacial bonding between aggregates and geopolymer binders it has been shown that the presence of soluble silicates, as Betol39T® in the case of this study, in the initial activating solution is beneficial.[132] However, at this point it must be mentioned that the experimental observations are highly dependent on the raw materials used for the geopolymer production[133,134] Studies on the binder to aggregate ratio using high calcium fly ash together with sodium metasilicate as binder and sand as aggregate have, for example, shown an inverse effect, where a reduction of the strength with increasing aggregate proportion was observed.[135] Similar observations were made for the alkali activation of low grade kaolin.[136]

6.4 Conclusions

Geopolymers gain more and more attention when trying to find sustainable alternatives to hydraulic binders (e.g., normal cements based on Portland cement clinker), especially with respect to a desired reduction of greenhouse gas emission. In this work, therefore the influence of different factors, such as the water content and the binder to aggregate ratio, on the formation of geopolymer mortars were investigated with the aim to find and predict an optimal mixing design. The main intention was hereby to combine a good workability of the fresh mortar with low porosity and high compressive as well as flexural strengths of the resulting mortar specimens. To achieve this, we have casted mortar specimens using different ratios of metakaolin and water ranging from water to solid contents of the fresh lime of 0.57 to 0.78. The porosity of these specimens was then evaluated by water absorption measurements, mercury intrusion porosimetry, micro X-ray computer tomography and scanning electron microscopy. Subsequently, the mechanical properties, such as the tensile and compressive strengths, of the mortars were determined. To investigate the impact of the addition of aggregates, such as quartz powder, the

binder to aggregate ratio was varied from 100 to 0 until 20 to 80, referring to the metakaolin to quartz powder ratio.

The major conclusions derived from the experimental study can be summarised as follows:

- A higher water content of the geopolymer mixture leads to a better workability, as indicated by the increase in flow spread from 190 mm for GP-Ref to over 300 mm for GP_150, of the fresh mortar. This enhanced workability is also indicated by the increase of relative flow spread from 2.6 for GP_Ref to 8.0 for GP_150. Simultaneously, the compressive strengths of the mortar specimens decrease from 54.3 MPa for GP_Ref to 29.1 MPa for GP_150, due to an increase in capillary porosity. Simultaneously, the flexural strength is declining from 4.4 MPa GP_Ref to 4.0 MPa for GP_150, as the water content increases. At the same time, the increasing water content led to an improved deaeration effect and therefore low air void content, as indicated by micro X-ray computer tomography.
- The binder to aggregate ratio is crucial for the compressive and flexural strengths of the mortar specimens. Through the addition of quartz powder up to a ratio of 20 : 80 of metakaolin to quartz, an increase in strength, can be witnessed. Whereas the compressive strength of the geopolymer obtained without any quartz powder amounts 46.55 MPa, the strength can be increased to 81.43 MPa in the case of the 20 : 80 mixture of metakaolin and quartz. Simultaneously, the flexural strength increases. This finding gives a new impulse for the optimal design of the geopolymer mixture.
- The geopolymer formation is a complex process, which requires a detailed knowledge of the underlying factors that can influence the fresh mortar properties as well as the mechanical properties of the final geopolymer mortars.

6.5 Acknowledgments

The authors would like to thank Mr. Florian Fuchs for µXCT imaging and the Workgroup of Prof. Dirk Enke for performing individual MIP measurements, both from the University of Leipzig.

6.6 Supporting information

6.6.1 Analytical investigation of the raw materials

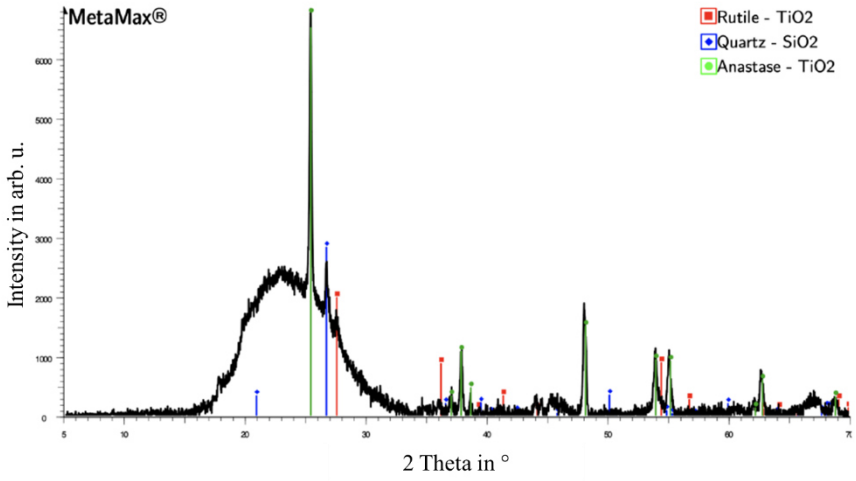

Figure 53: Powder X-ray diffractogram of the metakaolin Metamax®.

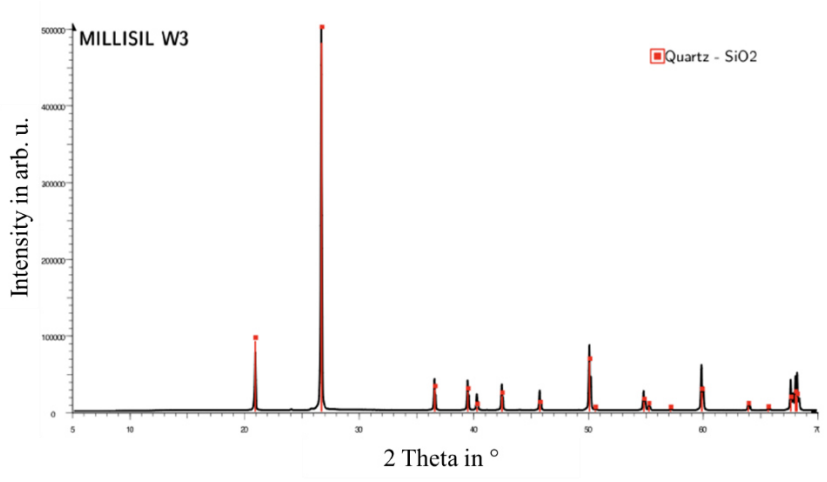

Figure 54: Powder X-ray diffractogram of the quartz powder MILLISIL W3®.

6.6.2 Analytical investigation of the mortar specimens

Incident light microscopy

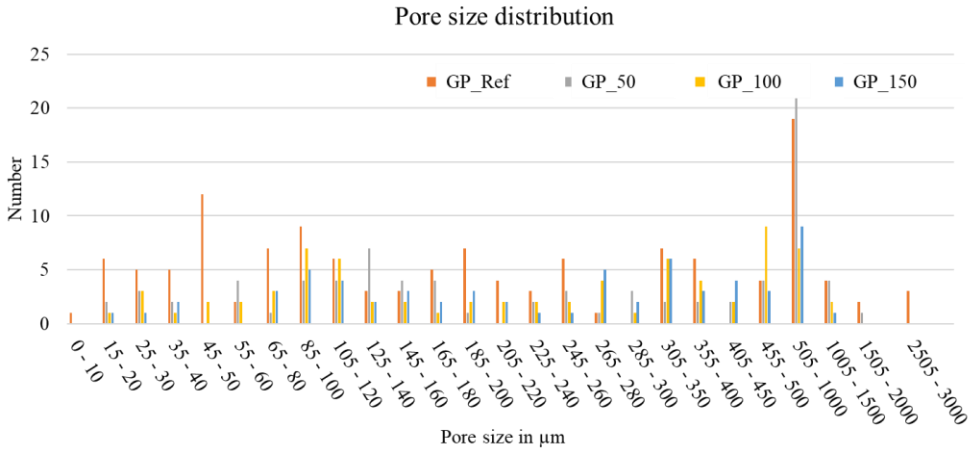

Figure 55: Pore size distributions according to incident light microscopy.

N_2 adsorption measurements

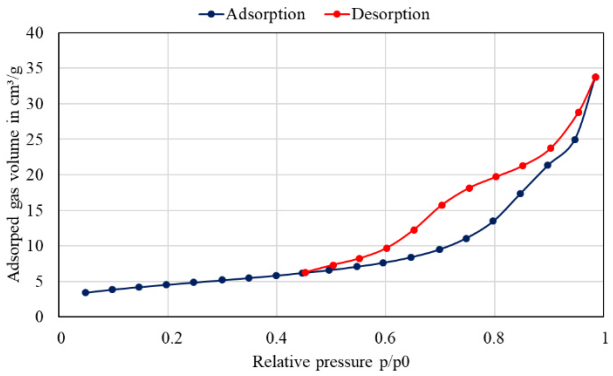

Figure 56: Nitrogen sorption isotherm for GP_Ref recorded at 77 K.

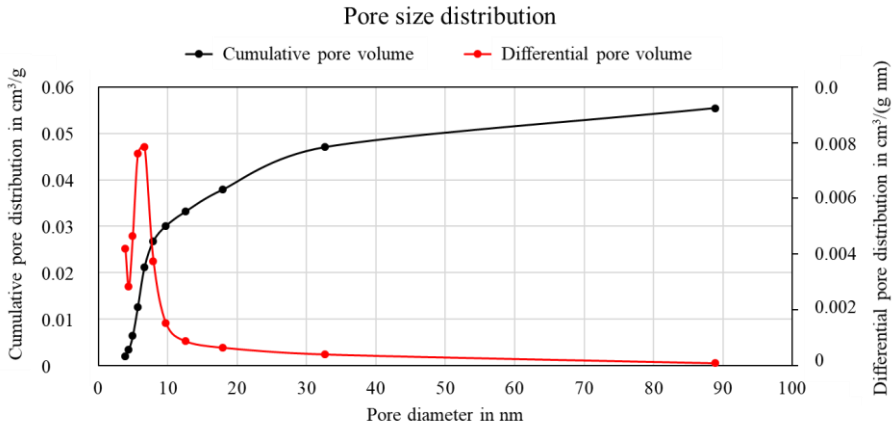

Figure 57: Pore size distribution according to the BJH method on the basis of the desorption data.

Mercury intrusion porosimetry

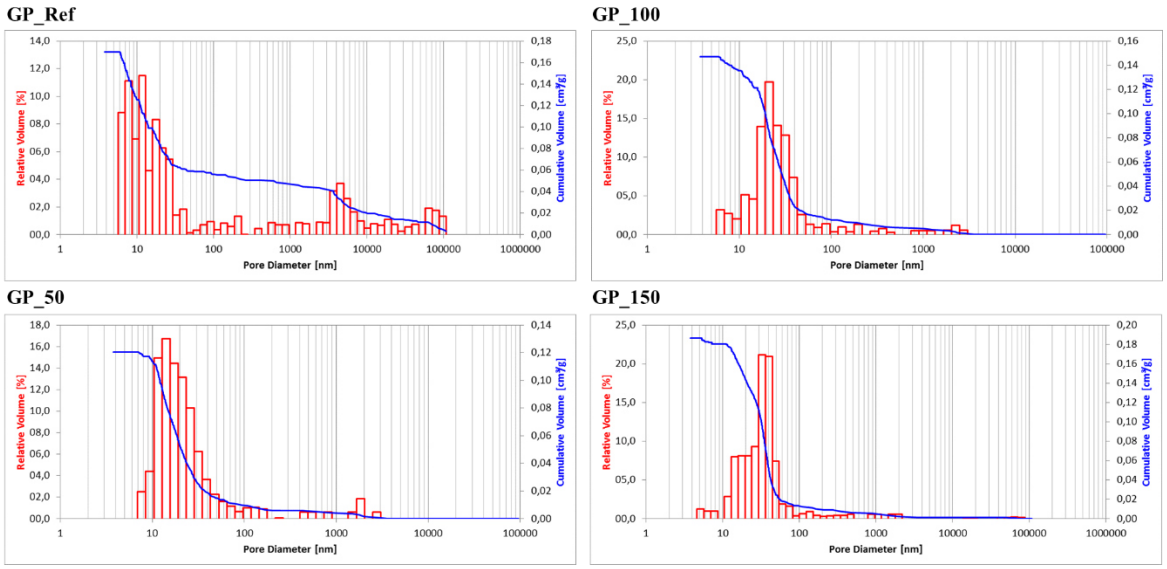

Figure 58: Results of the mercury intrusion porosimetry of the whole pore diameter area (3.5 - 100000 nm).

Powder X-ray diffraction

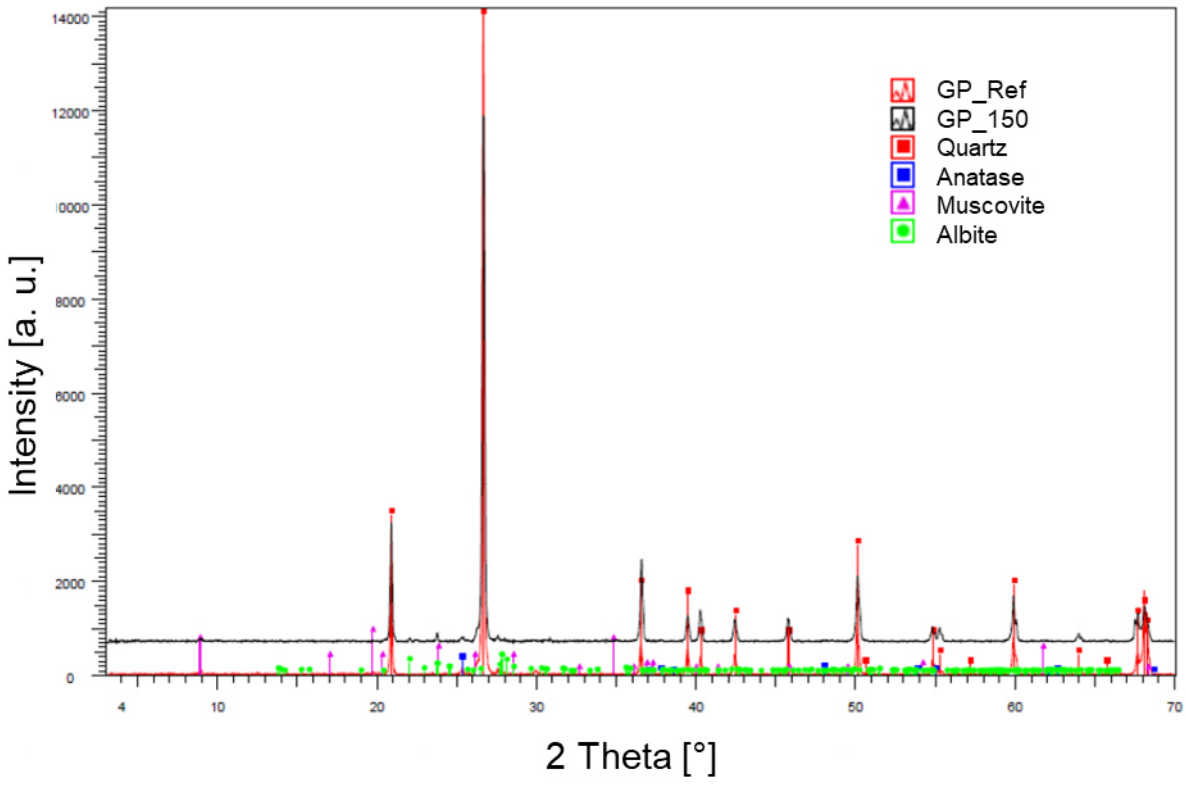

Figure 59: Powder X-ray diffractograms of GP_Ref and GP_150.

6.6.3 Mechanical properties

Table 14: Overview of the mechanical properties of the mortar specimens.

	Density [g/cm^3]	**Standard deviation**	**Tensile strength [N/mm^2]**	**Standard deviation**	**Compressive strength [N/mm^2]**	**Standard deviation**
GP_Ref	1.997	0.009	4.400	0.972	54.380	1.026
GP_50	2.022	0.011	5.057	0.117	44.997	0.455
GP_100	1.996	0.006	4.657	0.435	37.200	0.346
GP_150	1.970	0.008	4.047	0.175	29.183	0.571

6.6.4 Mixing design

Table 15: Molar ratios of the mixing design.

	Na_2O/SiO_2	**SiO_2/Al_2O_3**	**H_2O/Na_2O**	**Na_2O/Al_2O_3**
GP_Ref	1.24	1.52	1.63	1.34
GP_50	1.24	1.52	1.74	1.34
GP_100	1.24	1.52	1.87	1.34
GP_150	1.24	1.52	1.96	1.34
GP_100/0	1.27	1.52	1.63	1.34
GP_90/10	1.17	1.62	1.63	1.34
GP_80/20	1.07	1.72	1.63	1.34
GP_70/30	0.97	1.82	1.63	1.34
GP_60/40	0.87	1.92	1.63	1.34
GP_50/50	0.77	2.02	1.63	1.34
GP_40/60	0.67	2.12	1.63	1.34
GP_30/70	0.57	2.22	1.63	1.34
GP_20/80	0.47	2.32	1.63	1.34
GP_20/80 + 20 g H_2O	0.47	2.32	2.13	1.34

7. Conclusions and perspective

In this thesis, the application of geopolymers as an alternative to conventional cementitious materials was examined in depth, driven by the need to develop environmentally friendly construction materials with a significantly reduced CO_2 footprint. Currently, the construction industry, which has traditionally relied on Portland cement, is confronted with substantial challenges, due to the high carbon dioxide emissions associated with the production of cement. To date these emission account for approximately 8 % of the global CO_2 emissions. This number is expected to rise tremendously over the next decade due to growing economies, a trend that has to be seen very critically in the context of climate change. To counteract the rising greenhouse gas emissions, alternative construction materials with adaptable properties have to be identified, which are suitable for a range of construction-related applications. To address this challenge, geopolymers, which can be synthesised from abundant raw materials, such as industrial by-products or common clays, have been considered as alternative binder materials. These materials present a promising solution, due to their low energy production and reduced environmental footprint compared to traditional cement. However, the formation of geopolymers *via* the alkali activation of precursor materials with a low Ca-content and the subsequent geopolymerization reaction is a very complex reaction in a multi parameter setting. Therefore, this thesis aims to provide a better understanding of the underlying geopolymer chemistry by focusing on the selection of raw materials, the activation process, and the prediction and analyses of geopolymer mortar properties. This investigation also provides a detailed comparison of geopolymers with traditional cementitious materials in terms of performance metrics, including compressive strength, durability, workability and resistance to environmental impacts.

To identify suitable common clays as precursors for the geopolymer formation *via* an alkali activation procedure, a straightforward method, based on IR spectroscopy, was developed. As part of this work, a linear correlation between the surface area of the ATR-IR OH stretching band in kaolinite mixtures and the kaolinite content could be identified using an in-house developed IR setup. Based on this correlation and a subsequent calibration, a so-called clay activation index was determined for various common clays. This index gave insights into the quantity of reactive components after the calcination step of the common clay. Through this approach the necessary activator amounts (water glass and alkaline solution) for the alkali activation of calcined clays could be calculated, based on Davidovits geopolymer formation theory. This novel approach simplifies the alkali activation process by eliminating the need for empirical and iterative testing to determine the appropriate activator quantities. The mechanical tests of the resulting geopolymer mortars have proven the success of the developed method and confirmed the stability of the resulting binders.

In addition to this methodology study, the impact of calcium compounds on the properties of geopolymer binders has been investigated. It was found that when calcium is present in the form of calcite, the clays exhibit the expected mechanical properties after the calcination and activation procedures. However, if

the calcite phase decomposes during the thermal treatment, the properties of the binders change significantly. For instance, the calcination of two mineralogically similar clays from different deposits leads to different reaction products. Whereas in Clay1 an amorphous calcium-rich phase is formed, Clay2 produces crystalline lime. Free lime can cause issues, such as the crystallisation of sodium silicate, which leads to an uneven binder solidification. This makes the mortar unsuitable for construction-related applications. Interestingly, the decomposition of calcium carbonate within the common clays can be precisely controlled through a tailored calcination procedure. By the adjustment of the calcination temperature, the dehydroxylation of layered silicates within the clays and be decoupled from the calcium carbonate decomposition. In contrast, other carbonates, such as calcium magnesium carbonates as dolomite, undergo both processes simultaneously. Based on the adopted calcination procedure, mortars with compressive strengths over 20 MPa could be obtained, despite the low amount of reactive layered silicates and high unreactive mineral content (60 % quartz, illite). With the addition of superplasticisers and retarders, and through the optimisation of the activator types, strengths comparable to standard Portland cement (32.5 MPa) were achieved. Also, a 50 % post-solidification increase from 7 to 28 days was observed. Additionally, even small amounts of portlandite positively affect the carbonation resistance without compromising the mechanical properties. This indicates the suitability of the mortars for steel-reinforced components. Also, the high resistance of the mortars towards acids lay the foundation for various applications, such as the use in agricultural and wastewater buildings.

Further, various factors that affect the geopolymerization reaction, such as the water content and the binder-to-aggregate ratio, were investigated to identify an optimal mixing design for the alkali activation of common clays. The formation of geopolymer mortars is a very complex process, which requires a careful consideration of multiple factors that affect both fresh mortar properties and the final mechanical properties of the geopolymer mortars. Therefore, different ratios of metakaolin and water were investigated, with water-to-solid contents ranging from 0.57 to 0.78. Subsequently, the porosity and mechanical properties of the mortars were evaluated using various techniques, including water absorption, mercury intrusion porosimetry, micro X-ray tomography, and scanning electron microscopy. It became obvious that an increased water content improves the workability of the geopolymer mixture, evidenced by a rise in flow spread. However, simultaneously a reduction in compressive and flexural strengths, due to a higher capillary porosity, can be witnessed. This reduction in strength can be overcome by adjusting the binder-to-aggregate ratio. Through the addition of quartz powder up to a metakaolin-quartz ratio of 20:80 the compressive and flexural strengths can almost be doubled.

Overall, these insights significantly enhance our understanding of geopolymers, particularly regarding the selection of precursors, activation processes, and their resultant properties. However, this study also underscores the critical need for further examinations of various parameters during the activation procedure to achieve the desired, tuneable properties of the final geopolymer-based mortar product. Beyond a comprehensive parameter screening of the geopolymerization reaction, the impact of additives and superplasticisers in the context of geopolymer binders have to be studied in detail. This is crucial

for a real-world application of geopolymer mortars in the construction industry. These experimental studies should be accompanied by theoretical methods to deepen the knowledge regarding the underlying reaction mechanisms. Further, the scalability of the geopolymer mortar production has to be investigated in the future, also with respect to cost-efficient and environmentally friendly manufacturing processes. In this context, also the standardisation and the development of norms in the field of geopolymer-based mortars has to be pushed forward. This should include aspects like the production procedures, analyses, performance requirements and long-term durability studies.

8. References

[1] C. Meyer, *Cem. Concr. Compos.* **2009**, *31*, 601–605.

[2] C. Costa, *Mater. Constr. Civ. Eng. Sci. Process. Des.* **2015**, 1–52.

[3] International Energy Agency, Global Status Report: Towards a Zero-Emission, Efficient and Resilient Buildings and Construction Sector **2018**, available online: https://www.iea.org/reports/2018-global-status-report (accessed on 4th of June 2024)

[4] A. Petek Gursel, E. Masanet, A. Horvath, A. Stadel, *Cem. Concr. Compos.* **2014**, *51*, 38–48.

[5] G. Habert, S. A. Miller, V. M. John, J. L. Provis, A. Favier, A. Horvath, K. L. Scrivener, *Nat. Rev. Earth Environ.* **2020**, *1*, 559–573.

[6] A. Herrmann, A. Koenig, F. Dehn, *Struct. Concr.* **2018**, *19*, 918–929.

[7] Y. Cancio Díaz, S. Sánchez Berriel, U. Heierli, A. R. Favier, I. R. Sánchez Machado, K. L. Scrivener, J. F. Martirena Hernández, G. Habert, *Dev. Eng.* **2017**, *2*, 82–91.

[8] M. C. G. Juenger, F. Winnefeld, J. L. Provis, J. H. Ideker, *Cem. Concr. Res.* **2011**, *41*, 1232–1243.

[9] A. Wardhono, D. W. Law, A. Strano, *Procedia Eng.* **2015**, *125*, 650–656.

[10] D. L. Y. Kong, J. G. Sanjayan, K. Sagoe-Crentsil, *Cem. Concr. Res.* **2007**, *37*, 1583–1589.

[11] C. R. Gagg, *Eng. Fail. Anal.* **2014**, *40*, 114–140.

[12] M. Uwasu, K. Hara, H. Yabar, *Environ. Dev.* **2014**, *10*, 36–47.

[13] M. E. Bildirici, *Clean Technol. Environ. Policy* **2019**, *21*, 783–793.

[14] N. Sahoo, A. Kumar, Samsher, *Environ. Dev.* **2022**, *44*, 100767.

[15] N. A. Madlool, R. Saidur, M. S. Hossain, N. A. Rahim, *Renew. Sustain. Energy Rev.* **2011**, *15*, 2042–2060.

[16] P. J. Jackson, in *Lea's Chem. Cem. Concr.,* Vol. 4, Ed.: P. C. Hewlett, Elsevier, **2003**.

[17] H. Hong, Z. Fu, X. Min, *Cem. Concr. Res.* **2001**, *31*, 287–290.

[18] E. Taylor, *Cem. Concr. Compos.* **1998**, *20*, 335.

[19] K. Scrivener, A. Ouzia, P. Juilland, A. Kunhi Mohamed, *Cem. Concr. Res.* **2019**, *124*, 105823.

[20] International Energy Agency, Technology Roadmap - Low-Carbon Transition in the Cement Industry **2018**, available online: https://iea.blob.core.windows.net/assets/cbaa3da1-fd61-4c2a-8719-31538f59b54f/TechnologyRoadmapLowCarbonTransitionintheCementIndustry.pdf (accessed on 29th of August 2024)

[21] P. J. M. Monteiro, S. A. Miller, A. Horvath, *Nat. Mater.* **2017**, *16*, 698–699.

[22] E. Aramendia, P. E. Brockway, P. G. Taylor, J. Norman, *Glob. Environ. Change* **2023**, *83*, 102745.

[23] B. Bajželj, J. M. Allwood, J. M. Cullen, *Environ. Sci. Technol.* **2013**, *47*, 8062–8069.

[24] S. A. Miller, A. Horvath, P. J. M. Monteiro, *Environ. Res. Lett.* **2016**, *11*, 074029.

[25] C. Chen, G. Habert, Y. Bouzidi, A. Jullien, *J. Clean. Prod.* **2010**, *18*, 478–485.

[26] S. J. Davis, N. S. Lewis, M. Shaner, S. Aggarwal, D. Arent, I. L. Azevedo, S. M. Benson, T. Bradley, J. Brouwer, Y. M. Chiang, C. T. M. Clack, A. Cohen, S. Doig, J. Edmonds, P. Fennell, C. B. Field, B. Hannegan, B. M. Hodge, M. I. Hoffert, E. Ingersoll, P. Jaramillo, K. S. Lackner, K. J. Mach, M. Mastrandrea, J. Ogden, P. F. Peterson, D. L. Sanchez, D. Sperling, J. Stagner, J. E. Trancik, C. J. Yang, K. Caldeira, *Science* **2018**, *360*, eaas9793.

[27] E. Gartner, *Cem. Concr. Res.* **2004**, *34*, 1489–1498.

[28] A. Josa, A. Aguado, A. Cardim, E. Byars, *Cem. Concr. Res.* **2007**, *37*, 781–788.

[29] G. Habert, C. Billard, P. Rossi, C. Chen, N. Roussel, *Cem. Concr. Res.* **2010**, *40*, 820–826.

[30] R. Snellings, *RILEM Tech. Lett.* **2016**, *1*, 50–55.

[31] J. L. Provis, *Cem. Concr. Res.* **2018**, *114*, 40–48.

[32] H. Castillo, H. Collado, T. Droguett, M. Vesely, P. Garrido, S. Palma, *e-Polymers* **2022**, *22*, 108–124.

[33] V. B. Thapa, D. Waldmann, in *Vielfalt im Massivbau - Festschrift zum 65. Geburtstag von Prof. Dr. Ing. Jürgen Schnell*, Eds: M. Pahn, C. Thiele, C. Glock, Ernst & Sohn, **2018**.

[34] A. Palomo, M. W. Grutzeck, M. T. Blanco, *Cem. Concr. Res.* **1999**, *29*, 1323–1329.

[35] J. L. Provis, *Mater. Struct. Constr.* **2014**, *47*, 11–25.

[36] I. Pol Segura, N. Ranjbar, A. Juul Damø, L. Skaarup Jensen, M. Canut, P. Arendt Jensen, *Heliyon* **2023**, *9*, e15718.

[37] P. Cong, Y. Cheng, *J. Traffic Transp. Eng. (Engl. Ed.)* **2021**, *8*, 283–314.

[38] J. N. Y. Djobo, S. Tome, *Cem. Concr. Compos.* **2024**, *152*, 105660.

[39] F. Pacheco-Torgal, J. Castro-Gomes, S. Jalali, *Constr. Build. Mater.* **2008**, *22*, 1305–1314.

[40] *Alkali Activated Materials-State of the Art Report*, Eds: J. L. Provis, J. S. J. van Deventer, Springer, **2014**.

[41] H. Taghvayi, K. Behfarnia, M. Khalili, A. Wardhono, D. W. Law, T. C. K Molyneaux, H. Ye, A. Radlińska, M. Olalekan Yusuf, M. Azmi Megat Johari, Z. Arifin Ahmad, M. Maslehuddin, *J.*

Adv. Concr. Technol. **2018**, *16*, 293–305.

[42] C. Shi, D. Roy, P. Krivenko, *in Alkali-Activated Cements and Concrete,* CRC Press, **2003**.

[43] J. Davidovits, in *Geopolymer Chemistry and Applications,* Vol. 5, Geopolymer Institute, **2020**.

[44] A. Buchwald, *Bauverlag* **2006**, *7*, 42–49.

[45] R. Firdous, D. Stephan, J. N. Y. Djobo, *Constr. Build. Mater.* **2018**, *190*, 1251–1263.

[46] P. Kathirvel, S. R. M. Kaliyaperumal, *Constr. Build. Mater.* **2016**, *102*, 51–58.

[47] S. Chuah, W. H. Duan, Z. Pan, E. Hunter, A. H. Korayem, X. L. Zhao, F. Collins, J. G. Sanjayan, *Mater. Des.* **2016**, *92*, 571–578.

[48] M. Lahoti, K. K. Wong, K. H. Tan, E. H. Yang, *Mater. Des.* **2018**, *154*, 8–19.

[49] J. He, Y. Jie, J. Zhang, Y. Yu, G. Zhang, *Cem. Concr. Compos.* **2013**, *37*, 108–118.

[50] S. Lekshmi, J. Sudhakumar, S. Thomas, *Mater. Today Proc.* **2023**, DOI 10.1016/J.MATPR.2023.04.083.

[51] J. P. Hos, P. G. Mccormick, L. T. Byrne, *J. Mater. Sci.* **2002**, *37*, 2311–2316.

[52] D. Khale, R. Chaudhary, *J. Mater. Sci.* **2007**, *42*, 729–746.

[53] H. Yan, C. Xue-Min, M. Jin, L. P. Liu, X. D. Liu, J. Y. Chen, *Microporous Mesoporous Mater.* **2012**, *161*, 187–192.

[54] J. Davidovits, in *Second Int. Conf. Geopolymers*, **1995**, 9–40.

[55] J. Davidovits, *J. Mater. Educ.* **1994**, *16*, 91–139.

[56] M. Amin, Y. Elsakhawy, K. Abu el-hassan, B. A. Abdelsalam, *Case Stud. Constr. Mater.* **2022**, *16*, e00976.

[57] H. Xu, J. S. J. Van Deventer, *Miner. Eng.* **2002**, *15*, 1131–1139.

[58] H. Xu, J. S. J. Van Deventer, *Cem. Concr. Res.* **2002**, *32*, 1705–1716.

[59] B. Zhang, *Sustain. Mater. Technol.* **2024**, *40*, e00882.

[60] H. G. Dill, *Ore Geol. Rev.* **2020**, *119*, 103304.

[61] E. Galán, R. E. Ferrell, *Dev. Clay Sci.* **2013**, *5*, 83–126.

[62] F. Wypych, R. A. de Freitas, *Dev. Clay Sci.* **2022**, *10*, 3–35.

[63] *Tonminerale und Tone,* Eds: K. Jasmund, G. Lagaly, Steinkopff Verlag Darmstadt, **1993**.

[64] K. Emmerich, N. Giraudo, R. Schuhmann, F. Schnetzer, H. Kaden, P. Thissen, *J. Phys. Chem. C* **2018**, *122*, 7484–7493.

[65] S. C. Aboudi Mana, M. M. Hanafiah, A. J. K. Chowdhury, *Geol. Ecol. Landscapes* **2017**, *1*, 155–

161.

[66] R. K. Taylor, T. J. Smith, *Clay Miner.* **1986**, *21*, 235–260.

[67] S. Bailey, *Clay Miner.* **1980**, *15*, 85–93.

[68] *Crystal Structures of Clay Minerals and their X-Ray Identification,* Eds.: G. W. Brindley; G. Brown, Mineralogical Society, **1980**.

[69] *Advances in the characterization of industrial minerals: university textbook,* Ed.: G. E. Christidis, European Mineralogical Union, **2011**.

[70] H. Xu, J. S. J. Van Deventer, *Int. J. Miner. Process.* **2000**, *59*, 247–266.

[71] A. Herrmann, A. König, F. Dehn, *Cem. Int.* **2015**.

[72] J. S. Damtoft, J. Lukasik, D. Herfort, D. Sorrentino, E. M. Gartner, *Cem. Concr. Res.* **2008**, *38*, 115–127.

[73] F. Slaty, H. Khoury, J. Wastiels, H. Rahier, *Appl. Clay Sci.* **2013**, *75–76*, 120–125.

[74] F. Avet, R. Snellings, A. Alujas Diaz, M. Ben Haha, K. Scrivener, *Cem. Concr. Res.* **2016**, *85*, 1–11.

[75] N. Garg, J. Skibsted, *Cem. Concr. Res.* **2016**, *79*, 101–111.

[76] *Concrete Repair, Rehabilitation and Retrofitting III*, Vol. 1, Eds.: M. G. Alexander, H.-D. Beushausen, F. Dehn, P. Moyo, CRC Press, **2012**.

[77] F. Dathe, V. Strelnikova, N. Werling, K. Emmerich, F. Dehn, *Open Ceram.* **2021**, *7*, 100152.

[78] R. Prost, A. Dameme, E. Huard, J. Driard, J. P. Leydecker, *Clays Clay Miner.* **1989**, *37*, 464–468.

[79] European Patent EP0085902A2, *Verfahren Zur Kontinuierlichen Umwandlung von Metakaolin in Feinstteiliges Zeolithisches Natriumaluminiumsilikat*, **1983**.

[80] G. J. G. Gluth, K. Arbi, S. A. Bernal, D. Bondar, A. Castel, S. Chithiraputhiran, A. Dehghan, K. Dombrowski-Daube, A. Dubey, V. Ducman, K. Peterson, P. Pipilikaki, S. L. A. Valcke, G. Ye, Y. Zuo, J. L. Provis, *Mater. Struct. Constr.* **2020**, *53*, 1–17.

[81] A. Buchwald, *Habilitation: The Influence of Calcium on the Condensation of (Alumino-) Silicates in Alkali-Activated Binders*, Bauhaus-Universität Weimar, **2012**.

[82] Statusbericht der deutschen Kreislaufwirtschaft: Einblicke und Aussichten **2018**, https://www.bvse.de/images/pdf/Nachrichten_2018/Statusbericht_2018_Ansicht_und_Druck.pdf (accessed on 28th of August 2024)

[83] A. Trümer, *PhD thesis: Calcinierte Tone als Puzzolane der Zukunft : Von den Rohstoffen bis zur Wirkung im Beton*, Bauhaus-Universität Weimar, **2020**.

[84] *Applied Clay Mineralogy: Occurrences, Processing and Applications of Kaolins, Bentonites, Palygorskite-Sepiolite, and Common Clays,* Ed.: H. H. Murray, Elsevier, **2007**.

[85] A. Mehta, R. Siddique, *Constr. Build. Mater.* **2017**, *146*, 136–143.

[86] N. K. Lee, H. K. Lee, *Cem. Concr. Compos.* **2016**, *72*, 168–179.

[87] A. Koenig, A. Herrmann, S. Overmann, F. Dehn, *Constr. Build. Mater.* **2017**, *151*, 405–413.

[88] T. Bakharev, J. G. Sanjayan, Y. B. Cheng, *Cem. Concr. Res.* **2003**, *33*, 1607–1611.

[89] H. J. Zhuang, H. Y. Zhang, H. Xu, *Procedia Eng.* **2017**, *210*, 126–131.

[90] C. K. Ma, A. Z. Awang, W. Omar, *Constr. Build. Mater.* **2018**, *186*, 90–102.

[91] A. Koenig, A. Wuestemann, F. Gatti, L. Rossi, F. Fuchs, D. Fessel, F. Dathe, F. Dehn, F. Minelli, *Constr. Build. Mater.* **2019**, *211*, 583–593.

[92] R. Pouhet, M. Cyr, *Cem. Concr. Res.* **2016**, *88*, 227–235.

[93] *Lea's Chem. Cem. Concr.*, Vol. 5, Eds.: P. C. Hewlett, M. Liska, Elsevier, **2019**.

[94] N. Werling, F. Dehn, F. Krause, A. Steudel, R. Schuhmann, K. Emmerich, *Clays Clay Miner.* **2020**, *68*, 524–531.

[95] G. A. González-Montiel, E. N. Kaweesa, N. Feau, R. C. Hamelin, J. K. Stone, S. Loesgen, *Molecules* **2020**, *25*, 2359.

[96] F. Tittarelli, A. Mobili, C. Giosuè, A. Belli, T. Bellezze, *Corros. Sci.* **2018**, *134*, 64–77.

[97] C. Monticelli, M. E. Natali, A. Balbo, C. Chiavari, F. Zanotto, S. Manzi, M. C. Bignozzi, *Cem. Concr. Res.* **2016**, *80*, 60–68.

[98] M. Criado, I. Sobrados, J. M. Bastidas, J. Sanz, *Prog. Org. Coatings* **2016**, *99*, 11–22.

[99] N. Beuntner, *PhD thesis: Zur Eignung und Wirkungsweise calcinierter Tone als reaktive Bindemittel- komponente im Zement,* Universität der Bundeswehr München, **2017**.

[100] B. Franke, *Z. anorg. allg. Chem.* **1941**, *247*, 180–184.

[101] EN 196-1:2016, Methods of Testing Cement—Part 1 - Determination of Strength, European Committee for Standardization, Brussels, Belgium, **2016**.

[102] EN 196-3:2017-03, Bestimmung der Erstarrungszeiten und der Raumbestäständigkeit, European Committee for Standardization: Brussels, Belgium, **2017**.

[103] EN 13295:2004, Products and systems for the protection and repair of concrete structures - Test methods - Determination of resistance to carbonation, European Committee for Standardization:

Brussels, Belgium, **2004**

[104] R. M. McIntosh, J. H. Sharp, F. W. Wilburn, *Thermochim. Acta* **1990**, *165*, 281–296.

[105] A. Buchwald, M. Hohmann, K. Posern, E. Brendler, *Appl. Clay Sci.* **2009**, *46*, 300–304.

[106] F. Farooq, X. Jin, M. Faisal Javed, A. Akbar, M. Izhar Shah, F. Aslam, R. Alyousef, *Constr. Build. Mater.* **2021**, *306*, 124762.

[107] J. Davidovits, *J. Therm. Anal. Calorim.* **2005**, *37*, 1633–1656.

[108] *Geopolymers Structure, Processing, properties and industrial applications,* Eds.: J. L. Provis, J. S. J. van Deventer, Woodhead Publishing, **2009.**

[109] C. He, B. Osbaeck, E. Makovicky, *Cem. Concr. Res.* **1995**, *25*, 1691–1702.

[110] T. Seiffarth, M. Hohmann, K. Posern, C. Kaps, *Appl. Clay Sci.* **2013**, *73*, 35–41.

[111] Y. M. Liew, C. Y. Heah, A. B. Mohd Mustafa, H. Kamarudin, *Prog. Mater. Sci.* **2016**, *83*, 595–629.

[112] N. Werling, R. Schwaiger, F. Dathe, F. Dehn, K. Emmerich, *Appl. Clay Sci.* **2024**, *250*, 107259.

[113] S. V Patankar, S. S. Jamkar, Y. M. Ghugal, *Int. J. Adv. Technol. Civ. Eng.* **2012**, *1*, 296–300.

[114] S. Luhar, D. Nicolaides, I. Luhar, *Buildings* **2021**, *11*, 82.

[115] T. Bakharev, *Cem. Concr. Res.* **2005**, *35*, 1233–1246.

[116] A. Albidah, M. Alghannam, H. Abbas, T. Almusallam, Y. Al-Salloum, *J. Mater. Res. Technol.* **2021**, *10*, 84–98.

[117] E. Pulidori, C. Pelosi, M. Fugazzotto, S. Pizzimenti, M. R. Carosi, L. Bernazzani, A. Stroscio, M. R. Tiné, P. Mazzoleni, G. Barone, C. Duce, *J. Therm. Anal. Calorim.* **2024**, 1–13.

[118] G. Dal Poggetto, P. Kittisayarm, S. Pintasiri, P. Chiyasak, C. Leonelli, D. Chaysuwan, *Polymers* **2022**, *14*, 5091.

[119] A. D'Angelo, G. Dal Poggetto, S. Piccolella, C. Leonelli, M. Catauro, *Polymers* **2022**, *14*, 3380.

[120] Z. Zuhua, Y. Xiao, Z. Huajun, C. Yue, *Appl. Clay Sci.* **2009**, *43*, 218–223.

[121] X. Yao, Z. Zhang, H. Zhu, Y. Chen, *Thermochim. Acta* **2009**, *493*, 49–54.

[122] J. G. S. Van Jaarsveld, J. S. J. Van Deventer, G. C. Lukey, *Chem. Eng. J.* **2002**, *89*, 63–73.

[123] EN 480-11:2005- Admixtures for Concrete, Mortar and Grout—Test Methods—Part 11: Determination of Air Void Characteristics in Hardened Concrete, European Committee for Standardization, Brussels, Belgium, **2005**.

[124] A. Koenig, *Constr. Build. Mater.* **2020**, *244*, 118313.

[125] EN 1015-3:2007, Methods of Test for Mortar for Masonry—Part 3: Determination of Consistence of Fresh Mortar (by Flow Table), European Committee for Standardization, Brussels, Belgium, **2007**.

[126] H. Wang, H. Li, F. Yan, *Colloids Surfaces A Physicochem. Eng. Asp.* **2005**, *268*, 1–6.

[127] Z. Yunsheng, S. Wei, L. Zongjin, *Appl. Clay Sci.* **2010**, *47*, 271–275.

[128] A. C. A. Muller, K. L. Scrivener, *Cem. Concr. Res.* **2017**, *100*, 350–360.

[129] C. Pelosi, R. Occhipinti, C. Finocchiaro, G. Lanzafame, E. Pulidori, M. Lezzerini, G. Barone, P. Mazzoleni, M. Rosaria Tiné, *Mater. Lett.* **2023**, *335*, 133773.

[130] M. Kasaniya, M. D. A. Thomas, T. Moffatt, A. Hossack, *Cem. Concr. Res.* **2024**, *183*, 107575.

[131] N. Dujardin, T. Salem, V. Feuillet, M. Fois, L. Ibos, C. Poilane, R. Manuel, *Constr. Build. Mater.* **2020**, *245*, 118417.

[132] A. B. Abell, K. L. Willis, D. A. Lange, *J. Colloid Interface Sci.* **1999**, *211*, 39–44.

[133] S. H. Kang, Y. Jeong, K. H. Tan, J. Moon, *Cem. Concr. Compos.* **2018**, *94*, 238–247.

[134] S. Haruna, B. S. Mohammed, M. M. A. Wahab, A. Al-Fakih, *IOP Conf. Ser. Mater. Sci. Eng.* **2021**, *1101*, 012022.

[135] B. Joseph, G. Mathew, *Sci. Iran.* **2012**, *19*, 1188–1194.

[136] R. Arellano-Aguilar, O. Burciaga-Díaz, A. Gorokhovsky, J. I. Escalante-García, *Constr. Build. Mater.* **2014**, *50*, 642–648.

9. Apendix

9.1 List of abbreviations

AAMs	Alkali-activated materials
C-S-H	Calcium silicate hydrate
CCS	Carbon capture and storage
DSC	Differential scanning calorimetry
ESEM	Environmental scanning electron microscopy
GGBFS	Ground granulated blast furnace slag
IEA	International Energy Agency
IR	Infrared
MIP	Mercury intrusion porosimetry
μXCT	micro X-ray computer tomography
MS	Mass spectrometry
N-A-S-H	Sodium aluminosilicate hydrate
NMR	Nuclear magnetic resonance
OPC	Ordinary Portland cement
RH	Relative humidity
RT	Room temperature
SEM	Scanning electron microscopy
TG	Thermogravimetric analysis
UNEP	United Nations Environment Program
XRD	X-ray powder diffraction
XRD	X-ray fluorescence

9.2 Original publication concerning chapter 4

Dathe and Dehn *Int J Concr Struct Mater* (2024) 18:1
https://doi.org/10.1186/s40069-023-00627-y

International Journal of Concrete Structures and Materials

RESEARCH Open Access

Alkali Activation of Common Clay Deposits: Evaluation of the Suitability by an IR Spectroscopic Method

Felix Dathe[1*] and Frank Dehn[1]

Abstract

In the context of a sustainable use of resources with the aim of the reduction of the CO_2 footprint, the development of alternative concrete materials has attracted a great deal of attention. In this context, geopolymers, obtained from common clay deposits, are found to be interesting construction materials with very versatile properties. In this paper, a completely novel approach for the evaluation of the suitability of clays for the geopolymer formation is investigated. The method is based on simple and easy-to-handle IR spectroscopic measurements, through which the surface area under the OH stretching band in the IR spectrum of the clay can directly be correlated to the amount of reactive clay components. These reactive components are required for the success of the alkali activation of the clays in order to access geopolymers. Based on the theoretical reaction pathway of the geopolymer formation, the linear relationship between the OH stretching band area and the reactive components can be used for the estimation of the required activator amount for the alkali activation of calcined clays and predict the quality of the casted geopolymer mortar in terms of strength. This new method not only gives an insight into the suitability of a common clay for the geopolymer formation, but also facilitates a straightforward alkali activation procedure without tedious preliminary testing of the required activator amount.

Keywords Alkali activation, Clay, IR spectroscopy, Geopolymer binder, Clay activation index

1 Introduction

The components of clays are mainly based on the mineral relicts of their parent rocks. This fact causes a vast variety of clay deposits to occur. Most common clays are associated with sheet silicates, which are vital for the alkali activation of clays, since they comprise suitable hydroxyl groups for the calcination process prior to the alkali activation (Emmerich, 2011). Despite the sheet silicates also other minerals, such as quartz, hematite and feldspar, can be found in clay deposits. These minerals are inert towards calcination and activation processes (Xu & Deventer, 2000).

The alkali activation of raw materials has been studied in more depth recently, since it provides versatile access to novel construction materials. These materials are referred to as alkali activated binders or geopolymer binders, depending on the calcium content of the raw material (Herrmann et al., 2015). Furthermore, alkali activation represents a suitable and environmental friendly alternative to the cement production, which has a negative influence on the carbon dioxide content in the atmosphere (Damtoft et al., 2008). So far, the focus has been mainly on the alkali activation of fly ash, slag and metakaolin (Provis & Deventer, 2014) and not so much on common clays, due to the complexity of the clay material itself. This versatility of common clays causes

Journal information: ISSN 1976-0485 / eISSN 2234-1315.

*Correspondence:
Felix Dathe
felix.dathe@kit.edu
[1] Institute of Concrete Structures and Building Materials, Karlsruhe Institute of Technology (KIT), Gotthard-Franz-Str. 3, 76131 Karlsruhe, Germany

difficulties, since it is necessary to investigate the exact mineral composition of the clay before the activation to evaluate the right conditions for the calcination and subsequent activation of the raw material (Slaty et al., 2013). The calcination as well as the activation processes are extremely important not only for the development of new construction materials, but also for the application of calcined clay as an additive for ordinary concrete, due to its pozzolanic activity (Avet et al., 2016; Garg & Skibsted, 2016). Although there is a close relationship between the pozzolanic activity and the alkali activation, the hardening of the binder is caused by a different chemical reaction and makes a comparison difficult.

To obtain a geopolymer binder based on common clays, the raw material must be calcined first. During this step, the crystalline nature of the sheet silicates is destroyed under elevated temperatures and at the same time the hydroxyl groups of the crystal structure are eliminated in the form of water (White et al., 2012). The calcination process significantly impacts both the crystallinity of the material and its solubility in a basic pH solution. The amorphous material obtained after calcination represents the starting material for the alkali activation. During the alkali activation process, an aqueous base and water glass are commonly added to the calcined clay which leads to the formation of a geopolymer precursor. This precursor then undergoes a condensation reaction and forms an amorphous aluminosilicate network (Fig. 1) (Davidovits, 1994).

One of the major factors to consider during this process is the amount of base and water glass that is required for the geopolymer formation. Based on the studies of Davidovits et al. in 1994 it can be assumed that for 1 mol of metakaolin (which is a dehydroxylated form of kaolinite) 2 mol of water glass and in total 2 mol of base are required. However, if a calcined clay is used instead of pure kaolinite, which consists of a variety of mineral components, the situation becomes more complex. Therefore, it is necessary to determine the number of reactive components within clay deposits before the alkali activation. The amount of reactive components in the clay strongly depends on the OH groups present in the structure, since during the calcination process the clay structure is losing its OH groups in the form of water. This leads to the formation of so-called reactive centres, where the OH groups were present before, and the subsequent formation of geopolymer precursors. The positions of these reactive centres can then be cross-linked during the activation process via a condensation reaction (Dathe et al., 2021; Pacheco-Torgal et al., 2008).

Encouraged by this, a suitable method for the investigation of the amount of reactive components in clay deposits was developed. Therefore, a clay activation index, which represents the alkali activation potential of common clays, based on an IR spectroscopic method, is introduced. This clay activation index allows to estimate the suitability of a certain clay for the geopolymer formation, but also gives an estimation of the amount of activator that is required for the alkali activation of the calcined clay.

2 Materials and Methods

2.1 Clay Materials

Eight different deposits of common and materials (clays A–H) were analysed by powder X-ray diffraction (XRD) and simultaneous thermal analysis (STA) to gain information about their composition (Table 1). The phase components usually exhibit error values around ± 2%.

For the qualitative analysis of the composition of the clays the programme EVA™ was used, whereas the quantitative analysis was obtained by Rietveld analysis of the data, employing the programme PROFEX.

MetaMax® from BASF was used as reference material, since it is a high-reactivity pure metakaolin product, which shows no contamination of other minerals. The chemical purity of the kaolinite was investigated by powder XRD and STA. As aqueous base a 50 wt.% sodium hydroxide solution and as water glass a sodium metasilicate with a molar proportion of SiO_2 to Na_2O of 3.4 was used.

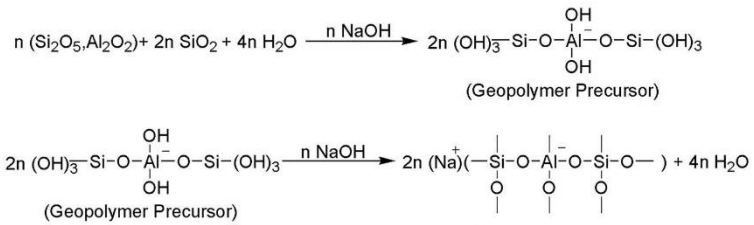

Fig. 1 Process of the formation of geopolymers based on metakaolinite (Davidovits, 2011)

Table 1 Composition of the clays A to D (in %)

Mineral component	Clay A	Clay B	Clay C	Clay D	Clay E	Clay F	Clay G	Clay H
Albite	–	–	4	–	–	3	2	–
Phyllosilicates	94	65	61	33	93	77	82	24
Quartz	2	28	29	44	2	20	12	74
Orthoclase	4	4	4	2	–	–	4	2
Anatase	–	3	1	1	2	–	–	–
Anhydrite	–	–	–	1	–	–	–	–
Haematite	–	–	2	–	–	–	–	–
Amorphous content	–	–	–	19	–	–	–	–
Phyllosilicates								
Kaolinite	78	40	23	12	87	68	5	6
Muscovite	16	10	19	21	6	9	4	18
Smectite	–	5	3	–	–	–	–	–
Montmorillonite	–	–	–	–	–	–	71	–
Chlorite	–	–	3	–	–	–	2	-
Strata chlorite/smectite	–	5	3	–	–	–	–	–
Strata illite/smectite	–	5	10	–	–	–	–	–

2.2 Analytical Methods

Powder X-ray diffraction (XRD) was carried out using a D8 Advance diffractometer (Bruker GmbH Karlsruhe, Germany) with a Lynxeye Detector (5° opening angle). Experiments were carried out with Cupper Kα radiation in a 2θ area between 5 and 70° in steps by 0.02° with a scanning time of 0.2 s. The quantitative analysis was carried out with the software PROFEX Version 4.1.0, by using an internal standard of 10 wt.% corundum.

Infrared spectroscopic measurements (IR) were carried out on a Bruker Tensor 27 FT-IR Spectrometer, with a modified ATR-IR Diamond setup. During the measurements, attention was paid on constant pressure on the sample.

Simultaneous thermal analysis (STA) About 100 mg of the raw materials were heated up to 1000 °C with a heating rate of 10 K/min under nitrogen atmosphere in corundum crucible, using a STA 409 apparatus (Netzsch, Selb, Germany).

Scanning electron microscopy (SEM) images were obtained using a Philips XL 30 FEG environmental scanning electron microscope (ESEM; FEI Europe, Eindhoven, The Netherlands). For the measurements all samples were glued onto aluminium SEM-holders using conductive tape (Leit-C, Plano GmbH, Wetzlar, Germany). To improve the quality of the SEM images, the samples were sputtered with a thin conductive layer (5 nm Au/Pd 80/20) and were investigated using an acceleration voltage of 20 kV.

2.3 General Preparation of the Clay Samples

Prior to the activation process, all clays were calcined in 1 kg charges, which were tempered to 700 °C for 3 h in a muffle oven under air. Afterwards, different components were added to the calcined clay to obtain mortar specimens (according to a slightly modified EN 196-1:2005-05 approach). Firstly, the calcined clay was placed in the mixer with the aqueous base. After 30 s of stirring, sand was added over 30 s and subsequently water glass was added to the mixture while the mixture was stirred (140 rpm). Afterwards, the mortar was stirred for another 30 s under stirring (280 rpm) and the specimens were cast in steel moulds.

Before the IR measurements of the clay, the samples were ground and sieved to obtain a particle size ≤ 32 µm. Furthermore, the clays and the material for the calibration were well dried under vacuum to remove any residual water. For the IR spectroscopic measurements of the common clays non-calcined samples were used. For the generation of the calibration curve (Fig. 4a) a certain amount of pure kaolinite was added to the calcined kaolin.

2.4 Strength Measurements

The compressive strength of the mortar specimens was determined according to EN 196-1:2005-05 with a TESTING Bluhm & Feuerherdt GmbH servo hydraulic compression and bending test device of the type RT 200/10-1s. After casting, the specimens were stored at

20 °C with a relative humidity of 65% for 7 days until the specimens were tested.

3 Results and Discussion

In order to measure the clay activation index of the clay samples and evaluate the activator amount that is needed for the alkali activation of common clay deposit, it is important to know the amount of reactive components within the clay. As mentioned before, this reactive amount is directly associated with the OH groups that are present in the clay. Therefore, IR spectroscopic measurements were utilised to gain information about the composition of the clay and the presence of hydroxyl groups.

3.1 Description of the Experimental Setup

The developed experimental IR setup is shown in Fig. 2. The setup consists of a modified diamond ATR-IR unit from "PIKE Technology". In order to obtain a constant pressure on the sample, a load cell was installed in axial position to the pressure stamp. With the aid of a fine thread, the contact pressure can be adjusted precisely. To guarantee a constant sample volume, a plate with a drilling was drafted on top of the IR diamond. This not only gives the possibility to use a certain sample volume, but also enables an efficient cleaning of the instrument after the measurement.

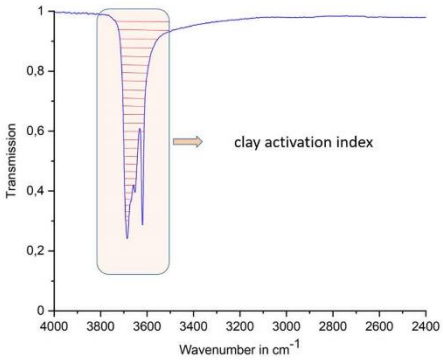

Fig. 3 Example of an IR measurement of a clay using the before described experimental setup

In Fig. 3, an example of an IR spectrum of a clay material using the before described setup is shown. The important region for the determination of the clay activation index is in the area of 3800–3500 cm^{-1}.

3.2 Calibration of the Experimental Setup

As starting point for this method, different mixtures of pure kaolinite with amorphous calcined kaolin, which was used as hydroxyl free support material, were

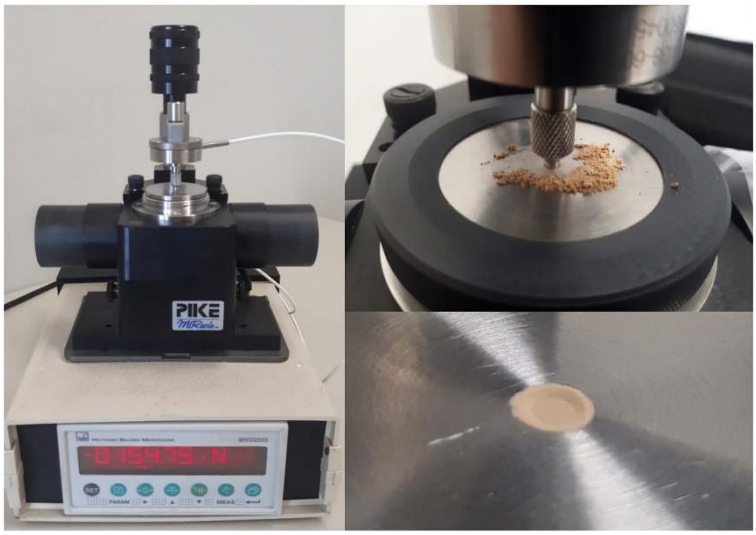

Fig. 2 Picture of the experimental IR setup for the determination of the clay activation index of common clays

prepared. The proportion of the mixtures were 0 to 100 wt.% of the kaolinite content with a stepwise increase of 5 wt.%. Kaolinite was the mineral of choice, since it represents the sheet silicate with the most hydroxyl groups and therefore a material that can easily be used for alkali activation (Prost et al., 1989). The samples were dried under vacuum prior testing to ensure that no free water influences the measurement. The purity of the samples was previously determined by powder XRD and STA measurements. Also, the samples were analysed via SEM imaging, showing the sheet like structure of the clay minerals. The mixtures were then further examined by the before introduced ATR-IR setup. As expected, an increase of the surface area of the OH stretching band around 3800–3500 cm^{-1} was observed moving from mixtures with a small kaolinite content to a higher kaolinite content (Fig. 4). To verify this observation quantitatively, the surface area under the OH stretching band was integrated and plotted against the kaolinite content, resulting in a linear correlation. Based on this, it can be assumed that the kaolinite content/the amount of OH groups correlate directly with the number of reactive centres present after the calcination process.

3.3 Clay Activation Index of Common Clays

After the calibration procedure, the clays were also analysed by ATR-IR spectroscopy using the developed setup (Fig. 5). Fig. 5 provides a clearer overview by displaying only four of the investigated clays. It is essential to note that all clays underwent vacuum drying before being utilised in this study.

The integrals of the OH IR stretching bands of the different clays were then related to the calibration curve obtained before (Fig. 6). Since, the integral is related to the amount of OH groups present in the clay sample, which is crucial for the alkali activation process, it can be converted into the clay activation index based on the calibration shown before. The clay activation index varies from 0 to 100% depending on the content of the active species within the clay that can be used for the alkali activation process.

3.4 Application of the Clay Activation Index for the Alkali Activation of Clays

The observations made during the ATR-IR spectroscopic measurements and the calculated clay activation indexes were now applied to the design of a suitable mixture of calcined clay, water glass and base during the alkali activation process to form a geopolymer binder mortar. Therefore, clays were calcined prior to the alkali activation process.

For the mixing design for the alkali activation procedure, it was assumed that a high hydroxyl content within a clay and thus a high clay activation index is related to large amounts of reactive centres. Therefore, a high clay activation index should also result

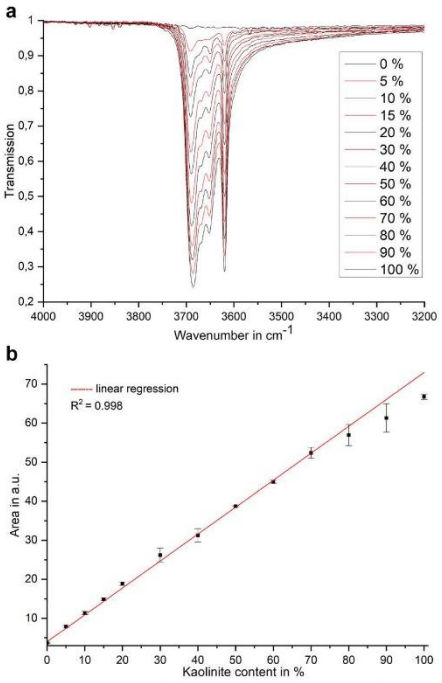

Fig. 4 **a** Investigation of different kaolinite/kaolin mixtures by IR spectroscopy and **b** the relationship between the area under the OH stretching bands and the kaolinite content

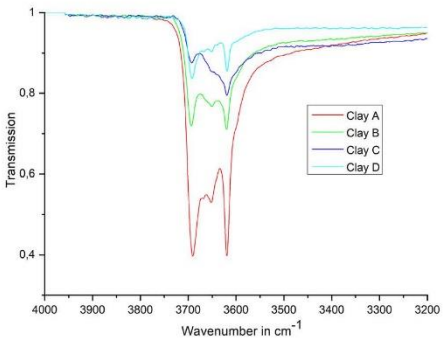

Fig. 5 Investigation of four different clay deposits by ATR-IR spectroscopy

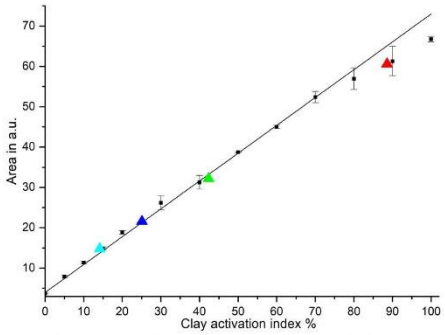

Fig. 6 The relationship between the surface area under the OH stretching bands and the clay activation index of the common clays (**A** red; **B** green; **C** blue; **D** light blue) and the kaolinite/kaolin calibration curve (black)

Table 2 Alkali activation mixtures based on the IR spectroscopic determination of the clay activation index

Calcined clay sample	Clay activation index in %	NaOH in mol	Na_2SiO_3 in mol
Clay A	88.6	1.77	1.77
Clay B	42.4	0.85	0.85
Clay C	25.1	0.5	0.5
Clay D	14.2	0.28	0.28
Clay E	95.3	1.9	1.9
Clay F	64.4	1.29	1.29
Clay G	20.2	0.4	0.4
Clay H	4.3	0.09	0.09
Ref. pure metakaolin	100	2	2

All mixtures consisted of 450 g calcined clay, 1350 g CEN-sand and the calculated activator amount

in good mortar quality after the alkali activation. The stoichiometry of the different components was based on Davidovits' studies, in which 1 mol of metakaolin, 2 mol of water glass and in total 2 mol of base were used (Davidovits, 1994). The previously defined clay activation index (Fig. 6) can now be utilised to calculate the required activator dosage (Table 2). In this context water glass as well as the aqueous base were both considered as activators, since the addition of base without water glass to the calcined clay only leads to the formation of a crystalline material (zeolite) (Christophliemk, 1989). In case of a lower clay activation index, the clay demands a smaller amount of activator solution, because the amount of reactive centres responsible for forming geopolymer precursors is lower. The reference mixture with a pure metakaolin (MetaMax®) consumes the highest amount of activators during the chemical reaction.

For the examination of the geopolymer binder specimens, which were obtained by the alkali activation described before, the compressive and flexural tensile strength was measured (Fig. 7).

These investigations have shown, that almost all specimens hardened without any special treatment (heat, etc.), which was not observed when random mixtures of calcined clay, activators (water glass, base) and sand were used. This already shows the success of this IR spectroscopic method for the evaluation of the necessary activator content for the alkali activation. Only clay H did not harden and consequently no compressive and flexural tensile strength measurements could be carried out.

As expected, the reference material MetaMax®, with the highest clay activation index, has shown the highest compressive strength among all clay materials. The compressive strengths then decrease with decreasing clay activation index from clay E to clay G. Therefore, the clay activation index is not only a great tool to estimate the suitability of common clays for the alkali activation, but it also gives clear information about the mixing design for the alkali activation procedure. Only in the case of clay D a slight inconsistency can be witnessed, since clay D shows a little higher compressive strength than clay G, despite the lower clay activation index. This points out, that not only chemical processes, like the alkali activation process, are responsible for the mortar performances but also physical effects, such as the grain size or the porosity, influence the material characteristics.

The obtained results were also verified via SEM imaging. Clays with a high activation index, and a therewith-associated high compressive strength, such as clay E, show a well-structured binder surface, whereas samples with a lower clay activation index, such as clay D, exhibit a more inhomogeneous microstructure that leads to a fragile connection between the particles.

4 Conclusions

The current study has shown a linear correlation between the surface area of the ATR-IR OH stretching band in kaolinite mixtures, and the kaolinite content using the developed ATR-IR setup. Based on this correlation and a subsequent calibration, the clay activation index, which gives insights into the amount of reactive components after the calcination process, of various common clays was determined. This allowed the calculation of the activator (water glass and base) amount required during the alkali activation of the calcined clay based on Davidovits' proposed geopolymer formation. This completely novel approach simplifies the alkali activation of clay material

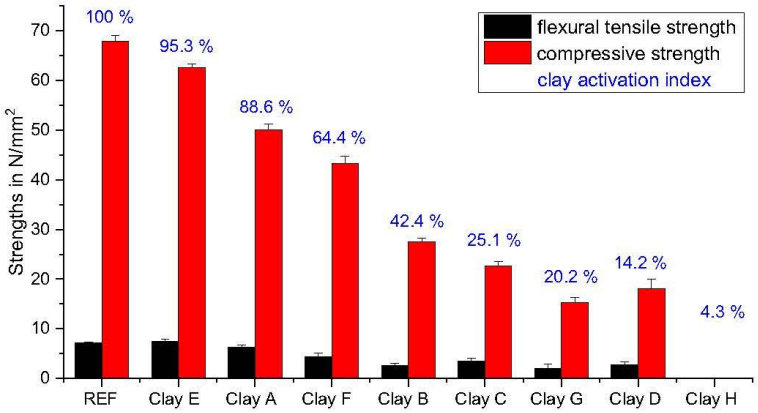

Fig. 7 Compressive strength and flexural tensile strengths of the geopolymer mortars, sorted by decreasing clay activation index

enormously and provides a straightforward access to a variety of geopolymer binders without the need of preliminary empirical and often iterative testing of the necessary activator amount. Tests of the compressive as well as the flexural tensile strength have underlined the stability of the geopolymer binders after the activation process and therefore shown the success and the wide applicability of this method.

Supplementary Information

The online version contains supplementary material available at https://doi.org/10.1186/s40069-023-00627-y.

Additional file 1. Appendix: Powder X-ray diffractograms: **Figure S1.** Powder X-ray diffractograms of clay A. **Figure S2.** Powder X-ray diffractograms of clay B. **Figure S3.** Powder X-ray diffractograms of clay C. **Figure S4.** Powder X-ray diffractograms of clay D. **Figure S5.** Powder X-ray diffractograms of clay E. **Figure S6.** Powder X-ray diffractograms of clay F. **Figure S7.** Powder X-ray diffractograms of clay G. **Figure S8.** Powder X-ray diffractograms of clay H. Selected SEM images: **Figure S9.** SEM image of clay D. **Figure S10.** SEM image of mortar D after the alkali activation. **Figure S11.** SEM image of clay E. **Figure S12.** SEM image of mortar E after the alkali activation. **Figure S13.** SEM image of clay H. **Figure S14.** SEM image of mortar H after the alkali activation.

Acknowledgements
This work would not have been accomplished without the Faculty of Chemistry and Mineralogy of Leipzig University. We also like to thank the staff of the Competence Center for Material Moisture (CMM) from KIT for the support during this work, and the German Research Foundation (DFG) for funding (Projektnummer 325967999).

Author contributions
FDa: conducted the experimental study, analysed the test results and drafted the manuscript. FDe contributed to the conception of the manuscript and supervision.

Funding
Open Access funding enabled and organized by Projekt DEAL. This study was supported by the German Research Foundation (DFG) for funding (Projektnummer 325967999).

Declarations

Ethics approval and consent to participate
All authors of the manuscript confirm ethical approval and consent to participate following the Journal's policies.

Consent for publication
All authors of the manuscript agree on the publication of this work in the *International Journal of Concrete Structures and Materials*.

Competing interests
Authors report no conflict of interest.

Availability of data and materials
All data relevant to this manuscript are given either in the manuscript or in Additional file 1: Appendix.

Received: 8 April 2023 Accepted: 31 July 2023
Published online: 02 January 2024

References

Avet, F., Snellings, R., Diaz, A. A., Haha, M. B., & Scrivener, K. (2016). Development of a new rapid, relevant and reliable (R3) test method to evaluate the pozzolanic reactivity of calcined kaolinitic clays. *Cement and Concrete Research, 85*, 1–11.

Christophliemk, P. (1989). *Henkel Kommanditgesellschaft, Verfahren zur kontinuierlichen Umwandlung von Metakaolin in feinstteiliges zeolithisches Natriumaluminiumsilikat.* 0085902B1, 05.04.89 (patent in German)

Damtoft, J. S., Lukasik, J., Herfort, D., Sorrentino, D., & Gartner, E. M. (2008). Sustainable development and climate change initiatives. *Cement and Concrete Research, 38*(2), 115–127.

Dathe, F., Strelnikova, V., Werling, N., Emmerich, K., & Dehn, F. (2021). Influence of lime, calcium silicate and portlandite on alkali activation of calcined common clays. *Open Ceramics, 7*, 100152.

Davidovits, J. (1994). Geopolymers: Man-made rock geosynthesis and the resulting development of very early high strength cement. *Journal of Materials Education, 16*, 91–138.
Davidovits, J. (2011). *Geopolymer Chemistry & Applications* (3rd ed.). Institut Geopolymere.
Emmerich, K. (2011). EMU Notes in Mineralogy: Advances in the Characterization of Industrial Minerals. Vol. 9, G. Christidis, Ed., Mineralogical Society, pp 129–170.
Garg, N., & Skibsted, J. (2016). Pozzolanic reactivity of a calcined interstratified illite/smectite (70/30) clay. *Cement and Concrete Research, 79*, 101–111.
Herrmann, A., König, A., & Dehn, F. (2015). *Proposal for the classification of alkali-activated binders and Geopolymer binders*. Cement International.
Pacheco-Torgal, F., Castro-Gome, J., & Jalali, S. (2008). Alkali-activated binders: A review Part 1. Historical background, terminology, reaction mechanisms and hydration products. *Construction and Building Materials, 22*, 1305–1314.
Prost, R., Dameme, A., Huard, E., Driard, J., & Leydecker, J. P. (1989). Infrared Study of Structural OH in Kaolinite, Dickite, Nacrite, and Poorly Crystalline Kaolinite at 5 to 600 K. *Clay and Clay Minerals, 37*, 464–468.
Provis, J. L., & van Deventer, J. S. J. (2014). *Alkali-activated materials, State-of-the-Art report, RILEM TC 224-AAM*. Springer.
Slaty, F., Khoury, H., Wastiels, J., & Rahier, H. (2013). Characterization of alkali activated kaolinitic clay. *Applied Clay Science, 75–76*, 120–125.
White, C. E., Provis, J. L., Riley, D. P., Proffen, T., Perander, L. M., & van Deventer, J. S. J. (2012). *Characterization and description of the structure of metakaolin by total scattering, density functional theory, and X-ray spectroscopy. Concrete Repair, Rehabilitation and Retrofitting III*. Taylor & Francis Group.
Xu, H., & van Deventer, J. S. J. (2000). The geopolymerisation of alumino-silicate minerals. *International Journal of Mineral Processing, 59*, 247–266.

Publisher's Note

Felix Dathe is a PhD student in the group of Prof. F. Dehn at the Karlsruhe Institute of Technology.

Frank Dehn is Professor in civil engineering at the Karlsruhe Institute of Technology.

9.3 Original publication concerning chapter 5

Open Ceramics 7 (2021) 100152

Contents lists available at ScienceDirect

Open Ceramics

journal homepage: www.editorialmanager.com/oceram

Influence of lime, calcium silicate and portlandite on alkali activation of calcined common clays

Felix Dathe [a], Vera Strelnikova [a], Nadja Werling [b], Katja Emmerich [b], Frank Dehn [a,*]

[a] Institute for Concrete Structures and Building Materials, Karlsruhe Institute for Technology (KIT), Gotthard-Franz-Straße 3, 76131 Karlsruhe, Germany
[b] Competence Center for Material Moisture, Karlsruhe Institute of Technology (KIT), Hermann-von-Helmholtz-Platz 1, 76344, Eggenstein-Leopoldshafen, Germany

ARTICLE INFO

Keywords:
Alkali activation
Geopolymers
Alkali-activated binders
Common clays
Calcium oxide

ABSTRACT

The application of calcite rich common clays has marked impact on the formation of alkali-activated binders. Experiments have shown that the carbonate decomposition can be well controlled via the calcination procedure, whereby the majority of the decomposition and the subsequent CO_2 release occurs above the calcination temperature of 750 °C. The decarbonation of the calcite can mostly be separated from the dehydroxylation of the layered silicates. Depending on the composition of the raw clay material, the $CaCO_3$ decomposition leads either to the formation of lime or other Ca rich minerals. The mechanical properties of the alkali-activated binders were investigated and despite the very low amounts of layered silicates of the clay raw materials and the high content of unreactive minerals, compressive strengths of above 20 MPa of the mortars could be obtained. The presence of lime in calcined clays up to an adequate amount has a positive effect on post-solidification and the carbonation resistance of the mortars.

1. Introduction

Recently, geopolymer (GP) and alkali-activated binders (AAB) have attracted a great deal of attention in research as alternative to conventional binding materials [1]. In contrast to the state-of-the-art construction material cement, the CO_2 footprint can be tremendously reduced through the application of such alternative binders in the field of civil engineering.

Both geopolymers and alkali-activated binders can be obtained from condensation reactions of Si and Al-rich precursors in the presence of a base. This process is also referred to as alkali activation. The transition from a geopolymer to an alkali-activated binder depends strongly on the soluble Ca content of the raw material, since this is crucial for the formation of different amorphous phases, such as N-A-S-H (low Ca content), C-A-S-H, C-(N)-A-S-H, and C–S–H(I) (very high Ca and low Al content) [2]. The nature of these amorphous phases is very complex and key to ongoing studies [3]. In general, GPs are considered as Ca-poor AABs with a high Al and Si content and whereas products resulting from fly ash with more than 7 wt% of CaO (according ASTM C618, type F) or 10 wt% CaO (according to EN 450–1), respectively, are classified as AAB, a lower calcium content is thought to result in the formation of a geopolymer. Further classification criteria are based on the Ca content within the crystallographic structure of the reaction products (<20 wt% CaO → geopolymer [4]) or the performance of the concretes/mortars (<10 wt% CaO → geopolymer [5,6]).

For the production of alkali-activated binders, usually industrial by-products, such as fly ash (FA) and ground-granulated blast-furnace slag (GGBS), have been used. The exploitation of these industrial by-products for the production of construction materials has been emphasised recently, especially with respect to a circular economy [7]. However, the availability of fly ash and slag in the European area is limited. This is mainly due to the continuous decrease of coal production and mining in the context of the energy revolution and the use of sustainable energy resources. In addition, the amount of ground-granulated blast-furnace slag lag from iron production cannot cover the global demand for mineral binders.

For these reasons, common clays have been investigated as precursors for the production of alkali-activated binders and as substitute in conventional cementitious systems with the ultimate aim of decreasing the amount of required cement clinker [8]. The term common clays is referring to structural clay products, which are fine grained and typically exhibit plastic behaviour when exposed to water [9] The main benefit of using common clays as precursors for alternative binders is the great availability since clay deposits are distributed widely around the globe. A

* Corresponding author.
E-mail address: frank.dehn@kit.edu (F. Dehn).

https://doi.org/10.1016/j.oceram.2021.100152
Received 30 December 2020; Received in revised form 18 June 2021; Accepted 21 June 2021
Available online 23 June 2021

further advantage of using clays for the GP production, are the moderate temperatures in the range of 700 °C–850 °C, which are required for the calcination. Consequently, only H_2O is released by the decomposing of the clay minerals and no CO_2 is formed as by product during the thermal treatment. The calcium-poor geopolymer binders, resulting from the alkali activation of these calcined clays, are very different from conventional cementitious systems in terms of their mineralogical properties and their microstructure. The very high thermal stability, the resistance towards acids [10–14] and the good mechanical performance [2,15,16] are particularly worth mentioning here.

Despite these advantages, the consumption of NaOH and the therewith-associated rapid decrease of pH of the binder during the condensation reaction is challenging since the basicity of binders is one of the most important material parameters in concrete technology. To protect the steel reinforcement of corrosion processes, a constant pH value above 11 is required to maintain the durability of the structure.

In ordinary Portland cements, the basicity results from the hydration product portlandite ($Ca(OH)_2$). The formation of $Ca(OH)_2$ in the microstructure of the cement will automatically stabilise the pH value at a constant level above 13 [17,18]. However, since during the hardening process of alkali-activated binders no portlandite is formed and the generation of sodium carbonates from sodium hydroxide through the presence of CO_2 in the air takes place [19], the basicity of the binder is reduced [20]. The consumption of NaOH and the thereof resulting reduction in the pH value influences in the corrosion of steel reinforcement [21–23].

As part of this study, calcite rich common clays were investigated as precursors for alkali-activated binders. Earlier studies focused almost exclusively on the utilisation of kaolin-rich deposits, which contain only very low amounts of calcium carbonate [24]. However, since carbonates, such as calcite and dolomite, are often geologically associated with layered silicates, the investigation of calcite rich common clays to produce AABs seems logical. Spurred by this, the author's attention in this area has turned towards the exploration of calcite rich common clays and their alkali activation. To investigate the influence of calcite on the alkali activation, the calcination temperature has been varied and the formation of CaO and the impact on the AAB properties have been explored. In that sense, the mechanical properties, such as the compressive and tensile strengths, of specimens made of alkali-activated common clays, have been measured. The investigation on calcium carbonate bearing clays for alkali-activation leads us to the grey area between the calcium-free geopolymers and calcium-rich alkali-activated binders and all because of the low solubility of the calcium carbonate and the high reactivity of lime.

In addition, the carbonation resistance has been looked at in detail, since through the formation of CaO from $CaCO_3$, an internal buffer is formed, which can react with the CO_2 from the air and consequently counteracts the-afore mentioned reduction in pH value.

2. Materials and methods

2.1. Raw materials

As part of this study two naturally occurring common clays were used, namely one clay from the Rhine Graben (Clay1) and one from a clay pit in central Germany (Clay2), both clays are secondary clay deposits. As a reference material (denoted as Refclay), a kaolin with a high purity of kaolinite from Hampshire UK mixed with 25 wt% $CaCO_3$ was utilised. For the reference materials pulverised $CaCO_3$ with a purity of >98.5% and a grainsize d_{50} of 1 μm as well as pulverised $Ca(OH)_2$ with a purity > 96% were selected (Carl Roth GmbH & Co.KG, Karlsruhe, Germany). All materials were milled and sieved to a grainsize below 90 μm and the particle sizes were determined by a particle size Analyser CILAS 1064 (LG), (3p instruments, Odelzhausen, Germany). The mineral composition of the two common clays was determined via powder X-ray diffraction (XRD) and X-ray fluorescence (XRF) analyses (Table 1 and Table 2).

As activators, a saturated NaOH solution with a concentration of 19.05 mol/L (50 wt%) and sodium silica solution Betol39T were blended. The applied water glass is based on a solution of sodium silicate with a solute concentration of 34.5 wt% and a molar ratio of SiO_2 and Na_2O of 3.4 (Woellner, Ludwigshafen, Germany).

2.2. Analytical techniques

2.2.1. Powder X-ray diffraction (XRD)

For the powder X-ray diffraction analysis a D8 Advance diffractometer (Bruker GmbH Karlsruhe, Germany) with a Lynxeye Detector (5° opening angle) was used. Experiments were carried out with Copper Kα radiation in a 2θ area between 5 and 70° in steps by 0.02° with a scanning time of 0.2 s. The quantitative analysis was carried out with the software PROFEX Version 4.1.0, by using an internal standard of 10 wt% corundum.

2.2.2. X-ray fluorescence (XRF)

The elementary composition was determined using a S4 Explorer for the raw clay and the surface of the AAB specimens investigated by a M4 Tornado (Bruker GmbH Karlsruhe, Germany) using energy dispersive X-ray fluorescence (XRF) spectrometer.

2.2.3. Simultaneous thermal analysis (STA)

About 100 mg of the raw materials were heated up to 1000 °C with a heating rate of 10 K/min under nitrogen atmosphere in corundum crucible, using a STA 409 apparatus (Netzsch, Selb, Germany).

2.2.4. Simultaneous thermal analysis (STA) coupled Mass spectrometry (MS)

About 100 mg of the raw materials were heated up to 1000 °C with a heating rate of 10 K/min under nitrogen (50 mL/min)/synthetic air (25 mL/min) atmosphere (Jupiter 449, Netzsch, Selb, Germany). The coupled mass spectrometer was a Quadrupol 409 (Aeolos, Netzsch, Selb, Deutschland).

2.3. Calcination

100 g of each clay were calcined at different temperatures in a laboratory muffle furnace (Heraeus Instruments, Hanau, Germany). Based on the STA results, one of the following temperatures 650, 700, 750, 800 and 850 °C was selected. These temperatures are based on the decomposition of the carbonate species and crystallisation of lime or calcium silicates in the clays. The clays were analysed quantitatively and qualitatively via powder XRD after the thermal treatment. After the calcination, the clays were milled with a vibrating mill to destroy the small aggregates that were formed.

Table 1
Proportions (wt.%) of the mineral phases within the common clays and the references clay obtained from powder XRD analysis and particle size from laser granulometric measurements.

	Clay1 Rhine Graben	Clay2 central Germany	Kaolin Hampshire UK
Calcite	25.4 ± 0.5	27.5 ± 0.5	0
Dolomite	4.9 ± 0.5	0	0
Quartz	21.3 ± 0.5	26.5 ± 0.5	3.2 ± 0.5
K-feldspar	2.5 ± 0.8	0	0
Plagioclase	5.3 ± 0.4	3.8 ± 0.8	0
Kaolinite	8.7 ± 1	14.5 ± 1	94.5 ± 1
Muscovite/Illite	16.6 ± 1	15.0 ± 0.5	2.2 ± 0.5
Smectite	6.7 ± 0.4	10.0	0
Microcline	1.7 ± 0.5	0	0
Chlorite	4.8 ± 0.6	2.5 ± 0.5	0
Hematite	0	1.8 ± 0.5	0
Particle size			
d(0,5)% < [μm]	8.5	27.8	9.4

Table 2
Elemental compositions of the raw materials determined by XRF analysis. LOI loss of ignition.

Constituents	SiO_2	Al_2O_3	CaO	Fe_2O_3	MgO	Na_2O	K_2O	LOI
Clay1	44.5	11.5	14.4	4.7	3.1	0.7	2.1	18.0
Clay2	45.3	17.5	15.7	8.1	0.2	1.5	0.8	12.5
Kaolin	44.3	42.9	0.1	0.7	0.1	0.3	0.1	10.5

2.4. Determination of the lime content

The soluble calcium content was determined by the following procedure developed by Franke [25]. Therefore, 50 g of the calcined clay samples were taken and completely sieved to 0.063 μm. Weighted with the accuracy of 0.001 g, 1.0 g of the sieved sample was mixed with 12 mL of ethyl acetoacetate and 80 mL of 2-butanole. The mixture was heated under reflux for 3 h and subsequently filtered. The precipitate was washed with 2-propanole and the washing liquid was combined with the mother liquor. To this clear solution, the indicator (TYP) was added, and the solution was titrated with 0.1 M HCl until a colour change from colourless to yellow occurred. This titration was carried out twice.

2.5. Alkali activation

After the calcination, the clays were mixed with the alkali activator solution and sand. The resulting mortars were then cased based on DIN EN 196–1 [26]. Hereby, two different sample sizes were cased 2*2*8 cm and 4*4*16 cm. For a better workability, the powder grain content of the used CEN standard sand was removed by sieving <125 μm. The mix ratio is shown in Table 3.

The development of the formulation started from the theoretical hypothesis given from Davidovits [27] for the optimal proportion for a geopolymer network. From the former research done on zeolite materials is known that the most stable ratio of silicon to aluminium is 3 to 1 because of the fourfold bonding of Al as energetic unstable coordination sphere. Considering this aspects and calculating with pure metakaolin as precursor, a theoretical optimal proportion of precursor to sodium silicate and sodium hydroxide can be achieved estimating a complete reaction. On the other hand, the practical realization is often difficult due to the different water demand of each calcined clay and the actually reactive amount of metaclay after the calcination process. Several different mixing designs were investigated always with the aim to minimise the activator amount with regard to environmental aspects. The chosen formulation was free of shrinkage cracks, showed good setting time and the specimens did not show efflorescence on the surface. However, a certain amount of activator had to be added to achieve an adequate workability for constructional applications which was determined via the slump test.

The portlandite containing metakaolin mortar "$Ca(OH)_2$ Metakaolin Mortar" was cased with the same mix design from the calcined kaolin clay from the UK (Kaolin). There for 10 wt% of the metakaolin was replaced by portlandite $Ca(OH)_2$.

2.6. Determination of the physical properties

Like in DIN EN 196–1 [26] described, the fresh mortars were tested for their slump, density and solidification time based on DIN EN 196–3:2017–03 [28]. All three clays show a comparable water demand, so that the water binder ratio of 1:1 led to a stiff fresh mortar with a resulting slump test around 15–20 cm. All samples were demoulded 24h after casting and stored wrapped in foil at 65% relative humidity and 20 °C until further tests were carried out. The compressive and flexural strengths were measured 7 and 28 days after casting on a ToniPRAX testing station Model 2031 (Toni Technik, Germany).

Table 3
Alkali activation procedure.

Mortar	Alumosilicate precursor calc. clay (750 °C; 850 °C)	Activator solution Betol39T + NaOH (50 wt%)	CEN standard sand 125 μm 2 mm
Mix ratio	450 g	450 g Betol39T, 225g NaOH (162 g sodium silicate, 112.5 g NaOH, 400.5 g H_2O)	1350 g

2.7. pH value

The hardened mortars were ground and powdered. 5 g of this powder <90 μm, were suspended in 50 mL distilled water and the pH value of this suspension was measured with a pH electrode.

2.8. Carbonation tests

Based on EN 13295:2004[29], a accelerated carbonation testing was performed on 4*4*16 cm mortar pricks after 7 days of curing wrapped in foil at 65% relative humidity (RH) and 20 °C. The specimens were transferred to a carbonation cabinet, with an atmosphere of 2% CO_2 atmosphere and 65% RH. After a certain time of CO_2 exposure, the depths of carbonation were determined by cracking the specimens and spraying a 1% phenolphthalein solution on the freshly broken surface. After 60 s, the carbonation depth was measured on four sides of the specimens and an average value was calculated. Hereby it became obvious, that the carbonation depth was not dependent on the determination time. Similar observations were already reported by Gluth et al. [1].

3. Results and discussion

3.1. Characterisation of the raw materials

The two clays and the reference material were analysed by simultaneous thermal analysis (STA, Fig. 1). During the STA experiments, different phase transitions were observed. At around 100 °C the loss of water bound in the materials can be observed. All three clays showed a dehydroxylation of the clay minerals, especially the dehydroxylation of kaolinite, around 520 °C. However, differential scanning calorimetry (DSC) and the thermogravimetric analysis (TG) of this decomposition process are overlapping with the dehydroxylation of the minerals. The CO_2, formed by the decomposition of dolomite, could be detected starting at 700 °C by STA coupled to a mass spectrometer (see supporting information) [30]. Further, mass losses starting at around 700 °C occurred, which result from the decomposition of the dolomite and calcite in the raw materials. At temperatures above 850 °C, all carbonates were decomposed. Afterwards no further mass losses could be observed by TG. However, for Clay1 and Clay2 the formation of a high temperature phase could be observed at 902 °C via differential scanning calorimetry and for the reference clay the formation of spinel phase at high temperatures consisting of Si and Al could be witnessed at 994 °C.

To gain further insight into the before described phase transitions, the clays were calcined at different temperatures (650, 700, 750, 800, 850, 950 °C) and the resulting materials were analysed via powder X-ray diffraction (Fig. 2). Clay1 consists of a broad range of minerals and the calcination at 650 °C results in the disappearance of kaolinite and dolomite. Nevertheless, still a strong reflex, which can be attributed to calcite, can be observed. When Clay1 is calcined at higher temperatures,

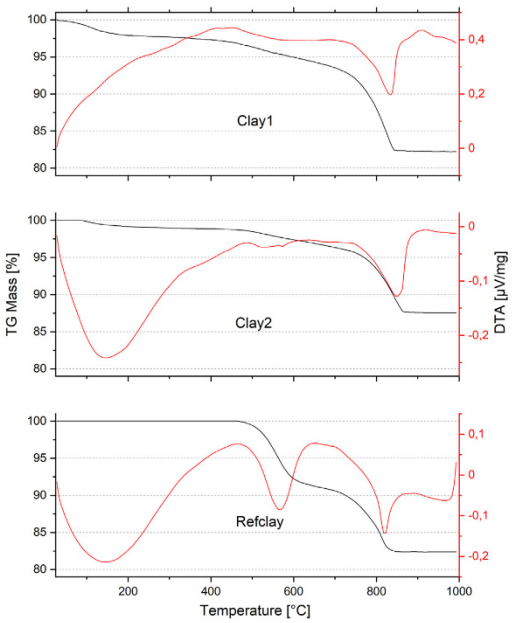

Fig. 1. STA measurements of the three investigated clays heated from room temperature to 1000 °C; Sample weight 100 mg, atmosphere 75 ml/min N_2.

the intensity of the calcite reflex is decreased, however, only very little recrystallisation of calcite to lime does occur even at a calcination temperature of 850 °C. With Rietveld analysis only a lime content of 2 wt% could be determined. The calcium oxide within the clay (14.4 wt% in the raw material) forms most likely an insoluble amorphous phase during the thermal treatment, which is not detectable via powder X-ray diffraction.

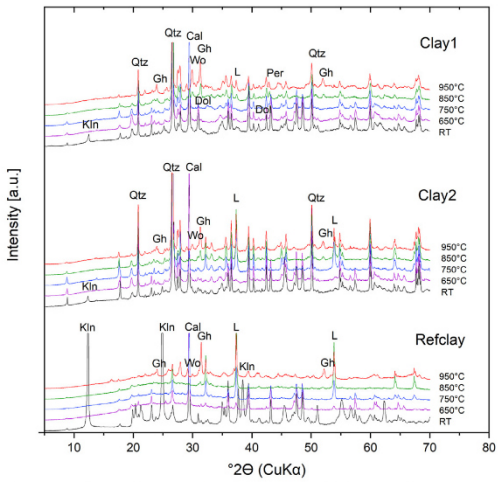

Qtz Quartz; Cal Calcite; L Lime; Kln Kaolinite; Gh Gehlenite; Wo Wollastonite; Dol Dolomite; Per Periclase

Fig. 2. Powder X-ray diffractograms of the two clays and the reference material, which were calcined at different temperatures (RT, 650, 750, 850, 950 °C).

This is confirmed by the fact, that when Clay1 is calcined at temperatures above 902 °C, different calcium minerals, such as Gehlenite ($Ca_2Al[AlSiO_7]$) and Wollastonite ($CaSiO_3$) can be observed. The transition of the Calcite to Gehlenite and Wollastonite via an amorphous transition state is favoured over the formation of crystalline lime. In addition, the variation of the calcination duration could not change the outcome of the powder diffraction experiments.

In the case of Clay2, the decomposition of calcite starting at 750 °C leads mainly to the formation of lime 10 wt% (15.7 wt% in the raw material). However, again not the whole amount of calcite is converted into lime. At 850 °C gehlenite and wollastonite can already be observed, which shows that not all the calcium is bound in the form of crystalline lime after the calcination. At higher temperatures above 950 °C the lime reacts further with the aluminosilicate to form more gehlenite.

For the reference clay, kaolinite is decomposing when the material is calcined at temperatures in the range of 650–750 °C. At a calcination temperature of 850 °C the complete decomposition of calcite to lime can be observed. When the Refclay is heated up further to 950 °C, the lime and the amorphous metakaolin forms gehlenite ($Ca_2Al[AlSiO_7]$). Also, small reflexes belonging to wollastonite ($CaSiO_3$) can be detected.

The information gathered by powder XRD is underlined by the measurement of soluble free calcium in the calcined clays according to the method described by Franke [25]. The results are depicted in Fig. 3. It becomes obvious, that the soluble content of calcium follows different trends for the three clays. Whereas for Clay1 with 14.4 wt% CaO in the raw material only 1.7 wt% calcium oxide is soluble after the complete decarbonation of the calcite, in Clay2 9.3 wt% out of 15.7 wt% in the at 850 °C calcined material are soluble. In the case of the reference clay, consisting of 14 wt% CaO in the raw material, a soluble CaO content of 13.6 wt% was determined.

3.2. Exploration of the mortars

Alkali activations of the calcined common clays and the reference kaolin were carried out to obtain mortars prisms. Hereby it has to be mentioned that CaO is quite reactive and reacts with water to form $Ca(OH)_2$ with an exothermic reaction enthalpy of 65 kJ/mol. This high exothermic heat release may influence hardening process and leads to changes in the mechanical strength development. The compressive strengths of these specimens were analysed depending on the calcination temperature of the clays 28 days after casting (Fig. 4). All three mortars show an enhancement of the compressive strength until a calcination

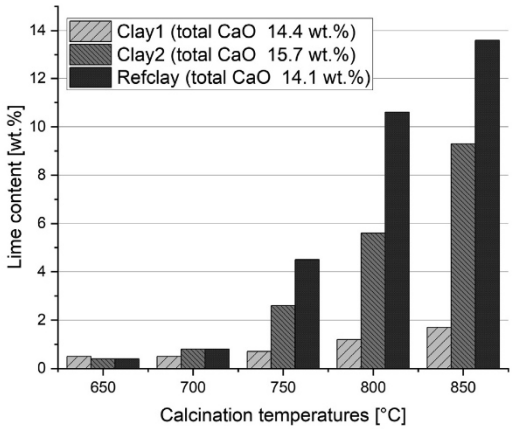

Fig. 3. Calcium oxide content depending on the calcination temperatures. The soluble CaO content was determined according to Franke et al. [25].

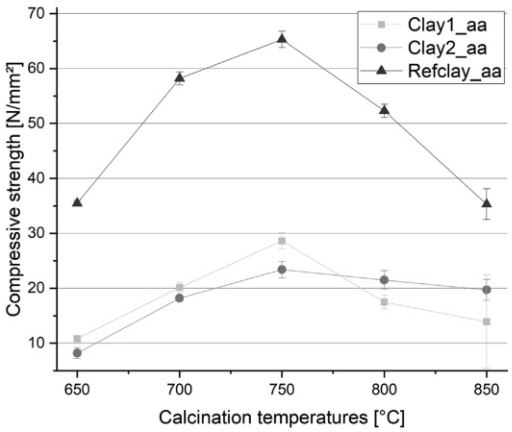

Fig. 4. Compressive strengths of the two alkali activated clays and the alkali activated reference clays depending on the calcination temperature. Strengths were measured 28 days after casting.

temperature of 750 °C. Hereby a maximum compressive strength of 65.3 MPa could be obtained for Refclay, whereas compressive strengths of 28.6 MPa for Clay1 and 23.4 MPa for Clay2 were measured. The reason for the lower compressive strengths of the clays, in comparison with the reference clay, is the lower amount of reactive layer silicates, which can be calcined and converted into the strength giving N-A-S-H phases. Whereas the reference clay contains 94.5 wt% kaolinite, Clay1 consists of 8.9 wt% and Clay2 14.5 wt% kaolinite. When the clays are calcined at temperatures above 750 °C a tremendous decrease of compressive strength can be witnessed. For that reason, the optimal calcination temperature for the investigated clays was chosen to be 750 °C. At this temperature, that CO_2 release is quite low and the mechanical properties are optimal considering a constructional application.

Comparable calcite-free clays show usually a very similar increase of the compressive strength up to calcination temperatures of 750 °C. However, such calcite-free clays do not exhibit a significant loss in compressive strengths in temperature ranges between 750 °C and 900 °C. Only when calcination temperatures above 900 °C are applied, a decrease in compressive strength is observed for calcite-free clays, due to the formation of unreactive spinels formed from the metaclay minerals [31]. The observed loss of compressive strength up to 50% is therefore a direct consequence of the presence of high calcium contents, since Ca species influence the hardening process of the binder paste.

Based on the results of the compressive strengths in dependence of the calcination temperature, only clays calcined at 750 °C and 850 °C were considered for further testing.

During the casting of the specimens, also the properties of the fresh mortar properties were explored. There was a major change in workability and the solidification time observed depending on the calcination temperature of the clays.

With constant activator/clay ratio for the alkali activation, the workability of the mortars is clearly increased for all three clays when the calcination temperature is enhanced. This is based on the fact, that the particle size is enhanced with increasing calcination temperature, as laser granulometric measurements have shown (Table 4). This leads to a reduced water consumption and consequently to a higher flow spread of the fresh mortars. As shown in Table 4, the slump test results of all three materials were significantly increased.

Especially for the mortar cased from Clay1 calcined at 850 °C, an inhomogeneous solidification was observed, whereby the softer binder covers solidified areas. This inhomogeneous solidification also leads to a high standard deviation of the obtained compressive strengths (Fig. 6).

To study the inhomogeneous solidification further, the mortars casted of Clay1 were analysed in more detail by powder X-ray diffraction and micro x-ray fluorescence. Thereby it could be shown, that two phases were formed with very different crystallographic and mechanical properties (Fig. 5). In the hard areas crystalline sodium silicate hydrate (Na_2SiO_3 x H_2O) crystallised (Fig. 6). This observation can most likely be attributed to the fact that the activator solution of Betol39T does not react with the amorphous clay minerals to form N-A-S-H or C-A-S-H phases, but directly crystallises and forms Na_2SiO_3. This leads to a local inhomogeneous distribution of aluminium and calcium as shown in Fig. 5.

The compressive strength development over the first 28 days (Fig. 7) shows that there is a significant post solidification from 7 days to 28 days. Such a development is typical for cementitious systems or slag based AABs, since a reaction is occurring through which strengthening crystalline phases, such as calcium silicate hydrate (CSH) phases, are formed. Also in the case of the calcite containing clays, the post solidification could be due to the formation of CSH phases. This assumption is supported by the appearance of the typical reflex of CSH phases in the XRD of the reference clay after six days (Fig. 9). In contrast, for alkali-activated calcite free clays, which form N-A-S-H phases, usually no major post solidification can be observed over time (see Fig. 7).

3.3. Lime consumption

The solidified binder paste was analysed by powder XRD 7 days after casting (Fig. 8). These investigations show that the calcite stays untouched by the activation process. In addition, a lot of other minerals such as Quartz, Albite, Hematite and Muscovite show an inert behaviour. The binder paste of Clay2 calcined at 850 °C shows no Ca species in crystalline form, such as lime. This finding points towards the fact, that Ca is taking part in the alkali activation reaction and is consumed during this reaction.

A similar behaviour can also be observed for the alkali-activated reference clay (Fig. 9). Again, CaO in the binder is consumed over the time and Ca species are implemented into amorphous networks. Further, the beginning formation of calcium silicate hydrate phases can be observed.

3.4. Carbonation resistance

Since measurements of the pH values of the ground mortars have shown higher values than expected (Fig. 10), the question arose whether the CaO within the mortar can protect the specimen from carbonation, similar to the role of $Ca(OH)_2$ in concrete systems.

As it is shown in Fig. 9, the pH value inside the mortars is decreased over time. Starting from 14, due to the pure NaOH used for the activation, the pH value is reduced to 10.8 after 90 days for a calcium free metakaolin mortar. In contrast, the investigated calcite containing clays show a higher pH value after 90 days, which was found to be between 12 and 13. Based on these results, accelerated carbonation experiments were carried out (Fig. 10).

For comparison, a reference mortar consisting of pure metakaolin without any calcium content was also investigated, named further as

Table 4
Particle size, slump test and hardening time for 750 °C and 850 °C alkali activated calcined clays.

	Particle size d(0.5)% < [μm] 750 °C → 850 °C	Slump test [cm] 750 °C → 850 °C	Solidification time [h] 750 °C → 850 °C
Clay1_aa	10.5 → 13.5	15,5 → 20	5 → 2
Clay2_aa	30.5 → 35.4	17 → 21.5	6 → 1.5
Refclay_aa	9.4 → 12.1	15.5 → 19.5	4,5 → 2.5

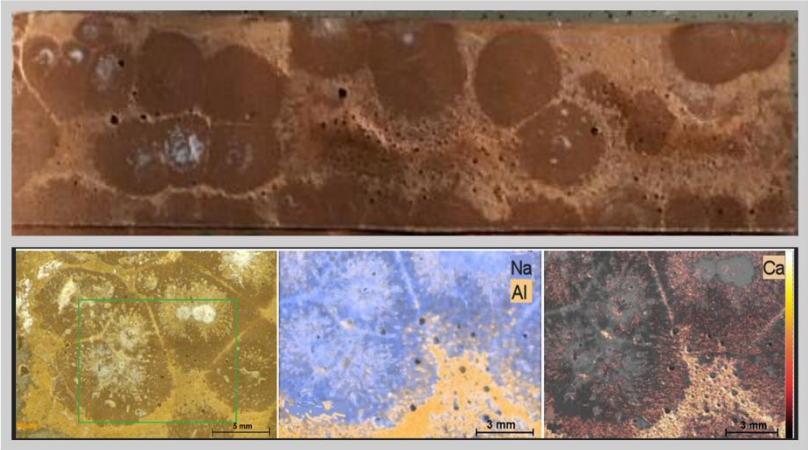

Fig. 5. Top: surface of the mortar specimen of Clay1 aa calcined at 850 °C. Bottom: the inhomogeneous distribution of Al, Na and Ca determined by μXRF.

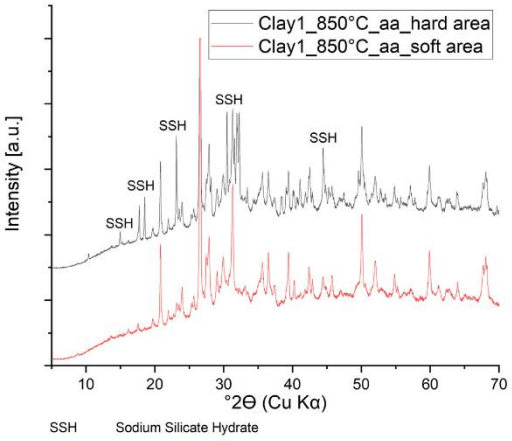

Fig. 6. Powder X-ray diffractograms of the inhomogeneous solidification measured on two different parts of one specimen casted from Clay1, soft and hard area. The Formation of Sodium Silicate Hydrate is shown.

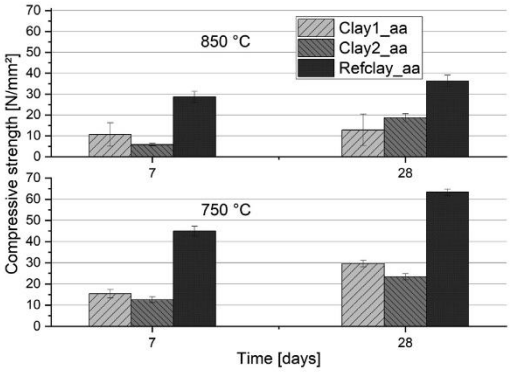

Fig. 7. Post-solidification of the mortar specimens between 7 and 28 days after casting.

"Metakaolin Mortar". It becomes obvious that the carbonation depths of the clays significantly differ from the Ca-free mortar. The carbonation depth was measured by spraying phenolphthalein on the fresh broken cross-section of the specimens. After 90 days the calcium free system shows a carbonation depth of 9.5 mm. In comparison, the three investigated clays show a carbonation depth between 4.8 and 7.2 mm. That underlines that the attack of CO_2 on the specimen is occurring much slower due to an enhanced OH^- content in the pore solution.

3.5. Replacement of lime by portlandite

Based on the before described results, two CaO-free mortars were casted, since very high CaO contents were found to have a negative impact on the solidification time and the compressive strength. More precisely, a standard metakaolin mortar, referred to as "Metakaolin Mortar" and a metakaolin mortar mixed with $Ca(OH)_2$, denoted as "$Ca(OH)_2$ Metakaolin Mortar", were utilised for the investigations. The intention was hereby to implement an alternative Ca-source beside CaO, which does not react that exothermically with water and is therefore thought to be a more unreactive Ca species in the context of this study.

The $Ca(OH)_2$ Metakaolin Mortar was casted replacing 10 wt% of the metakaolin binder by $Ca(OH)_2$. The resulting specimens reached to a compressive strength of 61.3 MPa (Metakaolin Mortar) and 60.7 MPa ($Ca(OH)_2$ Metakaolin mortar). The fresh mortar properties were similar. The investigation of the mechanical properties have shown that the $Ca(OH)_2$ does not have a negative impact on solidification time and the mechanical properties, as seen before for the CaO containing clays. Also, the accelerated carbonation tests of the $Ca(OH)_2$ Metakaolin Mortar show a very high carbonation resistance. Again, as seen before for the calcite containing clays, the soluble Ca is consumed after the alkali activation and most likely imbedded in amorphous Al and Si containing phases. 24 h after casting the XRD investigation show that the crystalline portlandite hast been completely dissolved. The Results of the accelerated carbonation tests are shown in Fig. 11, the admixture of $Ca(OH)_2$

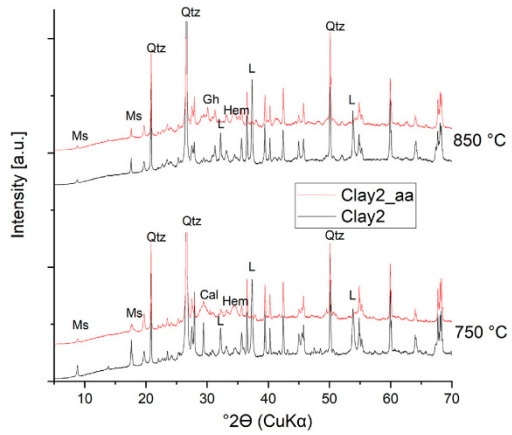

Qtz Quartz; Cal Calcite; L Lime; Gh Gehlenite; Ms Muscovite; Hem Hematite

Fig. 8. Powder X-ray diffractograms of binder paste casted from calcined Clay2 at two different calcination temperatures.

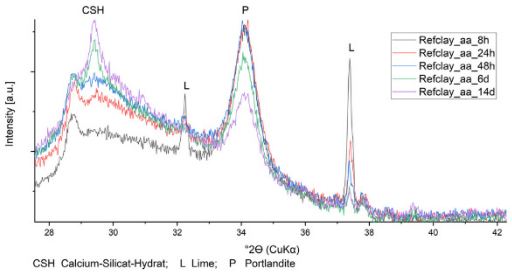

CSH Calcium-Silicat-Hydrat; L Lime; P Portlandite

Fig. 9. Powder X-ray diffractograms of the reference clay mortar showing the CaO consumption over the time of 14 days.

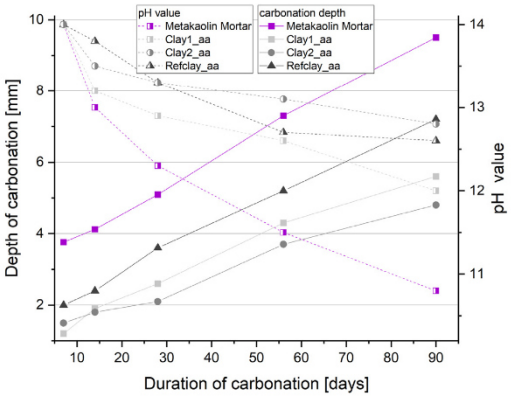

Fig. 10. Accelerated carbonation test 2% CO_2 atmosphere. The depths of carbonation of all three mortars made of the clays calcined at 750 °C and the overall pH value of the hardened mortars are shown. A comparable Ca-free metakaolin mortar is used.

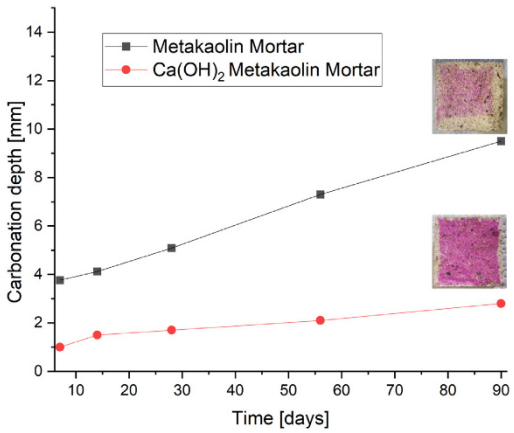

Fig. 11. Carbonation depth of $Ca(OH)_2$ tuned metakaolin mortar. The pictures in the graph show the freshly broken cross sections sprayed with phenolphthalein.

leads to a 3 times higher carbonation resistant compared to the Ca free system. The results show that after 90 days the carbonation depth of the Ca free Metakaolin Mortar is 9.5 mm while the tuned Mortar shows a carbonation depth of 2.8 mm. After 270 days the Ca free specimens are completely carbonated while the tuned $Ca(OH)_2$ Metakaolin Mortar show a carbonation depth of 14 mm.

One observation made on all alkali-activated specimens was that the casting side of the beams always shows a much lower carbonation depth than the sides that were in the mould while casting. The surface of the specimens, that has contact to air while setting, seems to be much denser than the other sides this lowers the diffusion rate of CO_2 in to the specimen. These observations have to be further investigated in the different scientific setup.

4. Conclusions

Calcium-rich common clay deposits have gained more and more attention recently in the field of construction materials, due to the frequent occurrence of such clay deposits. In this context, also the utilisation of calcium rich common clays as precursors for the alkali activation and formation of alternative binders has been considered.

In this work, the authors investigated the influence of calcium compounds on the properties of the alkali-activated binders. Hereby, it could be shown that, if calcium was present in the form of calcite, the two investigated common clays showed expected mechanical properties after calcination and alkali activation. However, if calcite decomposition occurs during the thermal treatment, the properties of the alkali-activated binders are altered tremendously. Although the calcination of Clay1 and Clay2 leads to calcite decomposition, different reaction products are observed. Whereas Clay1 forms an amorphous Ca-rich transition phase, the thermal treatment of Clay2 leads to the formation of crystalline lime. The formation of lime has an enormous impact on the mechanical properties, such as the setting behaviour and the workability of the mortars. With very large lime amounts, undesired damage processes can be observed, such as the crystallisation of sodium silicate, which leads to an inhomogeneous solidification of the binder. Ultimately, this makes the binder not suitable for any application as construction material. However, lime in adequate amounts leads to an increase in basicity and consequently an enhancement of carbonation resistance, which is beneficial for the application of such binders in steel reinforced components. Combined whit the high acid resistance that alkali activated systems

naturally show an application in agriculture buildings could be an interesting place of use.

As part of this work, the authors could show that the calcium carbonate decomposition can be well controlled via the calcination process. It became obvious that for pure calcium carbonate, the carbonate decomposition and the dehydroxylation of the layered silicates can be separated via the temperature. Only for MgCa carbonates, such as dolomite, the decarbonation and dehydroxylation takes place simultaneously within a similar temperature range. Based on this, the desired amount of lime can be adjusted via the calcination of the calcite-rich common clays without any recrystallisation processes of the amorphous layered silicates. The consideration of the free lime content is not only important for the formation of alkali-activated binders but has also to be considered when common clays are applied as additives in conventional cementitious systems.

The mechanical properties of the alkali-activated binders were investigated and despite the low content of layered silicates that are reactive after calcination, and the high content of unreactive minerals (60 wt% quartz, Illite) compressive strengths of above 20 MPa of the mortars could be obtained. Considering the kaolin content in Clay1 with 9 wt% and Clay2 with 15 wt%. We are convinced that after the addition of additives, such as super plasticizers and retarders, and the optimisation of the activator species, compressive strengths of 32.5 MPa similar to standard ordinary Portland cementitious systems are feasible. Such investigations are part of our ongoing studies.

The investigations have confirmed that even low amounts of free lime lead to an increase of basicity and have therefore a positive impact of the carbonation resistance of the mortars. Thereby, no negative effect on the mechanical properties was observed and even a post-solidification of 50% from 7 to 28 days of the mortars were observed for the first time in the field of alkali-activated binders based on common clays.

In ongoing studies, the mechanism of the $CaCO_3$ decomposition in combination with different clay minerals should be clarified further, since it can react either to form lime, as expected, or to form Ca-rich amorphous phases, which leads to an immobilisation of the calcium.

Funding

This project was funded by the Deutsche Forschungsgemeinschaft (From common clay to geopolymer binder - fundamental crystallographic and structural engineering investigations, 325967999).

Declaration of competing interest

The authors declare that they have no known competing financial interests or personal relationships that could have appeared to influence the work reported in this paper.

References

[1] G.J.G. Gluth, K. Arbi, S.A. Bernal, D. Bondar, A. Castel, S. Chithiraputhiran, A. Dehghan, K. Dombrowski-Daube, A. Dubey, V. Ducman, K. Peterson, P. Pipilikaki, S.L.A. Valcke, G. Ye, Y. Zuo, J.L. Provis, RILEM TC 247-DTA round robin test: carbonation and chloride penetration testing of alkali-activated concretes, Mater. Struct. 53 (2020) 1 17, https://doi.org/10.1617/s11527-020-1449-3.

[2] J.L. Provis, J.S.J. van Deventer, Alkali Activated Materials: State-Of-The-Art Report, RILEM TC 224-AAM, Springer Netherlands, Dordrecht, The Netherlands, 2014.

[3] F. Pacheco-Torgal, J. Castro-Gomes, S. Jalali, Alkali-activated binders: a review, Construct. Build. Mater. 22 (2008) 1305 1314, https://doi.org/10.1016/j.conbuildmat.2007.10.015.

[4] A. Buchwald, The Influence of Calcium on the Condensation of (Alumino-) Silicates in Alkali-Activated Binders, Habilitation, Weimar, 2012.

[5] A. Herrmann, A. Koenig, F. Dehn, Structural concrete based on alkali-activated binders: terminology, reaction mechanisms, mix designs and performance, Struct. Concr. 19 (2018) 918 929, https://doi.org/10.1002/suco.201700016.

[6] A. Herrmann, A. Koenig, F. Dehn, Proposal for the classification of alkali-activated binders and Geopolymer binder, Cem. Int. 2015 (2015) 63 69.

[7] e.V. Verband kommunaler Unternehmen, Statusbericht der deutschen Kreislaufwirtschaft, 2018.

[8] A. Trümer, Calcinierte Tone als Puzzolane der Zukunft Von den Rohstoffen bis zur Wirkung im Beton, 2020. Weimar.

[9] H.H. Murray, in: Applied Clay Mineralogy: Occurrences, Processing and Application of Kaolins, Bentonites, Palygorskite-Sepiolite, and Common Clays, first. ed., Elsevier, Amsterdam, 2007.

[10] A. Mehta, R. Siddique, Sulfuric acid resistance of fly ash based geopolymer concrete, Construct. Build. Mater. 146 (2017) 136 143, https://doi.org/10.1016/j.conbuildmat.2017.04.077.

[11] N.K. Lee, H.K. Lee, Influence of the slag content on the chloride and sulfuric acid resistances of alkali-activated fly ash/slag paste, Cement Concr. Compos. 72 (2016) 168 179, https://doi.org/10.1016/j.cemconcomp.2016.06.004.

[12] A. Koenig, A. Herrmann, S. Overmann, F. Dehn, Resistance of alkali-activated binders to organic acid attack: assessment of evaluation criteria and damage mechanisms, Construct. Build. Mater. 151 (2017) 405 413, https://doi.org/10.1016/j.conbuildmat.2017.06.117.

[13] T. Bakharev, J.G. Sanjayan, Y.-B. Cheng, Resistance of alkali-activated slag concrete to acid attack, Cement Concr. Res. 33 (2003) 1607 1611, https://doi.org/10.1016/S0008-8846(03)00125-X.

[14] H.J. Zhuang, H.Y. Zhang, H. Xu, Resistance of geopolymer mortar to acid and chloride attacks, Procedia Eng 210 (2017) 126 131, https://doi.org/10.1016/j.proeng.2017.11.057.

[15] C.-K. Ma, A.Z. Awang, W. Omar, Structural and material performance of geopolymer concrete: a review, Construct. Build. Mater. 186 (2018) 90 102, https://doi.org/10.1016/j.conbuildmat.2018.07.111.

[16] A. Koenig, A. Wuestemann, F. Gatti, L. Rossi, F. Fuchs, D. Fessel, F. Dathe, F. Dehn, F. Minelli, Flexural behaviour of steel and macro-PP fibre reinforced concretes based on alkali-activated binders, Construct. Build. Mater. 211 (2019) 583 593, https://doi.org/10.1016/j.conbuildmat.2019.03.227.

[17] R. Pouhet, M. Cyr, Carbonation in the pore solution of metakaolin-based geopolymer, Cement Concr. Res. 88 (2016) 227 235, https://doi.org/10.1016/j.cemconres.2016.05.008.

[18] P. Hewlett, in: Lea's Chemistry of Cement and Concrete, fourthth ed., Elsevier, Burlington, 2004.

[19] N. Werling, F. Dehn, F. Krause, A. Steudel, R. Schuhmann, K. Emmerich, Solubility OF precursors and carbonation OF WATERGLASS-free geopolymers, Clay Clay Miner. (2020), https://doi.org/10.1007/s42860-020-00096-4.

[20] A. Koenig, H. Mahmoud, O. Baehre, F. Dehn, Alkalinity and its consequences for the performance of steel-reinforced geopolymer materials, Molecules 25 (2020) 2359, https://doi.org/10.3390/molecules25102359.

[21] F. Tittarelli, A. Mobili, C. Giosuè, A. Belli, T. Bellezze, Corrosion behaviour of bare and galvanized steel in geopolymer and Ordinary Portland Cement based mortars with the same strength class exposed to chlorides, Corrosion Sci. 134 (2018) 64 77, https://doi.org/10.1016/j.corsci.2018.02.014.

[22] C. Monticelli, M.E. Natali, A. Balbo, C. Chiavari, F. Zanotto, S. Manzi, M.C. Bignozzi, Corrosion behavior of steel in alkali-activated fly ash mortars in the light of their microstructural, mechanical and chemical characterization, Cement Concr. Res. 80 (2016) 60 68, https://doi.org/10.1016/j.cemconres.2015.11.001.

[23] M. Criado, I. Sobrados, J.M. Bastidas, J. Sanz, Corrosion behaviour of coated steel rebars in carbonated and chloride-contaminated alkali-activated fly ash mortar, Prog. Org. Coating 99 (2016) 11 22, https://doi.org/10.1016/j.porgcoat.2016.04.040.

[24] N. Beuntner, Zur Eignung und Wirkungsweise calcinierter Tone als reaktive Bindemittel-komponente im Zement, 2018. München.

[25] B. Franke, Bestimmung von Calciumoxyd und Calciumhydroxyd neben wasserfreiem und wasserhaltigem Calciumsilikat, Z. Anorg. Allg. Chem. 247 (1941) 180 184, https://doi.org/10.1002/zaac.19412470115.

[26] European Committee for Standardization, Methods of Testing Cement - Part 1, Determination of strength, 2016.

[27] J. Davidovits, in: Geopolymer: Chemistry and Applications, fifth ed., Institut Geopolymere, Saint-Quentin, 2020.

[28] European Committee for Standardization, DIN EN 196-3:2017-03, Prüfverfahren für Zement_- Teil_3: Bestimmung der Erstarrungszeiten und der Raumbeständigkeit; Deutsche Fassung EN_196-3:2016, Beuth Verlag GmbH, Berlin.

[29] European Committee for Standardization, Products and Systems for the Protection and Repair of Concrete Structures Test Methods Determination of Resistance to Carbonation, 2004. Brussels, Belgium.

[30] R.M. McIntosh, J.H. Sharp, F.W. Wilburn, The thermal decomposition of dolomite, Thermochim. Acta 165 (1990) 281 296.

[31] A. Buchwald, M. Hohmann, K. Posern, E. Brendler, The suitability of thermally activated illite/smectite clay as raw material for geopolymer binders, Appl. Clay Sci. 46 (2009) 300 304, https://doi.org/10.1016/j.clay.2009.08.026.

9.4 Original publication concerning chapter 6

minerals

MDPI

Article

The Role of Water Content and Binder to Aggregate Ratio on the Performance of Metakaolin-Based Geopolymer Mortars

Felix Dathe [1,*], Steffen Overmann [2], Andreas Koenig [3,†] and Frank Dehn [1,†]

[1] Institute of Concrete Structures and Building Materials, Karlsruhe Institute of Technology (KIT), Gotthard-Franz-Str. 3, 76131 Karlsruhe, Germany; frank.dehn@kit.edu
[2] Institute of Building Materials Research, RWTH Aachen University, Schinkelstr. 3, 52062 Aachen, Germany; overmann@ibac.rwth-aachen.de
[3] Department of Prosthodontics and Material Sciences, Leipzig University, Liebigstraße 12, 04103 Leipzig, Germany; akoenig@uni-leipzig.de
* Correspondence: felix.dathe@kit.edu
† These authors contributed equally to this work.

Abstract: Geopolymers are in many applications a perfect alternative to standard cements, especially regarding the sustainable development of green building materials. This experimental study therefore deals with the investigation of different factors, such as the water content and the binder to aggregate ratio, and their influence on the workability of fresh mortar and its mechanical properties and porosity on different size scales. Although increasing the water content improved the workability and flow behaviour of the fresh mortar, at the same time, a reduction in compressive strength in particular and a lesser reduction in flexural strength could be demonstrated. This finding can be attributed to an increase in capillary porosity, as demonstrated by capillary water uptake and mercury intrusion porosimetry measurements. At the same time, the increasing water content led to an improved deaeration effect (low air void content) and to initial segregation (see the µXCT measurements). An alternative approach to enhance the compressive and flexural strengths of the mortar specimens is optimization of the binder to aggregate ratio from 1 to 0.25. This study paves the way for a comprehensive understanding of the underlying chemistry of the geopolymerization reaction and is crucial for the development of sustainable alternatives to cementitious systems.

Keywords: geopolymers; CO_2 reduction; common clays; capillary porosity; geopolymerization; alkali activation; metakaolin

Citation: Dathe, F.; Overmann, S.; Koenig, A.; Dehn, F. The Role of Water Content and Binder to Aggregate Ratio on the Performance of Metakaolin-Based Geopolymer Mortars. *Minerals* **2024**, *14*, 823. https://doi.org/10.3390/min14080823

Academic Editors: Dariusz Mierzwiński, Wei-Ting Lin and Paulina Faria

Received: 20 June 2024
Revised: 2 August 2024
Accepted: 10 August 2024
Published: 14 August 2024

1. Introduction

According to the International Energy Agency (IEA) and the United Nations Environment Program (UNEP), the construction area contributes to more than 40% of the energy consumption worldwide and about a third of greenhouse gas emissions [1]. In this context, the production of concrete represents a significant environmental burden, since about 5 to 7% of anthropogenic CO_2 emissions come from global concrete production [2]. For the production of every ton of Portland cement about 1.5 tons of raw materials are needed, while about one ton of CO_2 is released [3]. These numbers are rising every year due to an increased demand for construction materials. The immense amounts of raw materials needed and the high level of CO_2 emissions make cement production extremely resource and energy intensive.

In order to ensure a sustainable development of the construction sector, alternatives to conventional cementitious binders with a low carbon footprint have to be found. In this context, geopolymers have attracted more and more attention [4]. The term geopolymer was established by Davidovits in 1978 and refers to binder materials based on alkali-activated alumosilicates [5,6]. Geopolymers can be obtained from a polymerization reaction of an

alumosilicate material in the presence of an alkaline solution, such as sodium hydroxide, sodium silicate, potassium hydroxide or potassium silicate, as an activator (Figure 1).

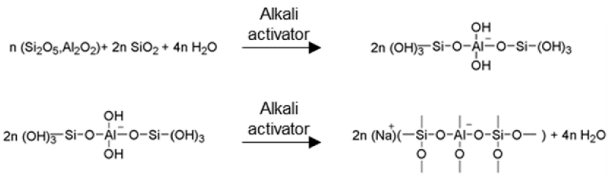

Figure 1. Geopolymerization reaction according to Davidovits [5].

As a starting material for the production of the geopolymer metakaolin, slag or alumosiliceous fly ash are commonly used [7,8]. Metakaolin is a dehydroxylated form of the clay mineral kaolinite and its structure is based on an amorphous (non-crystalline) aluminosilicate network, which can be activated by a base to form a corresponding geopolymer. Recently, also common clays, as widely occurring and cheap resources, have been investigated as raw materials for geopolymer production [9–13]. Such alternative binders based on sustainable resources are also being referred to as "Green Concrete" [14]. In addition to improved sustainability, these mortars/concretes have improved resistance to chemical agents (acids, sulfates) or high temperatures due to their alumosilicate network [15–17].

Despite the fact that geopolymers have been known for almost 50 years, the geopolymerization reaction is not completely understood. It is a very complex reaction that depends on many experimental factors. Consequently, a targeted mixing design to afford defined geopolymers with predictable properties, such as workability or tensile and compressive strengths, is challenging. To overcome this, attempts to rationalize the experimental parameters for the mixing design of metakaolin-based geopolymers, such as the sodium silicate to sodium hydroxide ratio and the alkaline solids to metakaolin ratio, were, for example, reported by Al-Salloum et al. Thereby, it was shown that the workability of the fresh mortars improved with an increased sodium silicate to NaOH ratio until a certain limit, while also the compressive strength was found to be increased [18]. In this context, it was also shown that by using a higher NaOH concentration during the activation, the polymerization degree within the mortar specimens could be increased [19]. The compressive strength of geopolymers was also reported to be improved through the addition of waste, such as pent abrasive powder, which was mainly composed of corundum grains [20]. Down this road, also the addition of dyes, such as bromothymol blue, cresol red, phenolphthalein, and methyl orange, to the geopolymer mixture has been described with the aim to provide colored geopolymers, which are suitable for design and restoration applications. Thereby, it was found that the fresh mortars exhibited a good workability, while there was no significant change in the microstructural 3D network of the geopolymer mortars observed [21].

Apart from these factors, the water content of the mixture and the associated solid to liquid ratio is also crucial, since it not only influences the fresh mortar properties but also the mechanical properties of the final mortar specimens [12]. Water is not only the reaction medium in which the dissolution of the raw materials and the ions takes place but also an integral part of the polymerization reaction itself, since it takes part in the hydrolysis and polycondensation of Al- and Si-containing oligomers [20]. In addition, water has a major influence on the workability of the fresh mortar. As the thickness of the water film on the particles increases, the internal friction is reduced, which results in increased flowability of the fresh mortar. Beside the positive effect of water in the context of the geopolymer formation, it has been reported that the addition of water and the associated reduction in alkalinity of the reaction system [21] can lead to a migration of ions away from the reaction zone. Also, an excess of water might influence the chemical equilibrium of the geopolymerization reaction according to the principle of Le Chatelier and push the equilibrium to the side of the starting materials, which leads to a reduction in

the polymerization rate [22]. This is complicated by the fact that the water is chemically bound to a lesser extent in the geopolymerization process compared to common cement hydration. This leads to the assumption that the porosity in the hardened geopolymer mortar/concrete is more clearly influenced by the water content. Therefore, the addition of water is a balancing act for the successful preparation of geopolymers via alkali solutions.

Although the role of water was investigated in some papers [14,20,23–25], no comprehensive studies using advanced analytic techniques, such as micro X-ray computer tomography, were carried out. In this paper, we therefore studied the alkali activation of metakaolin with the aim of finding a suitable water content and consequently an optimal formulation for the geopolymerization of calcined clay to produce geopolymer-based mortars with low porosity and high compressive as well as tensile flexural strengths. In this context, we also examined the binder to aggregate ratio in detail using various analytic techniques, such as X-ray powder diffraction (XRD), mercury intrusion porosimetry (MIP), and micro X-ray computer tomography (μXCT). This fundamental understanding of the geopolymer chemistry and the rationalization of the factors that can influence the geopolymerization reaction is crucial for the sustainable production of green building materials.

2. Materials and Methods

2.1. Raw Materials

Metakaolin (Metamax®) was purchased from BASF (Ludwigshafen, Germany), while the aqueous NaOH solution (50 wt.% NaOH) was obtained from Carl Roth GmbH & Co. KG (Karlsruhe, Germany). A sodium silicate solution (Betol39T®) from Woellner GmbH (Ludwigshafen, Germany) with a concentration of 34.5 wt.% and a SiO_2 to Na_2O molar ratio of 3.4 was used. Either quartz powder (MILLISIL W3®, Quarzwerke GmbH, Frechen, Germany) or CEN standard sand (0.08–2 mm) according to DIN EN 196-1:2016-11 were used as inert aggregates. The powder X-ray diffractograms of Metamax® and MILLISIL W3® are shown in the Supplementary Material (Figures S1 and S2).

2.2. Sample Preparation

All experiments were carried out under controlled laboratory conditions at 20 °C and 50% relative humidity. The manufacture and casting of the mortar specimens was carried out according to a modified DIN EN 196-1:2016-11 procedure [26]. Based on previous experiments and the successful formation of suitable geopolymer mortars [11], 450 g metakaolin powder was added to 225 g of an aqueous sodium silicate solution. While the mixture was stirred, aqueous sodium hydroxide solution (50 wt.%, 450 g) and water (according to the mixing designs shown in Tables 1 and 2) were added. The corresponding molar ratios are shown in the Supplementary Material (Table S2). Subsequently, CEN standard sand was added to the mixture while stirring. For the investigation of the influence of the binder to aggregate ratio on the workability of the fresh mortar and the strength of the mortar specimens, quartz powder was added as aggregate instead of CEN standard sand. The metakaolin/quartz powder ratio was varied from 100/0 to 20/80. The resulting mortars were then cast in standard prisms ($40 \times 40 \times 160$ mm^3) for the investigation of the influence of water or prisms of $20 \times 20 \times 80$ mm^3 for the investigation of the aggregate addition. The smaller prism size of the latter enabled a timely analysis of a large number of specimens. All samples were demolded 24 h after casting and stored wrapped in foil. The storing of the samples took place under controlled conditions (65% relative humidity and 20 °C) until further tests were carried out.

Table 1. Mixing design for the geopolymers mortars. W/S refers to the water to solid content of the fresh lime and the mortars, to which sand was added.

Code	Additional Water in g	W/S (Fresh Lime)	W/S (Mortar)
GP_Ref	0	0.57	0.20
GP_50	50	0.64	0.22
GP_100	100	0.71	0.25
GP_150	150	0.78	0.27

Table 2. Mixing design for the alkali activation of metakaolin and quartz powder (in g).

Code	Metakaolin	Quartz Powder	Sodium Silicate	50 wt.% NaOH	H_2O from Sodium Silicate and NaOH
GP_100/0	500	0	500	250	445.0
GP_90/10	450	50	450	225	400.5
GP_80/20	400	100	400	200	356.0
GP_70/30	350	150	350	175	311.5
GP_60/40	240	160	240	120	213.6
GP_50/50	200	200	200	100	178.0
GP_40/60	160	240	160	80	142.4
GP_30/70	120	280	120	60	106.8
GP_20/80	80	320	80	40	71.2
GP_20/80 + 20 g H_2O	80	320	80	40	91.2

2.3. Methods

For the powder X-ray diffraction analyses, a D8 Advance Bruker diffractometer with a Lynxeye Detector (Bruker, Ettlingen, Germany) was used. Experiments were carried out with Copper Kα radiation in a 2θ area between 5° and 70° in 0.02° steps with a scanning time of 0.2 s. The powder X-ray diffractograms of the precursor materials (metakaolin and quartz powder) and the mortar specimens (GP_Ref and GP_150) are shown in the Supplementary Material (Figures S1, S2 and S7). The light microscopic determination of the air void content was carried out on polished mortar samples with an Olympus SZX 10 microscope according to DIN EN 480-11:2005-12 [27]. The pore size distributions of all mortar specimens (GP_Ref, GP_50, GP_100, GP_150) according to incident light microscopy are shown in the Supplementary Material (Figure S3). A micro X-ray computer tomograph with a directional X-ray tube FXE 225.99 ($\leq$225 kV, focal spot diameter $\leq$3 mm, tungsten target) by YXLON International GmbH (Hamburg, Germany) and a 2D-detector 1621xN (2.048 × 2.048 pixels, CsI, pitch size 200 × 200 µm^2) by PerkinElmer (Waltham, MA, USA) were used to determine the macro pores and the grain distribution in the GP_Ref, GP_50, GP_100, GP_150 samples (Figure 5 and Figure 6). Measurements were carried out on drill cores of the diameter d = 6.5 mm and height h = 40 mm, which were extracted from the mortar specimens. The macro pore distribution analysis of the experimental data was carried out with software ImageJ 1.47v (National Institute of Health, Bethesda, MD, USA) and VG Studio Max 2.0v (Volume Graphics GmbH, Hamburg, Germany) based on [28]. For the SEM images, a LEO 1530 Gemini Carl Zeiss microscope with a secondary electron detector was applied to investigate the polished and unpolished fragments within the GP_Ref, GP_50, GP_100, and GP_150 samples (Figure 7). For the water absorption measurements, a cube with an edge length of 40 mm of each sample was dried until a mass constancy was reached (24 h, 105 °C). Afterward, the dried cubes were placed in a vessel with 400 mL of water and weighed after 4 h and 24 h to confirm a constant mass of the cubes, which results in a complete saturation of the mortar specimens (GP_Ref, GP_50, GP_100, GP_150) with water to detect open pores. The results are depicted in Figure 3, and based on these experiments, the pores filled with water can be calculated and the water absorption dependent porosities were obtained (Table 4) according to the following equation:

$$\varepsilon_w = \frac{(m_s - m_d)}{\rho_w * V} * 100$$

ε_w = porosity determined for water
m_s = mass of the water saturated specimens
m_d = mass of dried specimens
p_w = density of water
V = sample volume

Nitrogen adsorption measurements of GP_Ref were carried out using a NOVA Touch LX1 provided by Quantachrome under liquid nitrogen cooling to determine the specific surface of the pores with a diameter between 0.35 to 400 nm (Supplementary Material, Figures S4 and S5). For the determination of the pore size distribution of GP_Ref, GP_50, GP_100, and GP_150 via mercury intrusion porosimetry, a Pascal 440 device from Thermo Fisher Scientific was used (Figure 4, Supplementary Material, Figure S6). The additional module 140 (low pressure) could cover the pore radii between 3.6 and 100,000 nm. The measurement was performed on fragments. The compressive and flexural strengths of all mortar specimens, in standard prisms ($40 \times 40 \times 160$ mm^3) for the investigation of the influence of water or prisms of $20 \times 20 \times 80$ mm^3 size for the investigation of the aggregate addition, were determined seven days after their manufacture with a RT 200/10-1s device of the company Testing Bluhm & Feuerherdt according to DIN EN 196-1:2016-11 [26]. The applied loading rate for the determination of the compressive strength was 2400 N/s, whereas a loading rate of 50 N/s was used for the flexural strength. The results are depicted in Figure 9 and Figure 10 as well as in the Supplementary Material (Table S1). The workability of the fresh mortars (GP_Ref, GP_50, GP_100, GP_150) was tested via a flow spread test on a flow table according to DIN EN 1015-3:2007-05 [29] (Table 3). Right after the mixing process, the fresh mortar was placed in a truncated cone (Ø 100 mm) on a Hägermann flow table. After 15 hits, the spread of the fresh mortar was measured in both directions and the average flow spread was calculated.

Table 3. Flow spread test results of the fresh mortars.

Code	Flow Spread in mm	Relative Flow Spread	Consistency
GP_Ref	190	2.6	Plastic mortar
GP_50	245	5.0	Soft mortar
GP_100	275	6.6	Soft mortar
GP_150	>300	8.0	Very soft mortar

3. Results and Discussion

3.1. The Role of the Water Content in the Geopolymerization Process

3.1.1. Workability of the Fresh Mortar

In order to evaluate the workability of the fresh mortar, flow spread tests were carried out after varying the water content of the samples. As shown in Table 3, the flow spread increased with an enhanced water content of the geopolymer mixture. This corresponds to an easier to handle mortar, which is beneficial for the subsequent casting process.

3.1.2. Investigation of the Porosity of Mortar Specimens

The porosity of the mortar specimens was investigated in detail using light-based imaging methods, the examination of the water absorption, low temperature adsorption of nitrogen, mercury intrusion porosimetry and scanning electron microscopy (Figure 2) [30]. In addition to these analytical techniques, we used micro X-ray computer tomography to image micro-structures in three dimensions and to determine the porosity of the mortar specimens [19]. The existence of micropores (pores < 2 nm) within the mortar specimens was ruled out by N_2 adsorption measurements, as shown in the Supplementary Material (Figures S4 and S5).

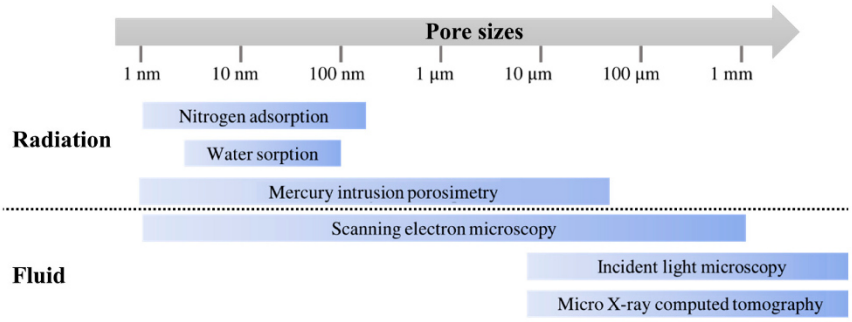

Figure 2. Relevant pore sizes and appropriate analytical methods for their determination.

The porosity of the mortar specimens was determined from the water absorption. During these experiments, the mass difference between dried mortar specimens and mortar specimens that were submerged in water was determined (Figure 3).

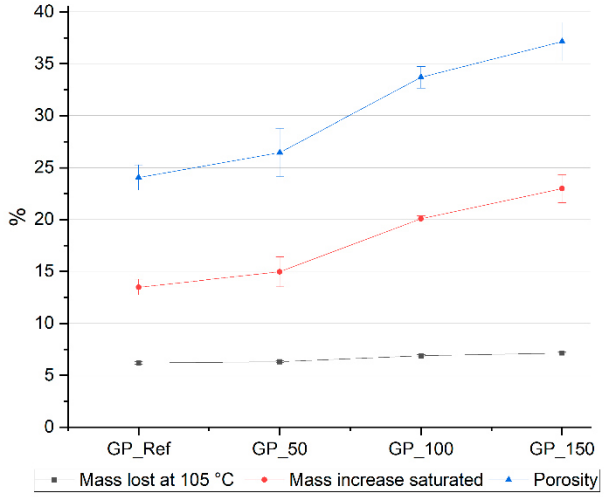

Figure 3. Determination of the water absorption and the porosity via drying and water uptake; mass loss at 105 °C to mass constancy (black); mass increase saturated (red); and calculated porosity (blue).

During the drying process, an almost linear mass loss of about 0.9% is witnessed with increasing water content of the geopolymer mixtures. After the drying process, fine cracks can be observed within the mortar specimens, which can be attributed to the shrinkage of the material and the different expansion coefficients of the various components. For the water uptake, again, an almost linear increase with increasing water content of the geopolymer mixture can be witnessed. The maximum difference amounts to 7.4% and is therefore about 10 times higher than the mass loss detected during the drying process.

Based on these experiments, the volume of the pores filled with water can be calculated and porosities between 24.05% and 35.8% were obtained. As it becomes obvious from Table 4, the porosity increased with increasing water content of the geopolymer mixture.

Table 4. Porosity determined via the investigation of the water absorption measurements.

Code	Porosity by Water Absorption in %
GP_Ref	24.05 ± 1.2
GP_50	26.5 ± 2.3
GP_100	33.7 ± 1.1
GP_150	37.1 ± 1.8

The meso- and macropores of the mortar specimens were analyzed by mercury intrusion porosimetry. The cumulative pore volume, the average pore diameter and the specific surface area obtained from mercury intrusion porosimetry are depicted in Figure 4. For these calculations based on the Washburn-equation [31], 3.050 nm was selected as the upper threshold (Supplementary Material, Figure S6).

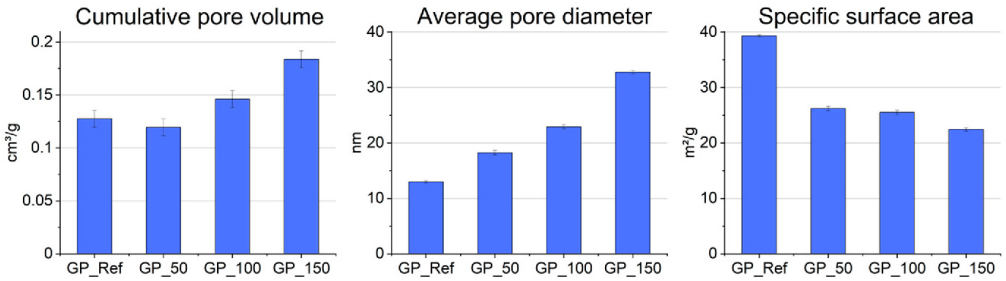

Figure 4. Results of the mercury intrusion porosimetry. Pore volumes are presented in cm^3/g of geopolymer with an error of ±0.008 cm^3, according to [32].

The cumulative pore volumes (Figure 4) and the resulting porosities (Table 5) show an almost linear increase with increasing water content. In cases of the average pore diameter, again, an increase can be witnessed when the water content in the geopolymer mixture is enhanced. While an enhancement of the average pore diameter with increasing water content was witnessed, the specific surface area decreased.

Table 5. Porosities of the mortar specimens determined via mercury intrusion porosimetry.

	Porosity in %	Cumulative Pore Volume in cm^3/g	Average Pore Diameter in nm
GP_Ref	24.2	0.128	13.0
GP_50	23.0	0.120	18.2
GP_100	26.8	0.146	22.9
GP_150	31.5	0.184	32.8

To gain structural information regarding the porosity in the size range of macro pores like air voids (Ø 0.020–10 mm), micro X-ray computer tomography (µXCT) measurements of the mortar specimens were carried out. Also, µXCT gives information about the distribution of the aggregated particles. With the used measurement setup, a resolution of 10 µm was achieved. The results of the µXCT of the drill cores for all mortar specimens are depicted in Figure 5.

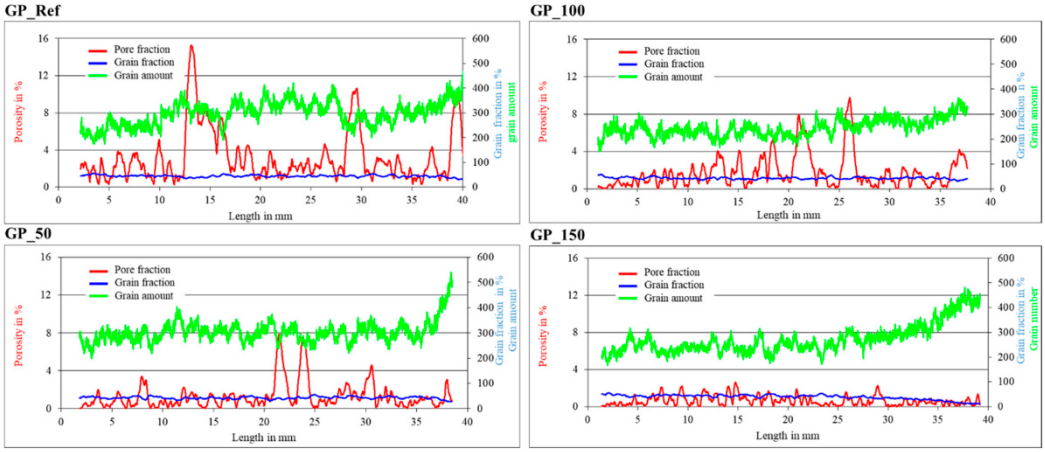

Figure 5. Pore and grain distribution through the cores of the mortar sample prisms obtained via µXCT measurements. The length of 0 mm corresponds to the bottom of the mortar sample prisms.

These results show that in the reference geopolymer mortar and in the mortars to which 50 g and 100 g of water were added, the grain fraction stays constant over the whole length of the drill core. However, the spatially resolved analysis of the drill core of the mortar, to which the highest amount of water (150 g) was added, shows a decrease of the grain fraction starting at a height of 30 mm. This is due to the low viscosity of the fresh mortar of GP_150, which leads to a gravity-related segregation of the grains and to the accumulation of the biggest grains within the bottom area of the drill core.

Obviously, not only the grain fraction is influenced by the water content of the mixture but also the porosity regarding air voids. It becomes clear that mixtures with a lower water content exhibit a higher amount of air voids than samples with a higher water content (Figure 6). A higher amount of air voids can be attributed to the high viscosity of the fresh mortar and the associated worse workability. Similar findings were made in the context of alkali-activated materials based on Sicilian volcanic precursors (i.e., volcanic ash and pumice), although here also the particle size of the applied precursors was shown to be a decisive factor in the porosity of the mortar specimens [33].

The observed porosity trend is inverse to the porosities determined via water absorption and mercury intrusion porosimetry since these techniques always indicated an increase in porosity with an enhanced water content. However, in the case of the µXCT measurements, only air voids that consist of 8 voxels were analyzed (Ø ~20 µm ≈ 8000 µm^3) and no smaller pores can be detected, which explains the different trends in comparison with the other analytical techniques. This finding is also supported by incident light measurements, where GP_Ref shows the highest number of pores over the whole size range as shown in the Supplementary Material (Figure S3).

The microstructures and porosities of the mortar specimens were investigated by scanning electron microscopy (Figure 7). From the images, a heterogeneous distribution of aggregates within the binder matrix becomes obvious. Also, cracks within the specimens can be witnessed, which most likely stem from the drying process. Similar microstructures have been reported for other metakaolin-based geopolymers [18].

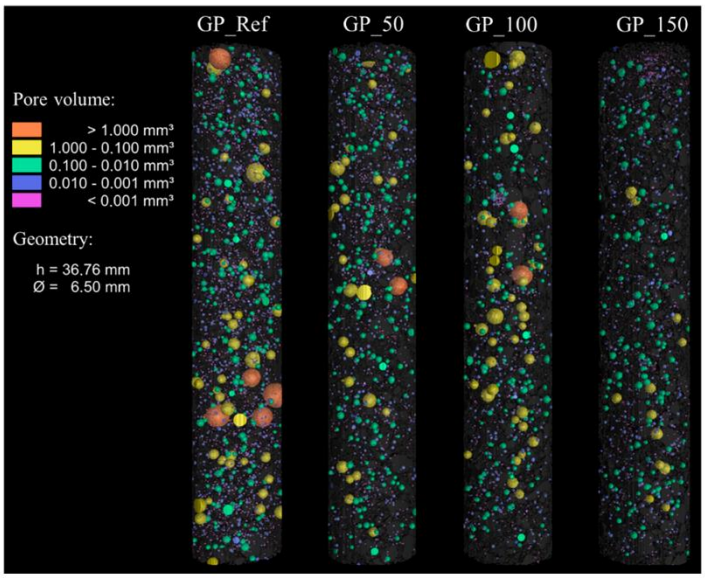

Figure 6. 3D representation of the pore size distribution within the drill core. The drill cores are oriented according to their casting direction, but cut off at about 1.6 mm.

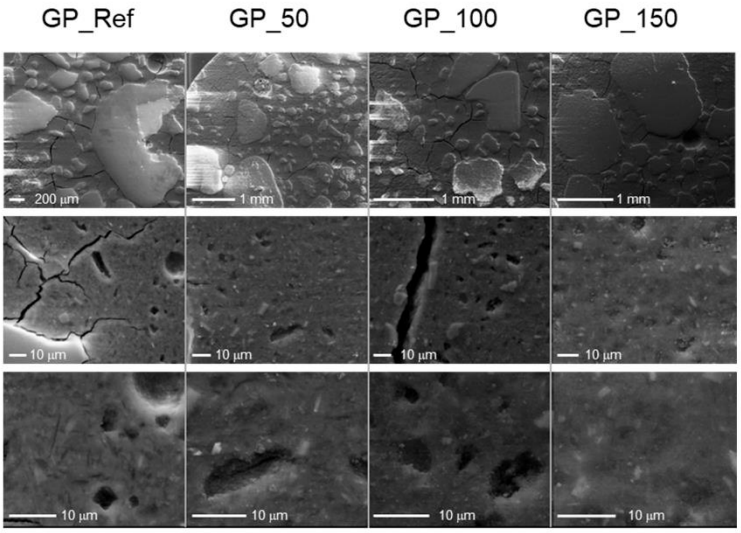

Figure 7. Scanning electron microscopy images of the mortar specimens. From left to right. GP_Ref, GP_50, GP_100, and GP_150. The resolution increases from the top to the bottom.

The mortar specimens GP_Ref and GP_150 were crushed and investigated by powder X-ray diffraction. In the resulting diffractogram (Figure 8), the crystalline phases of quartz, anatase, muscovite and albite can be identified. These phases belong to the aggregate used in the mortar. The geopolymer binder is amorphous and does not lead to any diffraction reflexes in the pattern. You can see clearly that the crystalline composition of GP_Ref and

GP_150 is identical. These results show us that the additional water does not lead to a change in crystallinity and the effect on porosity is due to other mechanisms.

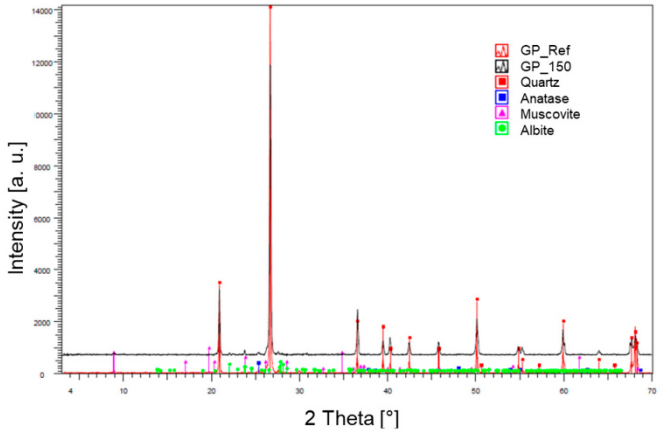

Figure 8. Powder X-ray diffraction of the mortar GP_Ref and GP_150.

3.1.3. Mechanical Properties of the Mortar Specimens

The compressive and flexural strengths of the mortar specimens were determined and it becomes obvious that a higher water content (w/s = 0.27 for mortar) leads to a reduction in the compressive strength (Figure 9). Consequently, the compressive strength is found to be inversely proportional to the water content of the geopolymer mixture, which is similar to observations made for the water-to-solid ratio in other metakaolin-based geopolymers [18] as well as for the water-to-cement ratio in conventional cementitious systems [34]. Similar observations were made for the tensile flexural strength of the mortar specimens. Only the reference mortar showed a slight deviation from this trend, but at the same time the highest standard deviation.

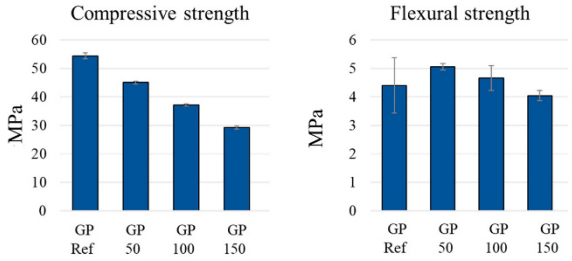

Figure 9. Compressive (6 values per mean value) and flexural (3 values per mean value) strengths with standard deviation of the mortar specimens.

The strength measurements clearly correlate with the porosities of the mortar specimens determined via capillary water uptake and mercury intrusion porosimetry measurements. It becomes obvious that a higher water content within the geopolymer mixture leads to an enhanced porosity of the mortar specimens, which results in a reduction of the compressive and flexural strengths. It is noticeable that the compressive strength decreases significantly more than the flexural strength due to the increasing water content. This behavior is unexpected. Normally, pores are usually compressed in compression testing and in flexural strength they have a reduced tensile cross-sectional area and a crack-initiating effect.

However, a low water content significantly reduces the workability of the fresh mortar, as the flow spread tests carried out have shown. Also, a low water content leads to a high amount of air voids, which were observed via micro X-ray computed tomography (Section 3.1.2 as well as incident light microscopy (see Supporting Information). Therefore, the macro pores have a lower influence than the smaller pores (<20 µm) on the mechanical performance. In order to produce geopolymers with good mechanical properties, the water content should be kept as low as possible.

3.2. The Role of the Binder to Aggregate Ratio

Although an increase in water content in a geopolymer mixture leads to a better workability of the mortar, a clear reduction in the compressive strength and a lesser reduction in the flexural strength was observed. Therefore, an alternative approach, namely the variation of the binder to aggregate ratio, was investigated with the aim of enhancing the workability of the mortar while good strengths of the mortar specimens are maintained. Whereas in the case of GP_Ref, GP,50, GP_100 and GP_150 a fixed amount of CEN sand (1350 g) was added as aggregate, in this section, a systematic study of the ratio variation of metakaolin and quartz powder as aggregate was carried out. In this case, quartz was selected as a non-reactive aggregate in powder form. In order to optimize the formulation of the geopolymer mortar, various binder to aggregate ratios varying between 1.0 and 0.25 were prepared.

Mechanical Properties of the Mortar Specimens

For the investigation of the effect of the quartz powder inclusion in the geopolymer mortars, the compressive and flexural strengths of the mortar specimens were determined depending on the binder to aggregate ratio (Figure 10). It becomes obvious that the geopolymerization of pure metakaolin without the addition of quartz powder results in mortar specimens with a compressive strength of 46.6 MPa and no detectible flexural strength. Very similar strength values were determined for the 90/10, 80/20 and 70/30 binder to aggregate mixtures. However, when the binder to aggregate ratio is reduced and the quartz powder content is increased, an enhancement of the compressive and flexural strengths can be witnessed. The maximum compressive strength of 81.4 MPa was achieved with a 20/80 binder to aggregate ratio. It is known from the development of ultra-high performance and eco-friendly concretes that the partial replacement of the reactive component (cement) by quartz powder can increase the packing density, due to the more finely tuned grain band, and thus the strength [27]. This physical mode of action can apparently be transferred for the metakaolin-based geopolymer since Li et al. demonstrated a similar increase in compressive strength (83/17 ratio) with a heat-treated metakaolin-based geopolymer. When 20 g of additional water is added to the 20/80 mixture, the compressive and flexural strength decrease. This is in complete accordance with the water content results shown before (Section 3.1).

These results are astonishing since the increase in aggregate ratio leads to an improvement of the compressive and flexural strengths of the mortar specimens within the investigated binder to aggregate ratio regime. Similar observations were made for geopolymer concrete made from alkali-activated fly ash, where an enhancement of the flexural strength of geopolymer concrete was observed with an increase in the total aggregate content [28]. Also, an increase in compressive strength has been observed for metakaolin-based geopolymers with a maximum at a 73.8% aggregate content. However, the reported compressive strengths were approximately 20 MPa below the compressive strength observed for the mortar specimens described in this study [18]. Consequently, these experimental findings can be considered as model experiments for the geopolymerization of common clays, since common clays can be considered as natural mixtures of aggregate with metakaolin, with a metakaolin content of below 50%.

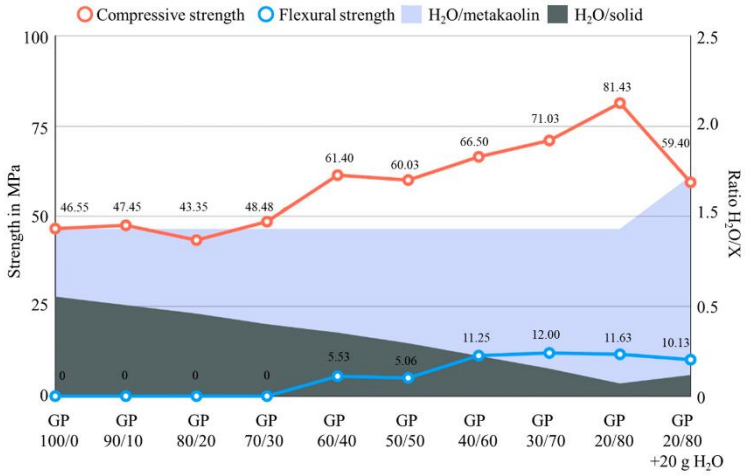

Figure 10. Compressive (six values per mean value) and flexural strengths (three values per mean value) of the mortar specimens depending on the metakaolin to quartz powder ratio.

The rationalization for this experimental observation is difficult, since the binder to aggregate interface within geopolymer binders is still poorly understood, especially at a molecular level. However, only recently, interfacial bonding including Al–O–Si, Na–O and H-bonding, was investigated using molecular dynamics simulations. The simulations have shown that the Si/Al ratio is crucial for the interfacial strength due to a higher degree of interaction and more cross-linking within the geopolymer [35]. In order to increase the interfacial bonding between aggregates and geopolymer binders, it has been shown that the presence of soluble silicates, as Betol39T® in the case of this study, in the initial activating solution is beneficial [36]. However, at this point, it must be mentioned that the experimental observations are highly dependent on the raw materials used for the geopolymer production [37,38]. Studies on the binder to aggregate ratio using high calcium fly ash together with sodium metasilicate as binder and sand as aggregate have, for example, shown an inverse effect, where a reduction of the strength with increasing aggregate proportion was observed [39]. Similar observations were made for the alkali activation of low grade kaolin [40].

4. Conclusions

Geopolymers have gained more and more attention when trying to find sustainable alternatives to hydraulic binders (e.g., normal cements based on Portland cement clinker), especially with respect to a desired reduction of greenhouse gas emissions. In this work, therefore, the influence of different factors, such as the water content and the binder to aggregate ratio, on the formation of geopolymer mortars were investigated with the aim of identifying an optimal mixing design. The main intention was hereby to combine a good workability of the fresh mortar with low porosity and high compressive as well as flexural strength of the resulting mortar specimens. To achieve this, we cast mortar specimens using different ratios of metakaolin and water ranging from water to solid contents of the fresh lime of 0.57 to 0.78. The porosity of these specimens was then evaluated by water absorption measurements, mercury intrusion porosimetry, micro X-ray computer tomography and scanning electron microscopy. Subsequently, the mechanical properties, such as the tensile and compressive strengths, of the mortars were determined. To investigate the impact of the addition of aggregates, such as quartz powder, the binder to aggregate ratio was varied from 100:0 to 20:80, referring to the metakaolin to quartz powder ratio.

The major conclusions derived from the experimental study can be summarized as follows:

- A higher water content of the geopolymer mixture leads to a better workability, as indicated by the increase in flow spread of the fresh mortar, from 190 mm for GP-Ref to over 300 mm for GP_150. This enhanced workability is also indicated by the increase of relative flow spread from 2.6 for GP_Ref to 8.0 for GP_150. Simultaneously, the compressive strengths of the mortar specimens decreased, from 54.3 MPa for GP_Ref to 29.1 MPa for GP_150, due to an increase in capillary porosity. Simultaneously, the flexural strength declined from 4.4 MPa GP_Ref to 4.0 MPa for GP_150 as the water content increased. At the same time, the increasing water content led to an improved deaeration effect and therefore a low air void content, as indicated by micro X-ray computer tomography.
- The binder to aggregate ratio is crucial for the compressive and flexural strengths of the mortar specimens. Through the addition of quartz powder up to a ratio of 20:80 of metakaolin to quartz, an increase in strength can be witnessed. The compressive strength of the geopolymer obtained without any quartz powder amounted to 46.55 MPa, and its strength can be increased to 81.43 MPa in the case of the 20:80 mixture of metakaolin and quartz. Simultaneously, the flexural strength increased. This finding gives new information for the optimal design of the geopolymer mixture.
- The geopolymer formation is a complex process, which requires a detailed knowledge of the underlying factors that can influence the fresh mortar properties as well as the mechanical properties of the final geopolymer mortars.

Supplementary Materials: The following supporting information can be downloaded at: https://www.mdpi.com/article/10.3390/min14080823/s1. Figure S1: Powder X-ray diffractogram of the metakaolin Metamax®. Figure S2: Powder X-ray diffractogram of the quartz powder MILLISIL W3®. Figure S3: Pore size distributions according to incident light microscopy. Figure S4: Nitrogen sorption isotherm for GP_Ref recorded at 77 K. Figure S5: Pore size distribution according to the BJH method on the basis of the desorption data. Figure S6: Results of the mercury intrusion porosimetry of the whole pore diameter area (3.5–100,000 nm). Figure S7: Powder X-ray diffractograms of GP_Ref and GP_150. Table S1: Overview of the mechanical properties of the mortar specimens. Table S2: Molar ratios of the mixing design.

Author Contributions: Conceptualization: F.D. (Felix Dathe), A.K., F.D. (Frank Dehn), writing—original draft—review, editing: F.D. (Felix Dathe), A.K. and F.D. (Frank Dehn), writing—original draft preparation—review, editing: F.D. (Felix Dathe), A.K. and F.D. (Frank Dehn), measurements: F.D. (Felix Dathe), S.O. and A.K.; analysis: A.K., visualization, F.D. (Felix Dathe), S.O. and A.K., supervision: A.K. and F.D. (Frank Dehn). All authors have read and agreed to the published version of the manuscript.

Funding: Parts of this project were funded by the German Research Foundation (DFG) (From common clay to geopolymer binder—fundamental crystallographic and structural engineering investigations, 325967999).

Data Availability Statement: The original contributions presented in the study are included in the article/supplementary material, further inquiries can be directed to the corresponding author.

Acknowledgments: The authors would like to thank Florian Fuchs for the µXCT imaging and the Workgroup of Dirk Enke for performing individual MIP measurements, both from the University of Leipzig.

Conflicts of Interest: The authors declare that they have no known competing financial interests or personal relationships that could have appeared to influence the work reported in this paper.

References

1. International Energy Agency, Glob. Status Report: Towards a Zero-Emission, Efficient and Resilient Buildings and Construction Sector. 2018. Available online: https://www.iea.org/reports/2018-global-status-report (accessed on 4 June 2024).
2. Petek Gursel, A.; Masanet, E.; Horvath, A.; Stadel, A. Life-cycle inventory analysis of concrete production: A critical review. *Cem. Concr. Compos.* **2014**, *51*, 38–48. [CrossRef]
3. Habert, G.; Miller, S.A.; John, V.M.; Provis, J.L.; Favier, A.; Horvarth, A.; Scrivener, K.L. Environmental impacts and decorbonization strategies in the cement and concrete industries. *Nat. Rev. Earth Environ.* **2020**, *1*, 559–573. [CrossRef]
4. Farooq, F.; Jin, X.; Faisal Javed, M.; Akbar, A.; Izhar Shah, M.; Aslam, F.; Alyousef, R. Geopolymer concrete as sustainable material: A state of the art review. *Constr. Build. Mater.* **2021**, *306*, 124762. [CrossRef]
5. Davidovits, J. Geopolymers: Man-Made Rock Geosynthesis and the Resulting Development of Very Early High Strength Cement. *J. Mater. Educ.* **1994**, *16*, 91–139.
6. Davidovits, J. Geopolymers: Inorganic polymeric new materials. *J. Therm. Anal. Calorim.* **2005**, *37*, 1633–1656. [CrossRef]
7. Palomo, A.; Grutzeck, M.W.; Blanco, M.T. Alkali-activated fly ashes: A cement for the future. *Cem. Concr. Res.* **1999**, *29*, 1323–1329. [CrossRef]
8. Provis, J.L.; van Deventer, J.S.J. (Eds.) *Geopolymers: Structures, Processing, Properties and Industrial Applications*; CRD Press: Boca Raton, FL, USA; Woodhead Publ.: Cambridge, UK, 2019.
9. He, C.; Osbaeck, B.; Makovicky, E. Pozzolanic reactions of six principal clay minerals: Activation, reactivity assessments and technological effects. *Cem. Concr. Res.* **1995**, *25*, 1691–1702. [CrossRef]
10. Seiffarth, T.; Hohmann, M.; Posern, K.; Kaps, C. Effect of thermal pre-treatment conditions of common clays on the performance of clay-based geopolymeric binders. *Appl. Clay Sci.* **2013**, *73*, 35–41. [CrossRef]
11. Dathe, F.; Strelnikova, V.; Werling, N.; Emmerich, K.; Dehn, F. Influence of lime, calcium silicate and portlandite on alkali activation of calcined common clays. *Open Ceram.* **2021**, *7*, 100152. [CrossRef]
12. Liew, Y.M.; Heah, C.Y.; Mohd Mustafa, A.B.; Kamarudin, H. Structure and properties of clay-based geopolymer cements: A review. *Prog. Mater. Sci.* **2016**, *83*, 595–629. [CrossRef]
13. Werling, N.; Schwaiger, R.; Dathe, F.; Dehn, F.; Emmerich, K. Micromechanical properties of geopolymers with different calcined clay precursors. *Appl. Clay Sci.* **2024**, *250*, 107259. [CrossRef]
14. Patankar, S.V.; Jamkar, S.S.; Ghugal, Y.M. Effect of water-to-geopolymer binder ratio on the production of fly ash based geopolymer conctrete. *Int. J. Adv. Technol. Civ. Eng.* **2012**, *1*, 296–300. [CrossRef]
15. Luhar, S.; Nicolaides, D.; Luhar, I. Fire Resistance Behaviour of Geopolymer Concrete: An Overview. *Buildings* **2021**, *11*, 82. [CrossRef]
16. Koenig, A.; Herrmann, A.; Overmann, S.; Dehn, F. Resistance of alkali-activated binders to organic acid attack: Assessment of evaluation criteria and damage mechanisms. *Constr. Build. Mater.* **2017**, *151*, 405–413. [CrossRef]
17. Bakharev, T. Durability of geopolymer materials in sodium and magnesium sulfate solutions. *Cem. Concr. Res.* **2005**, *35*, 1233–1246. [CrossRef]
18. Albidah, A.; Alghannam, M.; Abbas, H.; Almusallam, T.; Al-Salloum, Y. Characteristics of metakaolin-based geopolymer concrete for different mix design parameters. *J. Mater. Res. Technol.* **2021**, *10*, 84–98. [CrossRef]
19. Pulidori, E.; Pelosi, C.; Fugazzotto, M.; Pizzimenti, S.; Carosi, M.R.; Bernazzani, L.; Stroscio, A.; Tiné, M.R.; Mazzoleni, P.; Barone, G.; et al. Thermal behavior of Sicilian clay-based geopolymers. *J. Therm. Anal. Calorim.* **2024**, *23*, 1–13. [CrossRef]
20. Dal Poggetto, G.; Kittisayarm, P.; Pintasiri, S.; Chiyasak, P.; Leonelli, C.; Chaysuwan, D. Chemical and Mechanical Properties of Metakaolin-Based Geopolymers with Waste Corundum Powder Resulting from Erosion Testing. *Polymers* **2022**, *14*, 5091. [CrossRef] [PubMed]
21. D'Angelo, A.; Dal Poggetto, G.; Piccolella, S.; Leonelli, C.; Catauro, M. Characterisation of White Metakaolin-Based Geopolymers Doped with Synthetic Organic Dyes. *Polymers* **2022**, *14*, 3380. [CrossRef]
22. Zuhua, Z.; Xiao, Y.; Huajun, Z.; Yue, C. Role of water in the synthesis of calcined kaolin-based geopolymer. *Appl. Clay Sci.* **2009**, *43*, 218–223. [CrossRef]
23. Yao, X.; Zhang, Z.; Zhu, H.; Chen, Y. Geopolymerization process of alkali–metakaolinite characterized by isothermal calorimetry. *Thermochim. Acta* **2009**, *493*, 49–54. [CrossRef]
24. Davidovits, J. *Geopolymer Chemistry and Applications*, 5th ed.; Geopolymer Institute: Saint-Quentin, France, 2020.
25. Van Jaarsveld, J.G.S.; Van Deventer, J.S.J.; Lukey, G.C. The effect of composition and temperature on the properties offly ash- and kaolinite-based geopolymers. *Chem. Eng. J.* **2002**, *89*, 63–73. [CrossRef]
26. *EN 196-1:2016*; Methods of Testing Cement—Part 1, Determination of Strength. European Committee for Standardization: Brussels, Belgium, 2016.
27. *EN 480-11:2005*; Admixtures for Concrete, Mortar and Grout—Test Methods—Part 11: Determination of Air Void Characteristics in Hardened Concrete. European Committee for Standardization: Brussels, Belgium, 2005.
28. Koenig, A. Analysis of air voids in cementitious materials using micro X-ray computed tomography (μXCT). *Constr. Build. Mater.* **2020**, *244*, 118313. [CrossRef]
29. *EN 1015-3:2007*; Methods of Test for Mortar for Masonry—Part 3: Determination of Consistence of Fresh Mortar (by Flow Table). European Committee for Standardization: Brussels, Belgium, 2007.

30. Wang, H.; Li, H.; Yan, F. Synthesis and mechanical properties of metakaolinite-based geopolymer. *Colloids Surf. A Physicochem. Eng. Asp.* **2005**, *268*, 1–6. [CrossRef]
31. Yunsheng, Z.; Wei, S.; Zongjin, L. Composition design and microstructural characterization of calcined kaolin-based geopolymer cement. *Appl. Clay Sci.* **2010**, *47*, 271–275. [CrossRef]
32. Muller, A.C.A.; Scrivener, K.L. A reassessment of mercury intrusion porosimetry by comparison with 1H NMR relaxometry. *Cem. Concr. Res.* **2017**, *100*, 350–360. [CrossRef]
33. Pelosi, C.; Occhipinti, R.; Finocchiaro, C.; Lanzafame, G.; Pulidori, E.; Lezzerini, M.; Barone, G.; Mazzoleni, P.; Rosaria Tiné, M. Thermal and morphological investigations of alkali activated materials based on Sicilian volcanic precursors. *Mater. Lett.* **2023**, *335*, 133773. [CrossRef]
34. Kasaniya, M.; Thomas, M.D.A.; Moffatt, T.; Hossack, A. Microstructure and microanalysis of portland cement pastes with high *w/c* ratios. *Cem. Concr. Res.* **2024**, *183*, 107575. [CrossRef]
35. Dujardin, N.; Salem, T.; Feuillet, V.; Fois, M.; Ibos, L.; Poilane, C.; Manuel, R. Measurement of pore size distribution of building materials by thermal method. *Constr. Build. Mater.* **2020**, *245*, 118417. [CrossRef]
36. Abell, A.B.; Willis, K.L.; Lange, D.A. Mercury Intrusion Porosimetry and Image Analysis of Cement-Based Materials. *J. Colloid Interface Sci.* **1999**, *211*, 39–44. [CrossRef]
37. Kang, S.H.; Jeong, Y.; Tan, K.H.; Moon, J. The use of limestone to replace physical filler of quartz powder in UHPFRC. *Cem. Concr. Compos.* **2018**, *94*, 238–247. [CrossRef]
38. Haruna, S.; Mohammed, B.S.; Wahab, M.M.A.; Al-Fakih, A. Effect of aggregate-binder proportion and curing technique on the strength and water absorption of fly ash-based one-part geopolymer mortars. *IOP Conf. Ser. Mater. Sci. Eng.* **2021**, *1101*, 01202. [CrossRef]
39. Joseph, B.G.; Mathew, G. Influence of aggregate content on the behavior of fly ash based geopolymer concrete. *Sci. Iran.* **2012**, *19*, 1188–1194. [CrossRef]
40. Arellano-Aguilar, R.; Burciaga-Díaz, O.; Gorokhovsky, A.; Escalante-García, J.I. Geopolymer mortars based on a low grade metakaolin: Effects of the chemical composition, temperature and aggregate: Binder ratio. *Constr. Build. Mater.* **2014**, *50*, 642–648. [CrossRef]